UPC CTTC

# Numerical Simulation of the Thermal and Fluid Dynamics Behaviour of Liquid-Vapour Two-Phase Flow in Evaporators and Condensers.

Centre Tecnològic de Transferència de Calor
Departament de Màquines i Motors Tèrmics
Universitat Politècnica de Catalunya

Sergio Morales Ruiz
Doctoral Thesis

*Sergio Morales Ruiz*

DOCTORAL THESIS

*UPC – Marzo 2009*

# Numerical Simulation of the Thermal and Fluid Dynamics Behaviour of Liquid-Vapour Two-Phase Flow in Evaporators and Condensers.

Sergio Morales Ruiz

TESI DOCTORAL

presentada al

Departament de Màquines i Motors Tèrmics
E.T.S.E.I.A.T.
Universitat Politècnica de Catalunya

per a l'obtenció del grau de

Doctor Enginyer Industrial

Terrassa, Marzo 2009

# Numerical Simulation of the Thermal and Fluid Dynamics Behaviour of Liquid-Vapour Two-Phase Flow in Evaporators and Condensers.

Sergio Morales Ruiz

**Directors de la Tesi**

Dr. Joaquim Rigola Serrano

Dr. Carlos David Pérez-Segarra

Dr. Assensi Oliva Llena

**Tribunal Qualificador**

Dr. Esteve Codina Macià
Universitat Politècnica de Catalunya

Dr. Carles Oliet Casasayas
Universitat Politècnica de Catalunya

Dr. José Fernández Seara
Universidad de Vigo

Dr. Manel Soria Guerrero
Universitat Politècnica de Catalunya

Dr. José Manuel Pinazo Ojer
Universidad Politécnica de Valencia

**A Claudia, Manuela, y a mis padres**

# Contents

# Acknowledgements

Deseo agradecer a todos los miembros del Centro Tecnológico de Transferencia de Calor (CTTC), y en especial a su director el Profesor Asensi Oliva por su apoyo incondicional, comprensión y colaboración en momentos difíciles durante el tiempo que he sido miembro del CTTC.

A mi Director el Profesor Joaquim Rigola, por su colaboración en las diferentes tareas que llevaron a la culminación de esta Tesis, por acompañarme, guiarme y mostrarme los posibles caminos por los cuales conducir este trabajo, siempre dándome ánimos para continuar en las tareas que nos proponíamos.

Al Profesor Carlos David Peréz Segarra, por sus consejos, comentarios y recomendaciones en diversas tareas que fueron de gran utilidad para la elaboración de esta Tesis.

A todos los compañeros del CTTC, los que están y los que han marchado, con quienes he compartido muchos buenos momentos y a quienes agradezco sus consejos sobre como abordar tareas en las que no tenia suficiente experiencia, especialmente a Conxita e Ivette quienes me enseñaron la aplicación de la programación computacional y los métodos numéricos en la predicción del comportamiento fluido-dinámico de flujos en una sola fase.

A Carles Oliet, quien me aclaro conceptos relacionados con los diferentes mecanismos de transferencia de calor al interior de tuberías en intercambiadores de calor y quien me enseño varias estrategias de programación para la optimización de los código de simulación numérica.

A Gustavo Raush, quien me explico con detalle como utilizar la unidad de refrigeración por compresión de vapor y me guío en la tarea de obtener los datos experimentales para poder así llevar a cabo la validación de los modelos presentados en este trabajo.

A Manuel Ordoñez por su asistencia técnica y apoyo en las tareas de puesta a punto de la instalación experimental.

Al Profesor Francesc Reventós del Departamento de Física e Ingeniería Nuclear de la UPC y al Sr. Chris Allison director de Innovative Systems Software, por permitirme participar en el curso-seminario RELAP and SCDAP training workshop.

A toda mi familia, pero en especial a mis padres y a mi hermano por haber respetado mis decisiones a lo largo de todos esto años fuera de casa y por haberme apoyado a lo largo del desarrollo de mi vida personal y académica, sin el apoyo de ellos no hubiera alcanzado llegar hasta este punto.

A mi esposa Claudia, quien siempre me ha escuchado, apoyado, animado y contagiado de su gran espíritu de lucha y superación. Gracias por su compañía en todo momento y su complicidad en cada plan que nos proponemos. La culminación de está Tesis significa alcanzar uno de los objetivos que hace varios años nos planteamos,

gracias por estar siempre junto a mí y hacer que la vida sea más interesante.

A nuestra hija Manuela, quien nos ha llenado de energía para futuros retos y quien es la alegría de nuestro hogar.

# Abstract

A numerical study of the thermal and fluid-dynamic behaviour of the two-phase flow in conducts is presented. The numerical analysis is based on two different models. The first one is the quasi-homogeneous model, which assumes the two-phase flow as a mixture. The total mass flux, the pressure and the temperature of the fluid flow along evaporators and condensers are obtained by means of the numerical resolution of mass, momentum and energy conservation equations. The gas and liquid velocities are defined from the total mass flux result and the void fraction value, which is evaluated with an empirical correlation. Although the quasi-homogeneous model is capable to give well results in different applications where the two-phase flow occurs, this model can not evaluate each one of the phases separately. If the quasi-homogeneous model is applied judiciously considering their restrictions with some fluid flow configurations and limitations due to not including the interface exchanged terms, this model is able to be a very useful tool to estimate the thermal and fluid-dynamic behaviour of the two-phase flow in different thermal systems. The second one is the two-fluid model, which allows considering liquid and gas phases coexisting in a same control volume, although with different velocities and temperatures each one of the phases. This second model takes into account the interaction between each one of the phases and the interface recognising the influence of the exchange through the interface and non-thermal equilibrium conditions. The two-fluid model needs more empirical information than the quasi-homogeneous model to close and resolve the system of equations. The pressure, the void fraction, the gas and liquid velocities and the gas and liquid temperature are obtained by the numerical solution of two mass, two momentum and two energy conservation equations.

Both numerical simulation have been developed by means of the finite volume technique based on a one-dimensional and two-dimensional for the two-fluid model, transient integration of the continuity, momentum and energy conservation equations. The pressure, velocities, temperatures and distribution of the gas and liquid into the tube are obtained from the resolution of the set differential governing equations. A semi-implicit pressure based method SIMPLE-liked method have been used to resolve the governing equations proposed in each one of the models developed in this Thesis. Furthermore, the numerical algorithms are detailed.

The verification of the models developed has been carried out by means of a study of mesh density and precision criteria to make sure that the solution is free of numerical errors. Some specifics cases such as: the water faucet problem and the sedimentation problem have been compared with an analytical solution. The validation has been carried out with experimental data obtained from technical literature and CTTC's experimental facility. A comparison between quasi-homogeneous model and two-fluid model in one-dimensional numerical simulation of a refrigerant evaporator

is shown. On the other hand, two cases reported in the literature has been used to compare the two-fluid model 2D results, these cases are considered under isothermal conditions.

In order to show the applicability of the numerical models developed in this Thesis, these have been integrated into different CTTC's codes with the aim to be used for different applications like: i) A double-pipe heat exchanger is studied and the influence of different parameters on the thermal and fluid-dynamic behaviour is analysed; ii) A fin-and-tube heat exchanger working as an evaporator and a condenser is resolved numerically, and a comparison with experimental data are detailed; and ii) A solar panel with two-phase flow inside the pipes is studied numerically with the aim of avoid to reach the critical heat flux conditions, a dangerous working conditions for any kind of thermal installation.

# Chapter 1

# Introduction

## 1.1 Preamble

The two-phase flow phenomena is a particular case of the general multiphase flow. The general characteristic of the multiphase flow is the existence of one or several interfaces and discontinuities between two or more phases. The phase is a characteristic thermodynamic state of the matter. In standard conditions the matter has three different states: gas, liquid and solid. So, it is possible to classify a fluid flow as two-phase flow if a mixture of: gas-liquid, gas-solid, liquid-solid or immiscible liquid-liquid is present. In this Thesis the two-phase flow gas-liquid has been studied.

The numerical simulation of the two phase flow phenomena have a very important interest in academic and research fields, and play an important role on several industrial areas, e.g. mechanical, chemical, nuclear, oil industry, physics and mathematics. Different models and numerical methods of solution have been studied and developed during the last four decades, looking for the optimum working condition or the most efficient design of specific thermal devices, such as the different kind of heat exchangers, vapour generator, distillation towers, nuclear system, pipeline, fluidized beds,refrigerant systems, air-conditioning systems, etc., where two-phase flow phenomena occur. The evaporators and condensers are only one of the different industrial applications where the simultaneous flow of gas and liquid occur.

The two-phase flow can be classified in function of the structure of the flow and the topographic distribution of the each phase into the flow. Then, in a general form any two-phase flow can be get into three groups: separated flow, dispersed flow and mixed or transitional flow. Each one of these groups are divided in sub-groups called as regimes flow, which describe with more detail the geometry and configuration of the fluid flow. The regimes flow depend on the kind of mixture, and the characteristics of the fluid flow, such as: direction of the fluid flow (vertical or horizontal), mass flux or phase velocities and heat flux applied. The typical regimes flow used to define the fluid flow are: bubbly flow, slug flow, droplet flow, stratified flow, annular flow and

combination of these regimes. Along the last decades of the two-phase flow study, different classifications have been proposed in the literature, a summary can be see in [1].

The knowledge of the thermal and fluid dynamic mechanism of the two-phase flow is required to propose a numerical model capable to predict the behaviour of the phenomena correctly and to use the adequate empirical information. Great advancements in the numerical simulation and experimental techniques have been obtained in the computational fluid dynamics field for single-phase flow in last years. However, the complexity of the two-phase flows produces a lot of difficulties in the extension of these advancements developed to the two-phase flow, i.e. the usual experimental techniques for single-phase flow does not work very well when two-phase flow occurs. Due to these difficulties, the numerical simulations becomes an essential tool to understand and to investigate the two-phase flow phenomena lookin for the optimisation in the design of any thermal device in which the two-phase flow occurs.

The numerical simulation is a powerful strategy to predict the thermal and fluid dynamic behaviour of the two-phase flow, in some cases the only way to find the approximately evolution of a specific case, e.g. the two-phase flow without the influence of the gravity into the pipe. The adequate computational method in multiphase flow [2], which should correspond to the physical laws of transport of mass, momentum, and energy, is the best way to find the solution of the two-phase flow.

### 1.1.1 Numerical Models used in two-phase flow

Different resolutions of the two-phase flow phenomena by means of the numerical methods have been proposed. One of them is based on a simple heat global balance, depending on the inlet and the outlet conditions of the system. While, others are based on a local analysis by means of the solutions of the conservative equations of mass, momentum and energy, making up a governing equations.

The mathematical formulation of the governing equations can be written in different forms depending on the model applied and the hypothesis assumed. So, the solution of the two-phase flow can be a easy or complex task in function of the model chosen and the hypothesis assumed.

The earliest model of two-phase flow is the homogeneous mixture model. This model assumed that both phases are completely mixed and moved with the same speed at the same pressure and temperature. The flux is considered in thermal equilibrium and it has the same physical properties at the cross section. Three equations define the variation of the independent variables mixture velocity, mixture enthalpy and pressure as function of time and position [3]. A quasi-homogeneous model has been proposed as an alternative to define the liquid and gas velocities, where the hypothesis is define a mixture mass flux, and after evaluate two velocities as function on the volume, weight mass and void fraction [4] [5]. The quasi-homogeneous model make possible to

define the gas and liquid velocities in contrast to the homogeneous model, which only define a mixture velocity. These both models are used in one-dimensional simulations and well results are obtained depending on the characteristic of the fluid flow. These kind of models give more information than the heat global balance models and can be easily used for different industrial applications.

The separated models with no interface exchange assume equal gas and liquid temperature as in the case of homogeneous model, but different liquid and gas velocities are considered. The diffusion effect of each phases was considered, which mean that the two phase move with different speeds [6] [3]. The difference between velocities are evaluated by means of the constitutive equation, which evaluate the relative motion between phases from a kinematic constitutive expression. These models have the advantage of being inherently simple by assuming constant properties across the flow cross section and being able to apply single phase correlations directly [7]. However, these models not have into account the mass, momentum and energy exchanged on the interface. So, these models are valid only in cases where the exchange through the interface is not important on the behaviour of the fluid flow. The main disadvantage of these models is their empirical nature and their avoidance of deal with the detailed structure of the two-phase flow. Many studies have been carried out to find the most suitable constitutive equation in function of the different characteristics parameters of the two-phase flows, for example, horizontal flows, low flow conditions, counter-current flow, large pipe diameters, etc.

The two-fluid model assume that liquid and gas phases can be in thermal non-equilibrium and each phases have different velocities, temperatures, and pressure. The pressure is considered equal in many cases, it is a hypothesis than simplified the solution and not affect in an important manner the behaviour of the phenomena. Complex two-phase flow where non-equilibrium plays an important role require the two-fluid model, it model can calculated the kinematic and thermal non-equilibrium as a part of the solution [8]. These models consider exchange of mass, momentum and energy through the interface and can give more details of the phenomena that the methods mentioned above.

When two-fluid model is used, the number of equations is duplicated and then two equations for each phase are needed. So, two mass conservation equations, two momentum equations and two energy equations are defined and required to solve the two-phase flow based on a two-fluid model [9]. Each one of the equations needs a group of empirical correlations, by means of these empirical expressions is possible to link and relate each one of the phases with the interface and the wall. These empirical correlations are called the constitutive laws and are known to depend on the flow patterm, then a regimen maps must be defined previously [10].

## Empirical information

The set of empirical correlations and constitutive equations are required to close the system of equations defined as governing equations. This group of empirical expressions are called the constitutive laws.

The constitutive laws evaluate different parameters such as the frictional factors or the shear forces, the heat transfer coefficients, the interfacial area, the distribution of each phase into the volume and the volumetric mass exchanged. These parameters should be defined for each one of the phases and on the interface. Depending on the model chosen to solve the two-phase flow problem, the number of constitutive laws needed is different. The homogeneous and quasi-homogeneous model require at least two or three empirical expressions, while the two-fluid model needs at least nine different empirical correlations.

The constitutive laws depend on the regimen flow. So, in a two-phase flow the evaluation of the empirical parameters are function of the different regimen flows such as: stratified, bubbly, slug, annular, mist, and combination of them, while in the single phase only laminar or turbulent regimen should be considered. This characteristic make that the number of constitutive laws must be multiplied by the number of the different regimen flows. The determination of the regimen flow depends on the geometry, flow structure into the tube, position, distribution of the gas, and velocities.

The incorporation of flow regimen map in the numerical codes have been an improvement in the numerical simulation, because the value of the different empirical parameters should be function of the flow configuration defined by it. However, the problem is the complexity between regimes and the change value of the parameters. Many strategic have to be applied to do not fall in a discontinuity problem.

The empirical information used in the quasi-homogeneous model and the two-fluid model have been obtained from the technical literature. The local heat transfer coefficient of the two-phase flow mixture used in the quasi-homogeneous model is evaluated from traditional expressions such as [11] [12] [13], which are validate in a specific regime flow, and complex models that have taken into account the effect of the different regimen flows along the evaporation or condensation process such as [14] [15]. The quasi-homogeneous model is closed with the evaluation of the frictional factor from [16] or [17] and the void fraction from [18].

The number of constitutive laws needed in the two-fluid model is quite large and is not possible to list each one of the empirical expressions used. A basic information in function of a specific flow regimen is detailed in some papers such as [19] [20] [21], and a complete set of constitutive laws and a flow regimen map have been proposed in some commercial codes manuals as [22] [23] and technical books in the two-phase flow field such as [1] [10].

### Numerical resolution method

Different algorithm methods have been used to resolve the governing equations developed to find the numerical solution of the two-phase flow. The hypothetic process to find a numerical solution of the model developed, consists in discretize the governing equations suitably, and solve them by a method reliable for nonlinear problems, e.g. Newton-Rapshon iteration. However, the computational cost is prohibitive in storage requirement and execution time. Then, other alternative should be applied to find a solution.

The most important algorithms used in the numerical solution of the two-phase flow are: i) the step by step method implemented in an one-dimensional quasi-homogeneous model [4] [5]; ii) the segregated methods derived from the pressure-based method have been used in an one-dimensional quasi-homogeneous model [24] and an one-dimensional two-fluid model [25], and has been proposed to be used in two-dimensional two-fluid model [26], and; iii) the coupled or semi-coupled methods have been used in an one-dimensional two-fluid model and implemented in different nuclear reactor thermohydraulic safety codes [2], different alternatives such as first or second-order accurate scheme in a high-resolution method [27] have been proposed to solve the two-phase flow.

Other methods have been used to find a solution of the two-phase flow by means of mathematical approximation such as the linearized Riemann solver [28], or the flux vector splitting [29] based on the combination of the signal propagation along characteristic line with the property of accurate conservation of mass, momentum and energy.

The pressure-based methods are used in single phase flow, these are robust and efficient. Although an extention of the pressure-based method to two-phase flow has been developed, a disadvantage is the numerical dissipation of it, which tends to produce discontinuities if a grid size is not enough. This kind of method is suitable for relatively slow transients or phenomena with long duration such as flow in pipeline. On the other hand, the coupled methods are more suitable for fast transient such as the nuclear reactor applications.

## 1.1.2 Applicability: industrial interest

The constant search for improving the efficiency, to prevent the environment damage and to reduce the energy consumption, has had an important role in the design of the different thermal devices along the last decades. A lot of experimental and numerical investigations have been carried out looking for to understand and quantify the value of the different variables that take part in the two-phase flow phenomena.

The applicability of the two-phase flow simulation in industrial applications has a vital importance in the development of new thermal devices and in the control of

existing equipments to avoid dangerous working conditions.

The two-phase flow phenomena occurs in different thermal devices in several industrial field such as: air-conditioning and refrigerant systems, oil production and transport, automotion, nuclear steam supply system, chemical industry, food process, etc.

In the air-conditioning and refrigeration systems, the influence of new refrigerant fluids (alternative fluids) and their physical properties in the thermal and dynamic behaviour of the two-phase flow into the system have been extensively studied, together with the different geometries in a lot of heat exchanger configurations.

In the transport and production of oil the study of the behaviour of two fluids immiscible such as oil and water travel together in a pipeline, and the pressure drop are important aspects to know in this field.

In the automotion industry the spray injection into the combustion camera of the petrol-oil and air make up a two-phase flow. The well knownledge of the two-phase flow and the combustion phenomena can help to develop more efficient engines.

In the nuclear energy field a lot of studies have been proposed in the specific topic to prevent loss-of-coolant accident LOCA in the nuclear plants. The energy generation from nuclear plants has been one of the most interested field in the development of the computational methods to predict the thermal and fluid dynamic behaviour of the two phase flow to prevent possible damage problems in the reactor when critical heat flux conditions occur in the plant.

In chemical and food industry the use of the knowledge about the two-phase flow can help to improve the production mechanism, e.g. the transport of the particles suspended in a fluid flow of liquid or gas, increase the interfacial area for a gas-liquid chemical reaction, use the gas as a pump to lift part of the liquid.

In biomedical engineering the study of the two-phase flow particles suspensions can help to improve the knowledge about some hemodynamic problems from the computational multiphase flow methods. This kind of works contribute to improve people's life quality.

In the electronic industry the necessity of dissipate heat flux in the microprocessors has an important field of action, and a micro-channels working as micro-heat exchangers with two-phase flow inside have been used to reduce the heat produced during the work of data processing. Now, a lot of works about the two-phase flow phenomena assuming not gravity are been carrying out in different technical centers and the best manner to find answer is the computational methods, due to the experimental infrastructure is quite expensive.

This Thesis will show the application of the numerical methods developed for two-phase flow in the two different kind of heat exchangers and in a solar receiver working as a vapour generator.

## 1.2 Research Objective

Numerical simulation and experimental investigation in two phase flow is an important line of research in the CTTC (Centre Tecnologic de Transferencia de Calor). Attention has been focused on the analysis of different components such as condensers, evaporators, expansion devices and compressors. Also the complete refrigerant cycle has been studied. This Thesis is a work that complement and follow the line of research of the Group in the two-phase flow field.

The objectives of this Thesis have been: i) to build a complete numerical code to simulate the two-phase flow into the tubes, based on a quasi-homogeneous model. This model should be able to give good results of the two-phase flow phenomena, knowing the simplifications of this method that assume the two-phase flow as a mixture; ii) to develop a numerical simulation code based on the two-fluid model, this code should be able to describe the thermal and fluid dynamic behaviour of the liquid and gas phase flow into the tube, separately. The model implemented has to give realistic results about the two-phase flow variables that define this phenomena; iii) to use an experimental infrastructure to study the regimen of the flow present in different conditions of work at inner of the evaporator; iv) to validate the simulation code with help of the data obtained from the experimental refrigeration unit and the scientific literature, and v) to show the applicability of the numerical codes as a tool of design of different thermal devices where the two-phase flow occurs.

## 1.3 Outline of the Thesis

The results of the present Thesis has led to one journal publication and six papers published in international proceedings. The Thesis has been focused on detailed one-dimensional and two-dimensional numerical simulation of the two-phase flow phenomena. The numerical simulation is based on two different mathematical models, the first one is an equilibrium quasi-homogeneous model, it has been used in the numerical solution of one-dimensional two-phase flow inside pipes [24] [30], and applications of this model in the study of heat exchangers have been carried out [31] [32]. The second one is a non-equilibrium two-fluid model [33] [34] applied initially on one-dimensional cases and an extention to two-dimensional cases is presented in last Chapter.

Different numerical aspects have been evaluated with the aim of verifying the quality of the numerical solution. Convergence errors, discretization errors, and numerical schemes have been analysed. Effects of the boundary conditions, mesh sizes and initial value problem over numerical stability are also considered in the solutions. The differences between the numerical simulation data obtained with one-dimensional quasi-homogeneous model and two-fluid model into the tube are illustrated [34]. Furthermore a comparative between numerical results and experimental data obtained

from a CTTC's experimental set-up [35] is also shown.

The numerical quasi-homogeneous model developed in this work has been used recently in another Thesis [36] to study a vapour compression refrigerant system.

# References

[1] M. Ishii and T. Hibiki. *Thermo-fluid dynamics of two-phase flows.* Springer, 2006.

[2] A. Prospereti and G. Tryggvason. *Computational Methods for Multiphase Flow.* Cambridge University Press, 2007.

[3] G. B. Wallis. *One-dimensional two-phase flow.* McGraw-Hill, 1969.

[4] F. Escanes, C. D. Pérez-Segarra, and A. Oliva. Thermal and fluid-dynamic behaviour of double-pipe condensers and evaporators. *International Journal for Numerical Methods for Heat and Fluid Flow*, 5(9):781–795, 1995.

[5] O. García-Valladares, C.D. Pérez-Segarra, and J. Rigola. Numerical simulation of double-pipe condensers and evaporators. *International Journal of Refrigeration*, 27(6):656–670, 2004.

[6] N. Zuber and J. Findley. Average volumetric concentration in two-phase flow system. *Journal of Heat Transfer - Transactions of Asme*, 87:453–468, 1965.

[7] T. Hibiki and M. Ishii. One-dimensional drift-flux model and constitutive equations for relative motion between phase in various two-phase flow regimes. *International Journal of Heat and Mass Transfer*, 46:4935–4948, 2003.

[8] J. M. Delhaye, M. Giot, and M. L. Riethmuller. *Thermohydraulics of two-phase systems for industrial design and nuclear engineering.* Hemisphere Publishing Corporation, 1981.

[9] M. Ishii. *Thermo-fluid dynamic theory of Two-phase flow.* Eyrolles, 1975.

[10] S. Levy. *Two-phase flow in complex system.* Willey, 1999.

[11] M.M. Shah. A General Correlation for Heat Transfer during Film Condensation inside. *International Journal of Heat and Mass Transfer*, 22:547–556, 1979.

[12] M.M. Shah. Chart correlation for saturated boiling heat transfer: equations and further study. *ASHRAE Transactions*, 88(1):185–196, 1982.

[13] S.G. Kandlikar. A general correlation for saturated two-phase flow boiling heat transfer inside horizontal and vertical tubes. *Journal of Heat Transfer - Transactions of Asme*, 112(1):219–228, 1990.

[14] N. Kattan, J.R. Thome, and D. Favrat. Flow boiling in horizontal tubes: part 3 - development of a new heat transfer model based on flow pattern. *Journal of Heat Transfer - Transactions of Asme*, 120(1):156–165, 1998.

[15] L. Wojtan, T. Ursenbacher, and J.R. Thome. Investigation of flow boiling in horizontal tubes: part I - a new diabatic two-phase flow pattern map. *International Journal of Heat and Mass Transfer*, 48(14):2955–2969, 2005.

[16] D. Jung and R. Radermacher. Prediction of Evaporation Heat Transfer Coefficient and Pressure Drop of Refrigerant Mixtures. *International Journal of Refrigeration*, 16(5):330–338, 1993.

[17] L. Friedel. Improved Friction Pressure Drop Correlation for Horizontal and Vertical Two-Phase Pipe Flow. European Two-Phase Flow Group Meeting, Ispra, Italy. Paper E2., 1979.

[18] C.K. Rice. The Effect of Void Fraction Correlation and Heat Flux Assumption on Refrigerant Charge Inventory Predictions. *ASHRAE Transactions*, 93(1):341–367, 1987.

[19] M. Ishii. Two-fluid model and hydrodynamic constitutive relations. *Nuclear Engineering and Design*, 82(2-3):107–126, 1984.

[20] D. Bestion. The physical closure laws in the CATHARE code. *Nuclear Engineering and Design*, 124(3):229–245, 1990.

[21] A. Ullmann and N. Brauner. Closure relations for two-fluid models for two-phase stratified smooth and stratified wavy flows. *International Journal of Multiphase Flow*, 32:82–105, 2006.

[22] Idaho National Engineering Laboratory. *RELAP5/MOD3 Code Manual. Volumen IV: Models and correlations*, 2001.

[23] I. Tiselj, A. Hovard, G. Cerne, J. Gale, I. Parzer, B. Mavko, M. Giot, J. M. Seynhaeve, B. Kucienska, and H. Lemonnier. WAHA3 Code manual. Technical report, Jozef Stefan Institute, 2004.

[24] S. Morales-Ruiz, J. Rigola, C. D. Pérez-Segarra, and O. García-Valladares. Numerical analysis of two-phase flow in condensers and evaporators with special emphasis on single-phase / two-phase transition zones. *Applied Thermal Engineering*, 2008.

[25] M. R. Ansari and V. Shokri. New algorithm for the numerical simulation of two-phase stratified gas-liquid flow and its application for analyzing the Kelvin-Helmholtz instability criterion with respect to wavelength effect. *Nuclear Engineering and Design*, 237:2302–2310, 2007.

[26] M. Darwish and F. Moukalled. A unified formulation of the segregated class of algorithms for multiphase flow at all speeds. *Numerical Heat Transfer, Part B*, 40:99–137, 2001.

[27] I. Tiselj and S. Petelin. Modelling of two-phase flow with second-order accurate scheme. *Journal of Computational Physics*, 136:503–521, 1997.

[28] I. Toumi and A. Kumbaro. An approximate linealized Riemmann solver for two-fluid model. *Journal of Computational Physics*, 124:286–300, 1996.

[29] H. Staedtke, G. Franchello, and B. Worth. Numerical simulation of multidimensional two-phase flow based on flux vector splitting. *Nuclear Engineering and Design*, 177(1-3):199–213, 1997.

[30] S. Morales, J. Rigola, C. D. Pérez-Segarra, and A. Oliva. Numerical analysis of two-phase flow in condensers and evaporators with special emphasis on single phase - two phase transition zones. In *Proceedings of the 3rd International Symposium on Two-Phase Modelling and Experimentation*, pages 321–328, 2004.

[31] J. Rigola, S. Morales, G. Raush, and C. D. Pérez-Segarra. Analysis of two-phase flow in double-pipe condensers and evaporators with special emphasis on transition zones: Numerical model and experimental comparison. In *Proceedings of the 2004 International Refrigeration and Air Conditioning Conference at Purdue*, pages 1–10, 2004.

[32] J. Rigola, C. Oliet, S. Morales, and C. D. Pérez-Segarra. Numerical model of in-tube ammonia evaporation. Analysis of available heat transfer correlations. In *Proceedings of the 6th IIR Gustav Lorentzen Natural Working Fluids Conference*, pages 1–9, 2004.

[33] S. Morales, J. Rigola, C. D. Pérez-Segarra, and A. Oliva. Analysis of two-phase flow in Condensers and Evaporators based on Two-Fluid models: Numerical Model and Experimental Comparison. In *Proceedings of the 11th International Refrigeration and Air Conditioning Conference at Purdue*, pages 1–8, 2006.

[34] S. Morales, J. Rigola, C. D. Pérez-Segarra, and A. Oliva. Numerical Resolution of Two-fluid Models Equation for Condensation and Evaporation Flow in Ducts Using a Pressure Based Method. In *Proceedings of the 11th International Refrigeration and Air Conditioning Conference at Purdue*, pages 1–8, 2008.

[35] G. Raush, J. Rigola, S. Morales, C.D. Pérez-Segarra, and A. Oliva. Experimental analysis of two-phase flow in evaporators with special emphasis on single phase - two phase transition zones. In *Proceedings of the 3rd International Symposium on Two-Phase Modelling and Experimentation*, 2004.

[36] G. Raush. *Detailed experimental research on vapour compression refrigerant system.* PhD thesis, Universitat Politècnica de Catalunya, 2008.

# Chapter 2

# Numerical analysis of two-phase flow liquid-vapour in condensers and evaporators ducts by means of the Quasi-homogeneous model

**Abstract.**

A numerical study of the thermal and fluid-dynamic behaviour of the two-phase flow in ducts under condensation or evaporation phenomena is presented. The numerical simulation has been developed by means of the finite volume technique based on a one-dimensional and transient integration of the conservative equations (continuity, momentum and energy). The discretized governing equations are solved using the Semi-Implicit Method for Pressure-Linked Equations (SIMPLE) which allows back flow phenomena. Special emphasis is performed on the treatment of the transition zones between the single-phase and two-phase flow. The empirical inputs of single-phase and two-phase flow, including sub-cooled boiling and dry-out, have been adapted by means of adequate splines in the transition zones where the heat transfer correlations available in the literature are not suitable. Different numerical aspects have been evaluated with the aim of verifying the quality of the numerical solution.

## 2.1 Introduction

Heat exchangers are widely used in industrial applications, e.g. refrigeration and air-conditioning systems, where these equipments represent an important component. Condensers and evaporators in a vapour compression refrigeration system are an example. These elements have been studied for many years, and different experimental and mathematical modelling have been trying to explain the thermal and fluid dynamic behaviour of the fluid flow into the heat exchanger.

In many condensers and evaporators the fluid refrigerant flows inside tubes while the secondary fluid flows in the external part. In the refrigeration system, the heat exchanger are connected to other elements like compressors, expansion devices, receivers, etc. which have influence on the heat exchanger behaviour. The necessity of building equipment with higher energy efficiency and using non-contaminant refrigerants are important reasons for the continuous study and research on this topic.

The design of the heat exchanger can be developed by means of analytical methods. These methods give a quick and global approach of their behaviour. However, a large number of hypothesis and simplifications have to be assumed. Examples are the $F - factor$ or $\epsilon - NTU$ methods [1]. More general and accurate approaches require the use of numerical methodologies, which subdivide the heat exchanger into many elemental volumes and solve the governing equations for each volume. In the two-phase flow region, the governing equations (mass, momentum and energy) can be formulated in different forms depending on the model used. Homogeneous models [2], drift-flux models [3] or two-fluid models [4][5] can be employed to solve the two-phase flow present in the condensation and evaporation process.

To get a deep understanding of the mathematical model and the strategies for solving the governing equations, the double-pipe heat exchanger can be a good option for application due to its relatively simple geometry for the secondary flow. Different papers have been presented in the technical literature on this subject. For example, numerical and analytical results in steady and transient state have been compared in different studies on double-pipe heat exchangers [6][7][8]. Combination of the analytical expressions with numerical method are used in the double-pipe helical heat exchanger resolution [9], where a CFD modelling together with a $\epsilon - NTU$ method is used to solve the heat exchanger. Assuming thermodynamic non-equilibrium on the CV, the two-fluid model is used to solve the two-phase flow inside of the double-pipe heat exchanger. A condenser and evaporator are solved by means of this model in [10] and [11], respectively. Although this formulation shows the two-phase flow behaviour in a more detailed way, a large number of the empirical information is required and different hypothesis have to be assumed to simplify the resolution. A quasi-homogeneous model is used on double-pipe heat exchangers resolution (Escanes, Pérez-Segarra and Oliva [12] and García-Valladares, Pérez-Segarra and Rigola [13], where one-dimensional single-phase and two-phase flow are solved based on an implicit

step by step method.

The present chapter shows a more general approach for the resolution of the two-phase flow inside tubes in condensers and evaporators. The methodology is applied to double-pipe heat exchangers with the secondary fluid in the annulus region. This work is organised in different sections. The second section shows the mathematical formulation of the whole heat exchanger. Special attention is given to the analysis of the two-phase flow inside tubes by means of the Semi-Implicit Method for Pressure-Linked Equations (SIMPLE) (Patankar [14]) instead of the step-by-step method employed by the authors (Escanes, Pérez-Segarra and Oliva [12] and García-Valladares, Pérez-Segarra and Rigola [13]. The SIMPLE method is able to solve complex flow phenomena, e.g. when back flow appears due the interactions of the heat exchangers with other elements of the refrigeration system (compressor, expansion device, receivers, etc.). Furthermore, a group of different empirical correlations have been implemented to determinate the heat transfer coefficient in condensation (Shah [15]) and evaporation (Hewitt [16], Shah [17], Kandlikar [18] and [19], Groeneveld [20], Kattan, Thome and Fravrat [21], [22] and [23]), the void fraction (Rice [24]) and pressure drop (Jung and R. Radermacher[25] and Friedel [26]). The third section presents the numerical algorithm, together with different important aspects used in the solution. New criteria for the analysis of the transition zones to avoid discontinuities in the evaluation of the heat transfer coefficients between single-phase and two-phase are presented. This is an important topic that helps to prevent the appearance of non real wall temperature values and improves the numerical method. The fourth section shows the methodology to verify the numerical solutions to assure the quality of the results obtained. The mathematical model is validate in the fifth section by comparisons of the well verified numerical results with experimental data obtained from the scientific literature. The numerical results have been obtained considering R134a and R22 fluid refrigerants, while properties have been evaluated by means of the REFPROP properties program [27]. Illustrative results considering the whole double-pipe heat exchanger are given in section sixth. In the last section, the conclusions are presented.

## 2.2 Mathematical Formulation and Discretized Equations

This section presents the mathematical formulation for the whole double-pipe heat exchanger, i.e. the two-phase flow of refrigerant in the inner tube (subsections 2.2.1), the secondary fluid in the annulus (subsections 2.2.2), and the solids elements: inner tube, outer tube and insulator (subsection 2.2.3). A final subsection shows the empirical inputs needed to take into account fluid-solid interactions.

The main assumed hypothesis in the fluid flows are: one-dimensional flow, quasi-homogeneous model, negligible axial heat conduction and viscous stress in fluid and negligible heat radiation. The assumed hypothesis in the solid elements are: one-dimensional transient temperature distribution along inner and outer tubes length (but two-dimensional heat flux distribution), two-dimensional transient axisymmetric temperature and heat flux distribution in the insulator, and negligible heat radiation between tubes in the annulus and between insulator and the exterior.

The mathematical formulation is based on the conservation equations of mass, linear momentum and energy for the fluids contained in an arbitrary spatial region of volume V, bounded by a closed surface S in the Euclidean space:

$$\frac{\partial}{\partial t}\int_V \rho dV + \int_S \rho\vec{v}\cdot d\vec{S} = 0 \tag{2.1}$$

$$\frac{\partial}{\partial t}\int_V \vec{v}\rho dV + \int_S \vec{v}\rho\vec{v}\cdot d\vec{S} = \vec{F}_s + \vec{F}_m \tag{2.2}$$

$$\frac{\partial}{\partial t}\int_V \left(h - \frac{p}{\rho} + e_c + e_p\right)\rho dV + \int_S \left(h + e_c + e_p\right)\rho\vec{v}\cdot d\vec{S} = \dot{Q} - \dot{W}_s \tag{2.3}$$

These equations are integrated on the basis of staggered meshes. In this way, the domain is split into a number of control volumes (CVs). Mass and energy equations are discretized over the main CVs depicted in Figure 2.1a, while momentum equation is discretized over the staggered CVs as shown in Figure 2.1b.

The heat conduction in the solid elements is analysed by means of the heat equation, this equation is obtained from a energy conservation principle and is expressed as:

$$\rho C_p \frac{\partial T}{\partial t} = \frac{\partial}{\partial z}\left(\lambda\frac{\partial T}{\partial z}\right) + \frac{\partial}{\partial r}\left(\lambda\frac{\partial T}{\partial r}\right) + S \tag{2.4}$$

The heat equation is discretized over CVs indicated in Figure 2.2. Using this equation, the evaluation of the temperatures along the solid elements are obtained.

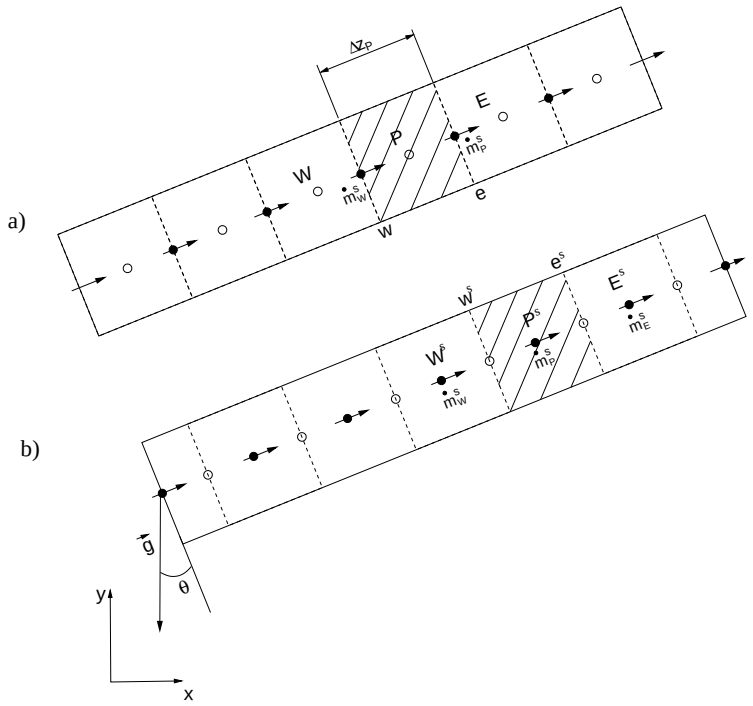


**Figure 2.1:** Schematic representation of the meshes used in the discretization of the fluid flow: a) Main control volumes for pressure and energy, b) Staggered control volumes for mass flux. Symbol (○) indicates the node of the main mesh, and (●) indicates the node of the staggered mesh.

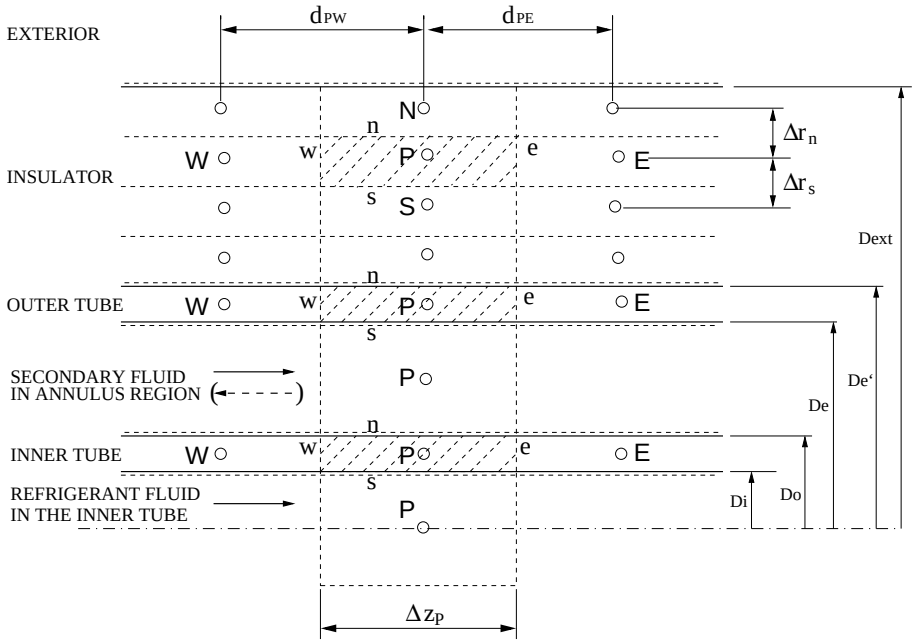


**Figure 2.2:** Discretization of the solid elements and fluids. Main nodes assigned to the selected CVs are denoted by P, while W,E,N,S indicated their neighbours. Cell-faces are denoted by lower-case letters (w,e,n,s).

### 2.2.1 Two-phase flow of refrigerant Fluid

The discretized form of the energy, momentum and mass (in terms of the pressure corrections) conservations equation of the refrigerant flow inside the inner tube is presented in this subsections.

#### Energy equation

The total energy equation is integrated over the main control volumes shown in Figure 2.1a. In a semi-discretized form, this equation can be written as:

$$\frac{\partial \tilde{\rho}_P \bar{e}_P}{\partial t} A\Delta z + \dot{m}_P^s e_e - \dot{m}_W^s e_w = \bar{\dot{q}}_P P \Delta z + \frac{\partial \tilde{p}_P}{\partial t} A\Delta z \tag{2.5}$$

where $\bar{e}_P$ represents the total specific energy ($e = h + e_c + e_p$), $\tilde{\rho}_P$ is the density, $\bar{\dot{q}}_P$ is the heat flux, $\tilde{p}_P$ is the pressure, $\dot{m}_P^s$ and $\dot{m}_W^s$ are the mass flow at the east and

west CV-faces respectively, $A$ is the cross sectional area, $P$ is the perimeter and $\Delta z$ is the CV length. The mean values over the CV used in equation (2.5) are defined as:

$$\tilde{\rho}_P = \frac{1}{V_P}\int_{V_P} \rho dV \;\; ; \;\; \tilde{p}_P = \frac{1}{V_P}\int_{V_P} p dV$$
$$\bar{e}_P = \frac{1}{\tilde{\rho}_P V_P}\int_{V_P} \rho e dV \;\; ; \;\; \bar{\dot{q}}_P = \frac{1}{\Delta z_P}\int_{z_w}^{z_e} \dot{q} dz$$

Transient terms are evaluated using a first order backward differencing scheme. Convective terms at the CV faces are evaluated using first or higher order schemes. When a first order scheme is used, the variables at a given face of the CV are taken equal to the nearest upstream nodal values (this is the upwind scheme). Higher order schemes, as Quick or Smart [28], are introduced using a deferred correction approach, i.e. the convective term is evaluated using the upwind scheme while an extra or correction term is introduced in the source term of the discretized equation keeping the diagonal dominance of the coefficient matrix. The convective heat flux is integrated along the CV heat transfer surface using local heat transfer coefficients and nodal temperatures for the inner tube and the refrigerant fluid.

Introducing all the above numerical schemes and models in the energy equation and approximating mean quantities by their values of the central node, the following fully discretized form is obtained.

$$\begin{aligned}(\rho_P e_P - \rho_P^o e_P^o)A\frac{\Delta z}{\Delta t} + \dot{m}_P^s e_e - \dot{m}_W^s e_w = \\ \alpha_P(T_P^t - T_P^f)P\Delta z + (p_P - p_P^o)A\frac{\Delta z}{\Delta t}\end{aligned} \tag{2.6}$$

Equation (2.6) can be re-written in the generic discretized form $a_P^h h_P = a_E^h h_E + a_W^h h_W + b_P^h$, in terms of the enthalpy as:

$$\begin{aligned} a_W^h = \;& max(\dot{m}_W^s, 0.0) \\ a_E^h = \;& max(-\dot{m}_P^s, 0.0) \\ a_P^h = \;& a_E^h + a_W^h + \rho_P^o A\frac{\Delta z}{\Delta t} \end{aligned} \tag{2.7}$$

$$\begin{aligned} b_P^h = \;& \left[\rho_P^o h_P^o - \rho_P(e_{cP} + e_{pP}) + \rho_P^o(e_{cP}^o + e_{pP}^o) + (p_P - p_P^o)\right]A\frac{\Delta z}{\Delta t} - \\ & \dot{m}_P^s[e_{ce} + e_{p_e}] + \dot{m}_W^s[e_{cw} + e_{p_w}] + \alpha_P(T_P^t - T_P^f)P\Delta z + \Delta conv \end{aligned} \tag{2.8}$$

High-order convective schemes are introduced through $\Delta conv$ in the source term $b_p^h$. This quantity is evaluated from:

$$\begin{aligned}\Delta conv = \quad & -[max(-\dot{m}_P^s, 0.0)(h_E - h_P) + \dot{m}_P^s(h_e^{ns} - h_P)] \\ & -[max(\dot{m}_W^s, 0.0)(h_W - h_P) - \dot{m}_W^s(h_w^{ns} - h_P)]\end{aligned}$$

where the variables $h_e^{ns}$ and $h_w^{ns}$ represent the fluid enthalpy at the CV faces itself evaluated by means of the selected high-order convective scheme. This is the deferred technique indicated above.

From the discretized energy equation, the nodal enthalpy $h_P$ is obtained at each CV. Considering thermodynamic local equilibrium in the flow, the mass gas weight fraction $x_{g,P}$ can be calculated in the two-phase flow zone as a function of the enthalpy $h_P$ and the local pressure $p_P$ as: $x_{g,P} = [h_P - h_l(p_P)]/[h_g(p_P) - h_l(p_P)]$, where $h_l$ and $h_g$ represent the saturated liquid and gas enthalpies, respectively.

## Momentum equation

The momentum equation in the axial direction is discretized over the staggered volumes indicated in Figure 2.1b. In a semi-discretized form the momentum equation can be written as:

$$\begin{aligned}V\frac{\partial \tilde{\rho}\bar{v}}{\partial t} + \dot{m}_{g,e^s} v_{g,e^s} + \dot{m}_{l,e^s} v_{l,e^s} - \dot{m}_{g,w^s} v_{g,w^s} - \dot{m}_{l,w^s} v_{l,w^s} = \\ (p_P - p_E)A - \bar{\tau}_w P \Delta z - mg\sin\theta\end{aligned} \tag{2.9}$$

Sub-indexes $g$ and $l$ indicate gas and liquid phase respectively. The gas mass flux $\dot{m}_g$ and the liquid mass flux $\dot{m}_l$ can be expressed as a function of the total mass flux of the refrigerant $\dot{m}$ and the gas weight flow fraction $x_g$ as: $\dot{m}_g = x_g\dot{m}$ and $\dot{m}_l = (1 - x_g)\dot{m}$. The gas and liquid velocities are expressed as a function of the void fraction, in the following form: $v_g = \dot{m}x_g/\rho_g\epsilon_g A$ and $v_l = \dot{m}(1 - x_g)/\rho_l(1 - \epsilon_g)A$. The mixture density can be expressed as: $\rho = \epsilon_g\rho_g + (1 - \epsilon_g)\rho_l$.

The local shear stress in the momentum equation (2.9) is obtained in terms of the friction factor, $\tau_w = (f/4)(\dot{m}^2/2\rho A^2)$. In the single-phase flow, the friction factor $f$ is determined by means of empirical information, while the mass flux $\dot{m}$ and the density $\rho$ are evaluated depending on the phase flow present, gas or liquid. In case of two-phase flow, the shear stress is determined by means of the friction factor corresponding to the gas phase, $f_g$, the gas mass flux $\dot{m}_g$, the gas density $\rho_g$ and the multiplier two-phase factor $\Phi$, as $f = f_g\Phi$. The friction factor and multiplier two-phase factor are empirically obtained.

Introducing in equation (2.9) the expressions commented above, and rearranging according to the general form of momentum equation, $a_P^v \dot{m}_{P^s} = a_E^v \dot{m}_{E^s} + a_W^v \dot{m}_{W^s} + b_P^v$, the following discretized coefficients are obtained:

$$
\begin{aligned}
a_W^v = \quad & max(\dot{m}_{w^s}, 0.0) K_{w^s} \\
a_E^v = \quad & max(-\dot{m}_{e^s}, 0.0) K_{e^s} \\
a_P^v = \quad & max(\dot{m}_{e^s}, 0.0) K_{e^s} - max(-\dot{m}_{w^s}, 0.0) K_{w^s} + \frac{f}{4}\left[\frac{\mid \dot{m}_{p^s} \mid}{2\rho_{P^s} A^2}\right] P\Delta z + \frac{\Delta z}{\Delta t} \\
b_P^v = \quad & (p_P - p_E)A + \dot{m}_P^o \frac{\Delta z}{\Delta t} - \rho_{P^s} g sin\theta A \Delta z + \Delta conv \\
\Delta conv = \quad & -[max(-\dot{m}_{e^s}, 0.0)\dot{m}_{E^s} - max(\dot{m}_{e^s}, 0.0)\dot{m}_{P^s} + \dot{m}_{e^s}\dot{m}_e^{ns}] K_E \\
& -[max(\dot{m}_{w^s}, 0.0)\dot{m}_{W^s} - max(-\dot{m}_{w^s}, 0.0)\dot{m}_{P^s} - \dot{m}_{W^s}\dot{m}_w^{ns}] K_P
\end{aligned}
\tag{2.10}
$$

where, $K = [x_g^2/\rho_g \epsilon_g A + (1 - x_g)^2/\rho_l (1 - \epsilon_g) A]$. This variable is evaluated at the node of the main mesh (in fact, $K_{e^s} = K_E$ and $K_{w^s} = K_P$). Using the Central Difference scheme (CDS) for the convective terms, the mass flux on the staggered volume faces are defined as: $\dot{m}_{e^s} = (\dot{m}_{E^s} + \dot{m}_{P^s})/2$ and $\dot{m}_{w^s} = (\dot{m}_{P^s} + \dot{m}_{W^s})/2$, and density value over the CV center of the staggered mesh are defined as: $\rho_{P^s} = (\rho_E + \rho_P)/2$. The mass flux $\dot{m}_e^{ns}$ and $\dot{m}_w^{ns}$ are evaluated using the Quick or Smart numerical scheme in the deferred correction term $\Delta conv$.

## Pressure correction equation

A pressure correction equation is evaluated over the main control volumes (Figure 2.1a) by means of the continuity equation and according to the SIMPLE method [14]. The strategy starts from the semi-discretized form of the continuity equation:

$$V_P \frac{\partial \tilde{\rho_P}}{\partial t} + \dot{m}_e - \dot{m}_w = 0 \tag{2.11}$$

The mass flow is estimated from the discretized momentum equation rewritten as: $\dot{m}_e = \dot{m}_e^* + d_e^v(p'_P - p'_E)$ and $\dot{m}_w = \dot{m}_w^* + d_w^v(p'_W - p'_P)$, where $\dot{m}_e^*$ and $\dot{m}_w^*$ indicate the mass fluxes obtained from the momentum equation assuming a guess pressure field $p^*$. The variable $p'_P$ represents the correction needed to verify the continuity equation. The coefficients $d_e^v$ and $d_w^v$ appear rearranging the discretized momentum equation (see [14] for details). Introducing the above expression of the cell face mass fluxes into equation (2.11), and approximating by their nodal value the mean CV quantities, the correction pressure equation can be written as:

$$\frac{\rho_P - \rho_P^o}{\Delta t} A \Delta z + [\dot{m}_{P^s}^* + d_e^v(p'_P - p'_E)] - [\dot{m}_{W^s}^* + d_w^v(p'_W - p'_P)] = 0 \tag{2.12}$$

This equation can be rewritten in terms of the generic discretized equation $a_P^p p'_P = a_E^p p'_E + a_W^p p'_W + b_P^p$, where the discretized coefficient can be easily obtained from equation (2.12). After pressure correction is obtained, the mass fluxes and pressure field are updated: $\dot{m}_{Ps} = \dot{m}^*_{Ps} + \dot{m}'_{Ps}$ and $p_P = p^*_P + p'_P$.

### 2.2.2 Secondary fluid in the annulus region

The secondary fluid flows in the annulus area, defined between inner tube and outer tube. The mathematical formulation of the governing equations is similar to the one presented for the refrigerant fluid in the inner tube, except that heat transfer and wall friction between the fluid and both the inner tube and outer tube must be considered. In this work, only single-phase flow is considered to occur in the annulus region. The general SIMPLE algorithm described above can be used. However, if no complex flow is expected (e.g. no back flow phenomena), the step by step method can also be used.

The fluid flow inside of the annulus is solved on the basis of a numerical implicit scheme, moving forward step by step in the flow direction. In each control volume, the set of governing equations is iteratively solved to calculate the mass flux, the pressure and the temperature at the outlet section, from the know values at the inlet section of the CV and in the whole CV at the preceding instant.

### 2.2.3 Heat conduction in solid elements

Three different solids are considered, the inner tube, the outer tube and the insulator. Details of the defined main control volumes (CVs) in the different parts of the heat exchanger are depicted in Figure 2.2. To solve the solid elements, the energy equation is applied over each CV. A general heat conduction equation can be integrated, obtaining the following generic form:

$$\rho c_p \frac{(T_P - T_P^o)}{\Delta t} V_P = \dot{Q}_w + \dot{Q}_e + \dot{Q}_n + \dot{Q}_s \tag{2.13}$$

where the left hand side indicates the internal energy increase in the CV, while the right hand represents the inlet net heat flux through the CV-faces (west, east, north, and south). Depending on which solid should be solved, the value of heat fluxes are different. For the inner tube the different heat fluxes through the CV-faces are the consequence of convective heat transfer with the refrigerant fluid and the secondary fluid, together with axial heat conduction through the tube itself. These fluxes can be approximated as:

$$\dot{Q}_w = \lambda_w^t \left( \frac{T_W^t - T_P^t}{d_{PW}} \right) A_{t,in}$$
$$\dot{Q}_e = \lambda_e^t \left( \frac{T_E^t - T_P^t}{d_{PE}} \right) A_{t,in}$$
$$\dot{Q}_s = \alpha^f (T_P^f - T_P^t) \pi D_i \Delta z_P$$
$$\dot{Q}_n = \alpha^{f.sec.o} (T_P^{f.sec} - T_P^t) \pi D_o \Delta z_P$$

where $\alpha^f$ and $\alpha^{f.sec.o}$ are the heat transfer coefficient of the refrigerant and the secondary fluid in the inner tube respectively, $T_P^f$ is the refrigerant fluid temperature and $T_P^{f.sec}$ is the secondary fluid temperature, $d_{PW}$ and $d_{PE}$ are the distance between nodes, and $A_{t,in}$ is the cross-section, $A_{t,in} = \pi(D_o^2 - D_i^2)/4$.

For the outer tube, the secondary fluid is in contact with the tube at south face, while heat conduction is applied on the other CV's faces. Thus, the heat fluxes can be approximated as:

$$\dot{Q}_w = \lambda_w^{t.out} \left( \frac{T_W^{t,out} - T_P^{t,out}}{d_{PW}} \right) A_{t,out}$$
$$\dot{Q}_e = \lambda_e^{t.out} \left( \frac{T_E^{t,out} - T_P^{t,out}}{d_{PE}} \right) A_{t,out}$$
$$\dot{Q}_s = \alpha^{f.sec.e} (T_P^{f.sec} - T_P^{t,out}) \pi D_e \Delta z_P$$
$$\dot{Q}_n = \lambda_n \left( \frac{T_N^{t,ins} - T_P^{t,out}}{\Delta r_n} \right) \pi D'_e \Delta z_P$$

where $T^{t,out}$ and $T^{t,ins}$ indicate the temperatures of the outer tube and insulator respectively. An harmonic mean thermal conductivity is used at the contact surface between the tube and the insulator, $\lambda_n = d_{PN}[d_{Pn}/\lambda_{wall} + d_{nN}/\lambda_{insulator}]^{-1}$. This criterion is obtained as a consequence of the condition of heat flux continuity at the interface, and after approximating temperature gradients by a backward (in the tube) and forward (in the insulator) first-order numerical scheme.

For the insulator, the conduction heat fluxes through any of the internal CV-faces can be approximated as:

$$\dot{Q}_w = \lambda_w^{ins}\left(\frac{T_W^{ins} - T_P^{ins}}{d_{PW}}\right)A_{ins}$$
$$\dot{Q}_e = \lambda_e^{ins}\left(\frac{T_E^{ins} - T_P^{ins}}{d_{PE}}\right)A_{ins}$$
$$\dot{Q}_s = \lambda_s^{ins}\left(\frac{T_S^{ins} - T_P^{ins}}{\Delta r_s}\right)\pi D_s \Delta z$$
$$\dot{Q}_n = \lambda_n^{ins}\left(\frac{T_N^{ins} - T_P^{ins}}{\Delta r_n}\right)\pi D_n \Delta z$$

The boundary conditions in the west and the east extreme nodes of the tubes and insulator can be a fix temperature or a null heat flux. Natural convection with the ambient is considered in the external part of the insulator.

## 2.3 Empirical information

The empirical information used to evaluate the local heat transfer coefficients $\alpha$ and the friction factors $f$ in single-phase and two phases, together with the void fraction $\epsilon_g$ are presented.

The single phase heat transfer coefficient is obtained using Nusselt [16] and Gnieliski [16] correlations, for laminar and turbulent regimes, respectively, while the friction factor is evaluated from Churchill [16] expression.

In case of condensation, the heat transfer coefficient is evaluated with Shah [15] correlation. Even though the Shah's correlation is defined only for annular flow, the expression is used along the flow. The empirical correlation given by Shah is available for gas weight fraction between 0.15 and 0.85. For the rest of the range there is no data available. In this case, two splines functions between single-phase and two-phase heat transfer correlations and vice-versa have been obtained for three-order polynomial equations considering continuity and derivability in the functions. The first one is ranged between 0.0 and 0.15, while the second one is ranged between 0.85 to 1.0. The spline coefficients are function of Re, Pr, duct geometry and fluid thermodynamic properties.

Three sub-zones are presented inside during evaporation when two phase flow appears, these sub-zones are sub-cooled boiling, saturated boiling and dry-out. The heat transfer coefficient during evaporation may be evaluated using different correlations depending on which sub-zone the flow is located.

Different correlations have been tested in the evaporation zone. The heat transfer coefficient in the sub-cooled zone is determined by Forster and Zuber correlation [16]

or by Kandlikar correlation [19]. These correlations are used when the wall temperature at a given location is equal to or greater than the local saturation temperature. The heat transfer for the saturated zone can be evaluated by means of the Shah correlation for evaporation [17], Kandlikar for saturated flow boiling [18], or Kattan et al. evaporation model [23]. The heat transfer coefficient in the dry-out zone can be obtained using Kattan et al. [22] [23] or Groeneveld [20] correlations. The Groeneveld correlation needs to determinate a previous point where the dry-out condition begins. The Kattan et al. [23] correlation estimates and recognizes the dry-out point by means of the evaporation flow pattern maps.

The Kandlikar correlations for sub-cooling boiling [19] and saturated flow boiling [18] do not present any discontinuity if both are used together. In this case, it is only necessary to take into account the transition zone from saturated boiling to dry-out, where Kattan et al. [22][23] or Groeneveld [20] correlations can be used.

The Shah correlation for evaporation [17] is only available in the saturation boiling zone. Therefore, splines functions between single-phase and two-phase phenomena are needed.

A more complete description of the heat transfer boiling phenomena is presented by Kattan et al. [21][22][23], which gives the value of heat transfer coefficient in saturation boiling and post dry-out zones.

The void fraction is calculated from the semi-empirical Premoli's equation [24]. The shear stress in condensation and evaporation is calculated from the Jung and Radermacher [25] or Friedel [26] correlations.

All thermodynamic properties are iteratively evaluated at each local position by means of the REFPROP program [27], as function of the local pressure and enthalpy. For the solid elements, Eckert and Drake [29] values have been implemented.

## 2.4 Numerical Resolution

This section presents the numerical resolution of the whole double-pipe heat exchanger. The global numerical algorithm takes into account, in a coupled manner, the thermal and fluid dynamical behaviour of the different elements of the system: i) the two-phase fluid flow in the inner tube (condensation and evaporation phenomena), ii) the single-phase flow in the annulus area, iii) the heat conduction through the solid elements (the inner tube, the outer tube and the insulator). Subsection 2.4.1 shows the global algorithm and the interactions between fluids and solids. Subsection 2.4.2 presents the initial and boundary conditions required by the numerical method. Finally, subsection 2.4.3 shows the phase change transition criteria used in the solution of single and two-phase flow.

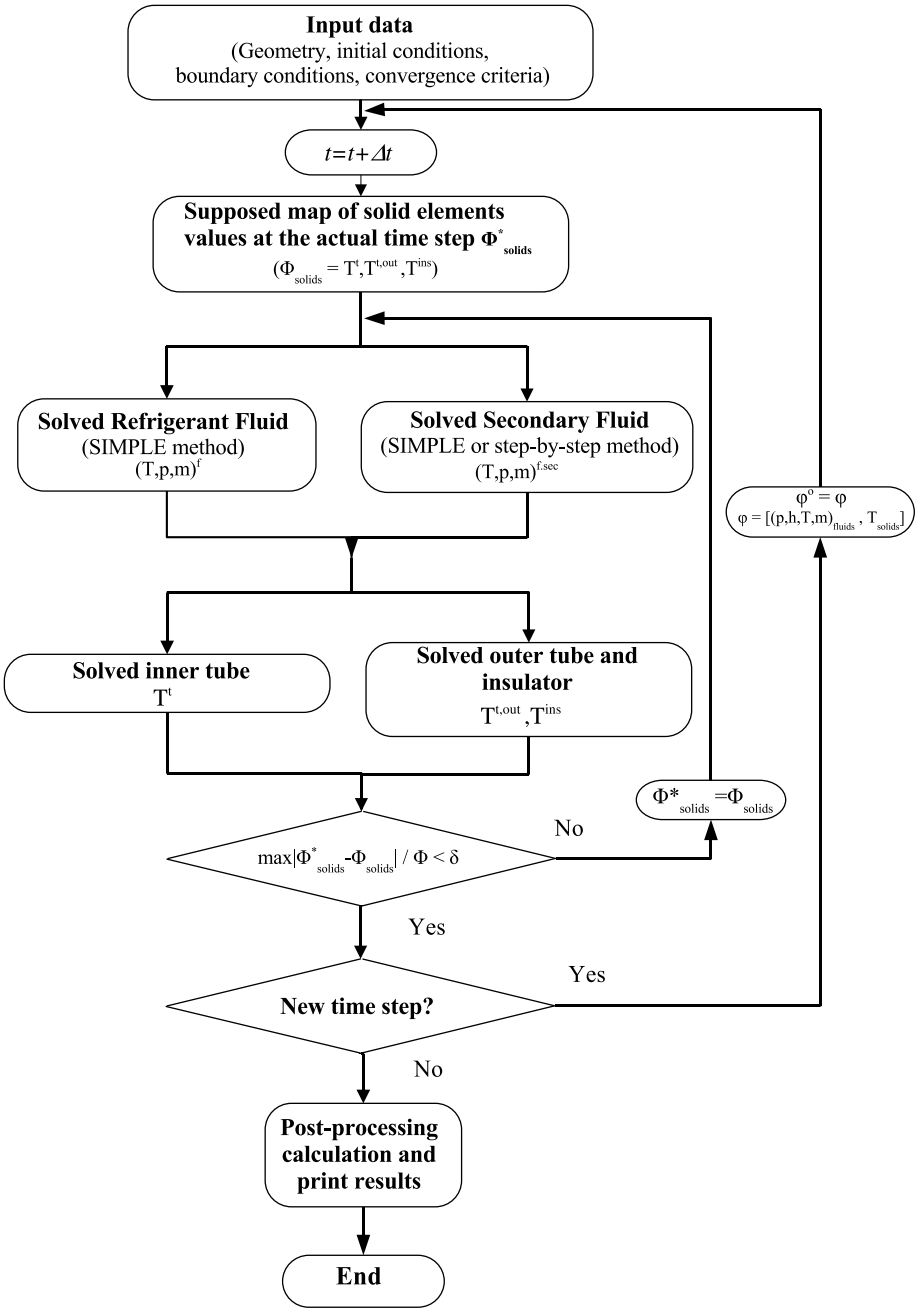


**Figure 2.3:** Global numerical algorithm

### 2.4.1 Numerical algorithm

The whole heat exchanger has been solved by means of a segregated fully implicit numerical scheme following the algorithm presented in Figure 2.3. The refrigerant inner fluid is solved using the general SIMPLE method [14] (see detail in section 2.2.1) to take into account the possibility of complex flow phenomena in the refrigeration system. The secondary fluid can be solved using the SIMPLE method described in this paper. However, the step by step method described in reference [12] or [13] is preferred when no back flow is expected. The temperature in the inner tube and in the outer tube and insulator are calculated using the discretized heat conduction equation (2.13).

The convergence of the different iterative loops is based on the maximum difference between the different local variables at the previous iteration $\phi^*$ and at the actual one $\phi$, i.e. $max|\phi^* - \phi|/\phi < \delta$, where $\delta$ is the convergence criteria. The process runs step-by-step in the time direction until some criteria is satisfied (e.g. steady-state conditions are reached, or just after some physical period of time).

### 2.4.2 Initial and boundary conditions

At the initial instant (t=0), pressure, mass flux and enthalpy distribution of the refrigerant and secondary fluids must be fully specified, together with temperatures in the solid elements.

For the refrigerant fluid in the inner tube, the SIMPLE method [14] solves the coupled governing equations considering the desired steady or unsteady boundary conditions, and allowing back flow phenomena if it is produced. For the secondary fluid, the SIMPLE method or step by step method can be used (no back flow phenomena is considered in this case). Two main boundary conditions can be used: i) the inlet mass flux $\dot{m}_{in}$, the inlet enthalpy $h_{in}$, and the outlet pressure $p_{out}$, or ii) the inlet pressure $p_{in}$, the inlet enthalpy $h_{in}$, and the outlet pressure $p_{out}$. The use of other boundary conditions are also possible.

For the solid elements, adiabatic boundary conditions are imposed at the lateral boundaries (z=0 and z= L). Pressure and temperature ambient conditions must also be given.

### 2.4.3 Phase change criteria for the refrigerant fluid

The transition criteria between the three main zones existing in both condensation and evaporation processes are evaluated depending on fluid enthalpy. These condition are: i) liquid region: the value of the enthalpy $h_P$ over the control volume is lower than the liquid saturation enthalpy $h_{l,sat}$ at local conditions; ii) two-phase region: the enthalpy $h_P$ over the control volume is greater than the local liquid saturation

enthalpy $h_{l,sat}$ but lower than the gas saturation enthalpy $h_{g,sat}$; iii) gas region: the enthalpy $h_P$ over the control volume is greater than the local gas saturation enthalpy $h_{g,sat}$.

The evaporation processes have two sub-zones or subregions: sub-cooled boiling and dry-out. The sub-cooled boiling criteria begins when the fluid enthalpy $h_P$ is lower than the liquid saturation enthalpy $h_{l,sat}$ and the wall temperature $T^t$ is greater than the saturation temperature of fluid $T^f_{sat}$. The dry-out criteria begins when the fluid enthalpy $h_P$ is lower than the gas saturation enthalpy $h_{g,sat}$, but is greater than the liquid saturation enthalpy, and gas weight fraction $x_g$ is greater than gas weight fraction $x_{g,do}$ at dry-out conditions. Using the previous criteria at each control volume is possible to define the proper zone.

## 2.5 Numerical Verification

This section shows the quality of the numerical solutions by means of a critical analysis of the different numerical sources of computational errors: convergence errors and discretization errors.

Two cases of two-phase flow of R134a inside a tube with specified heat flux at the wall are selected. The first one corresponds to a evaporation case inside a tube of 3 $m$ of length and 9.10 $mm$ of inner diameter. The refrigerant is evaporated with a constant heat flux through the tube walls of 10000 $W/m^2$. The pressure, mass flux and flow conditions at the inlet section (z=0) are $4.146{\cdot}10^5 Pa$, 0.0226 $kg/s$ and 230.0 $kJ/kg$, respectively.

The second case corresponds to a condensation process inside a tube with the same geometry as the one indicated above. The refrigerant is condensed with a constant extraction of the heat flux of 49000 $W/m^2$. The pressure, mass flux and flow conditions at the inlet section (z=0) are $1.047{\cdot}10^6 Pa$, 0.0201 $kg/s$ and 445.0 $kJ/kg$, respectively. Results obtained for both cases, evaporation and condensation considering different convergence criteria and number of CVs, are shown in Table 2.1. The values of temperature and enthalpy of the refrigerant fluid at the exit (z=L) are presented in both cases.

Numerical results tend to give an asymptotic solution when the grid is refined enough and when the convergence criteria is sufficiently low. A reference numerical solution is found for 2800 CVs and $10^{-12}$ as convergence criteria.

The influence of the convergence criteria is analysed changing its value from $10^{-6}$ to $10^{-12}$ and using 2800 CVs. Differences between $10^{-6}$ and $10^{-12}$ give a maximum discrepancies of 0.0721% and 2.759% in enthalpy and temperature for the evaporation case. However, when the convergence criteria is $10^{-10}$ the discrepancies between the obtained results and the reference solution are insignificant. The influence of the number of CVs is also evaluated. The condensation case gives higher discrepancies

**Table 2.1:** Numerical study of SIMPLE method

| Convergence criteria | Condensation | | Evaporation | |
|---|---|---|---|---|
| | $h_{out}$ $[kJ/kg]$ | $T_{out}$ $[^oC]$ | $h_{out}$ $[kJ/kg]$ | $T_{out}$ $[^oC]$ |
| $10^{-6}$ | 224.36 | 17.747 | 409.826 | 11.878 |
| $10^{-8}$ | 224.39 | 17.766 | 410.123 | 12.216 |
| $10^{-10}$ | 224.39 | 17.766 | 410.122 | 12.215 |
| $10^{-12}$ | 224.39 | 17.766 | 410.122 | 12.215 |
| Grid Number | Condensation | | Evaporation | |
| | $h_{out}$ $[kJ/kg]$ | $T_{out}$ $[^oC]$ | $h_{out}$ $[kJ/kg]$ | $T_{out}$ $[^oC]$ |
| 20 | 208.57 | 6.243 | 410.102 | 12.192 |
| 50 | 219.10 | 13.952 | 410.111 | 12.203 |
| 100 | 223.77 | 17.321 | 410.116 | 12.208 |
| 200 | 224.22 | 17.645 | 410.115 | 12.208 |
| 400 | 224.33 | 17.728 | 410.121 | 12.214 |
| 800 | 224.37 | 17.755 | 410.121 | 12.210 |
| 1600 | 224.38 | 17.765 | 410.122 | 12.214 |
| 2000 | 224.39 | 17.766 | 410.122 | 12.215 |
| 2800 | 224.39 | 17.766 | 410.122 | 12.215 |

between results obtained with different number of CVs. Eg., for 20, 50, 200 and 800 CVs, the discrepancies in temperature (in comparison with reference solution) has been 64.88%, 21.46%, 0.68% and 0.062%, respectively.

In order to show the influence of the different numerical schemes, Figure 2.4 depicts an illustrative condensation case considering Upwind, Quick and Smart schemes. The condensation occurs inside a tube with 2 $m$ of length and 6.0 $mm$ of inner diameter. The refrigerant R134a is condensed with a constant extraction of the heat flux of 14000 $W/m^2$. The inlet conditions (z=0) correspond to the gas phase at the following pressure, mass flux and enthalpy values: $1.496{\cdot}10^6 Pa$, 0.00338 $kg/s$ and 464.7 $kJ/kg$, respectively. The results are obtained with two different grid numbers, 20 CVs and 2000 CVs, and a convergence criteria of $10^{-12}$. The results obtained with 2000 CVs correspond to the reference grid independent solution.

The numerical comparative results of the fluid temperature at the exit section (z=L) between the three different numerical schemes used in the solution are presented for two different grid numbers. Results obtained for 20 CVs ($40.425^oC$, $40.135^oC$ and $40.135^oC$) in comparison with the reference solution ($39.573^oC$), present errors of 2.15%, 1.42% and 1.42% when Upwind, Quick and Smart schemes are applied, respectively. Difference not only affects the fluid temperature at outlet, but also along all condenser length (see details in Figure 2.4).

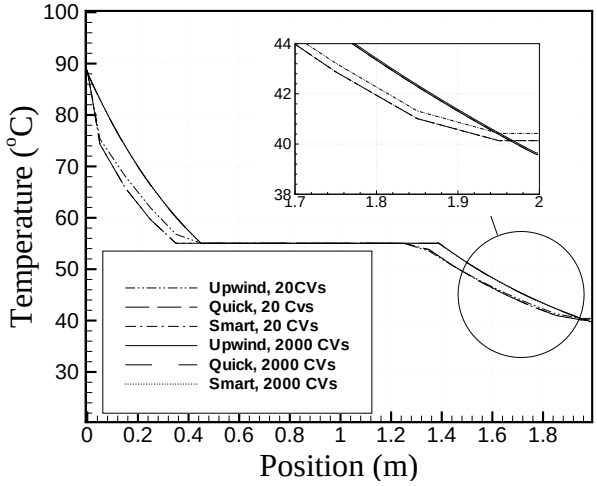


**Figure 2.4:** Comparison of the numerical solution using SIMPLE method depending on the convective scheme for 20 CVs and 2000 CVs.

## 2.6 Conclusions

A numerical model for analysing the condensation and evaporation phenomena inside ducts in double-pipe heat exchangers has been presented. The solution is obtained following a segregated numerical algorithm, where refrigerant inner fluid, secondary outer fluid and solid elements are iteratively solved.

The numerical simulation of two-phase flow is performed using the SIMPLE method with different numerical schemes for the convective terms: Upwind, Quick and Smart. The step by step method is applied to the secondary fluid in the annular region. Empirical information is needed in order to evaluate shear stress, heat flux and two-phase flow structure. The solid elements have been calculated solving the discretized conduction equation.

A numerical verification of the mathematical model is presented. The quality of the numerical solution has been assessed by means of a critical analysis of the different numerical sources of error (mainly convergence error and discretization error). The results clearly show the influence of different numerical parameters: convergence criteria, number of grid nodes, numerical schemes, etc. in order to obtain solutions not dependent of the numerical parameters chosen.

## 2.7 Nomenclature

A cross section area ($m^2$)
CV control volume
$e$ total energy $e = h + e_c + e_p$ ($W$)
$e_c$ kinetic energy ($W$)
$e_p$ potential energy ($W$)
$F_s$ superficial forces ($N$)
$F_m$ body forces ($N$)
f friction factor
h enthalpy ($J\ kg^{-1}$)
g acceleration of gravity ($m\ s^{-2}$)
$\dot{m}$ mass flux ($kg\ s^{-1}$)
m mass ($kg$)
P perimeter ($m$)
p pressure ($Pa$)
$\dot{Q}$ heat flux ($W$)
S surface ($m^2$)
T temperature ($^oC$)
t time ($s$)
V volume ($m^3$)
v velocity ($m\ s^{-1}$)
$x_g$ gas weight flow fraction
z length of tube (m)

**Greek symbols**
$\alpha$ heat transfer ($W\ m^{-2}\ K^{-1}$)
$\delta$ rate of convergency
$\epsilon_g$ void fraction
$\phi$ value of variable
$\rho$ density ($kg\ m^{-3}$)
$\tau$ shear stress
$\theta$ inclination

**Super- and Subscripts**
do dryout condition
i inlet section
g gas or vapour
l liquid
o outlet section
sat saturated condition

# References

[1] S. Kakaç and H. Liu. Heat Exchangers Selection, Rating and thermal Designs, 1998.

[2] S. Levy. *Two-phase flow in complex system*. Willey, 1999.

[3] G. B. Wallis. *One-dimensional two-phase flow*. McGraw-Hill, 1969.

[4] G. Yadigaroglu and R. Lahey. On the various forms of the conservation equations in two-phase flow. *International Journal of Multiphase Flow*, 2(5-6):477–494, 1976.

[5] M. Ishii and T. Hibiki. *Thermo-fluid dynamics of two-phase flows.* Springer, 2006.

[6] A. Zavala-Rio and R. Santiesteban-Cos. Reliable compartmental models for double-pipe heat exchangers: An analytical study. *Applied Mathematical Modelling*, 31:1739–1752, 2007.

[7] M. A. Abdelghani-Idrissi and F. Bagui. Countercurrent double-pipe heat exchanger subjected to flow-rate step change, Part I: New steady-state formulation. *Heat Transfer Engineering*, 23:4–11, 2002.

[8] M. R. Ansari and V. Mortazavi. Transiente response of a co-current heat exchanger to an inlet temperature variation with time using an analytical and numerical solution. *Numerical Heat Transfer, Part A*, 52:71–85, 2007.

[9] T. J. Rennie and G. S. Raghavan. Numerical studies of a double-pipe helical heat exchanger. *Applied Thermal Engineering*, 26:1266–1273, 2006.

[10] C. C. Wang. A numerical method for thermally non-equilibrium condensing flow in a double-pipe condenser. *Applied Thermal Engineering*, 17(7):647–660, 1997.

[11] W. Sripattranpan, T. Wongchang, and S. Wongwises. Heat transfer and two-phase flow characteristics of refrigerants flowing under varied heat flux in a double-pipe evaporator. *Heat and Mass Transfer*, 40:653–664, 2004.

[12] F. Escanes, C. D. Pérez-Segarra, and A. Oliva. Thermal and fluid-dynamic behaviour of double-pipe condensers and evaporators. numerical study. In *Proceedings of the 9th Conference on Numerical Methods in Thermal Problems*, pages 68–79, 1993.

[13] O. García-Valladares, C.D. Pérez-Segarra, and J. Rigola. Numerical simulation of double-pipe condensers and evaporators. *International Journal of Refrigeration*, 27(6):656–670, 2004.

[14] S. V. Patankar. *Numerical Heat Transfer and Fluid Flow*. Hemisphere Publishing Corporation, 1980.

[15] M.M. Shah. A General Correlation for Heat Transfer during Film Condensation inside. *International Journal of Heat and Mass Transfer*, 22:547–556, 1979.

[16] G.F. Hewitt. *Multiphase Fluid Flow and Pressure Drop,Heat Exchanger Design Handbook*. Hemisphere Publishing Corporation, 1983.

[17] M.M. Shah. Chart correlation for saturated boiling heat transfer: equations and further study. *ASHRAE Transactions*, 88(1):185–196, 1982.

[18] S.G. Kandlikar. A general correlation for saturated two-phase flow boiling heat transfer inside horizontal and vertical tubes. *Journal of Heat Transfer - Transactions of Asme*, 112(1):219–228, 1990.

[19] S.G. Kandlikar. Heat Transfer Characteristics in Partial Boiling, Fully Developed Boiling, and Significant Void Flow Regions of Subcooled Flow Boiling. *ASME J. Heat Transfer*, 244:141–150, 1997.

[20] D.C. Groeneveld. Post-Dryout Heat Transfer at Reactor Operating Conditions, 1973.

[21] N. Kattan, J.R. Thome, and D. Favrat. Flow boiling in horizontal tubes: part 1 - development of a diabatic two-phase flow pattern map. *Journal of Heat Transfer - Transactions of Asme*, 120(1):140–146, 1998.

[22] N. Kattan, J.R. Thome, and D. Favrat. Flow boiling in horizontal tubes: part 2 - new heat transfer data for five refrigerants. *Journal of Heat Transfer - Transactions of Asme*, 120(1):148–155, 1998.

[23] N. Kattan, J.R. Thome, and D. Favrat. Flow boiling in horizontal tubes: part 3 - development of a new heat transfer model based on flow pattern. *Journal of Heat Transfer - Transactions of Asme*, 120(1):156–165, 1998.

[24] C.K. Rice. The Effect of Void Fraction Correlation and Heat Flux Assumption on Refrigerant Charge Inventory Predictions. *ASHRAE Transactions*, 93(1):341–367, 1987.

[25] D. Jung and R. Radermacher. Prediction of Evaporation Heat Transfer Coefficient and Pressure Drop of Refrigerant Mixtures. *International Journal of Refrigeration*, 16(5):330–338, 1993.

[26] L. Friedel. Improved Friction Pressure Drop Correlation for Horizontal and Vertical Two-Phase Pipe Flow. European Two-Phase Flow Group Meeting, Ispra, Italy. Paper E2., 1979.

[27] NIST. Thermodynamic properties of refrigerants and refrigerant mixtures database (REFPROP). Version 6.0, 1998.

[28] M.S. Darwish and F. Moukalled. The normalized weighting factor method: a novel technique for accelerating the convergence of high resolution convective schemes. *Numerical Heat Transfer, Part B*, 30:217–237, 1996.

[29] E. R. G. Eckert and R. M. Drake Jr. *Analysis of Heat and Mass Transfer*. McGraw-Hill, 1972.

# Chapter 3

# Validation of Quasi-homogeneous model

**Abstract.**

An experimental comparison has been carried out with the objective to validate the mathematical model developed, previously detailed and numerically verified. The experimental data have been obtained from: i) scientific literature for two different refrigerant fluids, R134a and R22 and ii) a specific CTTC experimental set-up working with an electrically heated pipe with a specific geometry, working with R134a as refrigerant fluid to different conditions of pressure, mass and heat flux. The first experimental comparison is found on both condensation and evaporation phenomena into the pipe, while the second one is an evaporation phenomenon into the electrically heated pipe.

## 3.1 Introduction

An experimental validation of the numerical method proposed to evaluate the two-phase flow into the tubes have been carried out using experimental data obtained from technical literature [1] [2] [3] and a experimental set-up [4].

There are enough technical information about two-phase flow into tubes that allow to find experimental data to contrast the model proposed here. Usually, the heat transfer coefficient is the only value reported, the wall and fluid temperature are not presented. This aspect is because many papers are looking for define an empirical correlation be able to describe the thermal behaviour of fluid flow. Is not common to find a publication that give the wall and fluid temperature distribution, together with the pressure drop.

The experimental data of a particular set-up designed in the CTTC laboratory to research purposes has been used to validate the numerical results of different important variables in the study of the evaporation and condensation phenomena into the tubes, such as temperature, pressure, mass flux, etc.

The objective of this chapter is to show the good agreement between the numerical results, obtained with the numerical model proposed in Chapter 2, and the experimental data, obtained from literature and the CTTC experimental facility. The validation of the numerical simulation has been developed by means of the comparison between numerical and experimental results in condensation and evaporation cases.

Different kind of empirical correlations have been evaluated in both phenomena, evaporation and condensation. Furthermore, a numerical study of the best empirical correlation are reported in this chapter. The numerical results have been obtained considering R134a and R22 fluid refrigerants, while properties have been evaluated by means of the REFPROP properties program [5].

## 3.2 Condensation case from literature research

The numerical simulation of condensation process considers the adapted treatment of the heat transfer coefficient correlations detailed in Chapter 2. Between single gas phase and condensation the first spline function is used, while between the final step of condensation and single liquid phase the second one is applied.

Figure 3.1 depicts the values of the local heat transfer coefficient, the wall and fluid temperatures during condensation processes inside a tube with 2 $m$ of length and 6.0 $mm$ of inner diameter. The refrigerant R134a is condensed with a constant extraction of a heat flux of 14000 $W/m^2$. The pressure, mass flux and flow conditions at the inlet section (z=0) are $1.496{\cdot}10^6 Pa$, 0.00338 $kg/s$ and 464.7 $kJ/kg$, respectively. In this case, the splines are used (adapted correlations) based on the available correlation from the literature. The influence of the heat transfer coefficient adapted

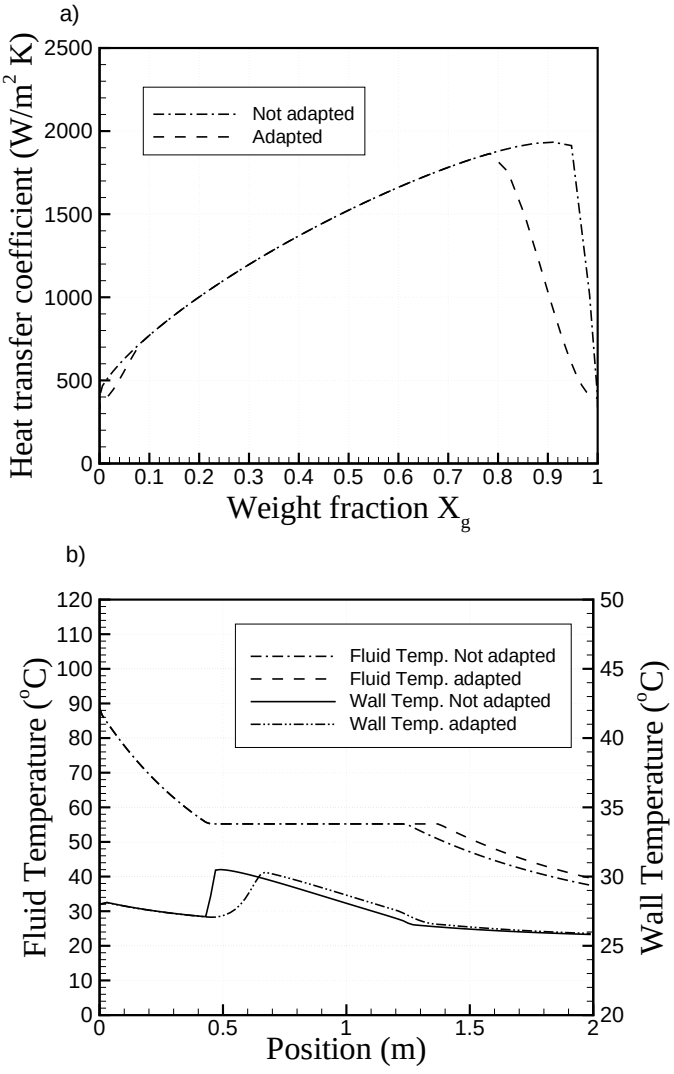


**Figure 3.1:** Heat transfer coefficient and temperatures.

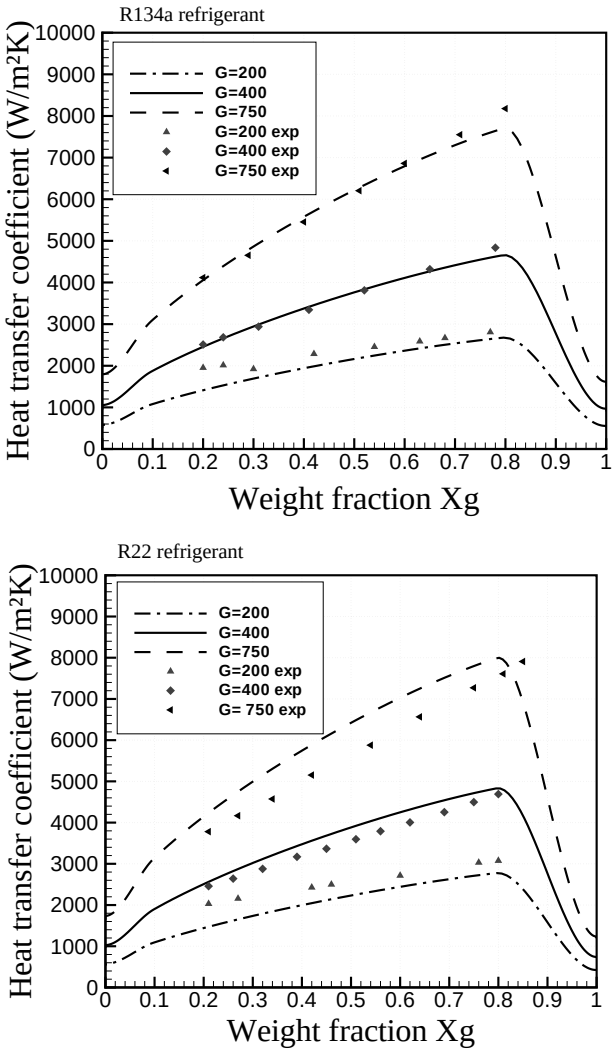


**Figure 3.2:** Numerical and experimiental comparison of the heat transfer coffi-cient.

over the wall temperature is shown in the jump wall temperature from single-phase to two-phase. The fluid temperature obtained with the adapted treatment shows significant differences in comparison with the not adapted one. A comparison between experimental and numerical value of the fluid temperature at the outlet section has been made. Discrepancies of 0.90% and 6.02% for adapted and not adapted treatment respectively have been obtained.

Using the adapted treatment for the empirical correlations, the experimental validation is performed by means of the comparison between the numerical results and the experimental data Cavallini et al. [1], who reported experimental heat transfer coefficients and pressure drop for condensation inside tubes and considering different refrigerants. Specific cases of condensation inside a tube of 8 $mm$ diameter with mass flux of 200, 400 and 750 $kg/m^2s$ for refrigerants R134a and R22 are depicted in Figure 3.2.

In the R134a condensation case, and for mass fluxes between 400 and 750 $kg/m^2s$ the agreement between numerical results and experimental data are quite good. However, for mass flux of 200 $kg/m^2s$, the numerical results under-predict the experimental data at low mass fractions. In the R22 condensation case, the numerical and experimental results present a similar behaviour, although the heat transfer coefficient is slightly over-predicted at high mass fluxes and under-predicted at low mass fluxes.

The numerical results with the adapted treatment of correlations do not produce abrupt alterations in the value of the local heat transfer coefficient or in the value of the wall temperature. The adapted treatment procedure gives stability to the numerical resolution process and does not allow discontinuities during the evaluation of the heat transfer.

## 3.3 Evaporation case from literature research

Two validation cases in the evaporation process are presented, Kattan et al. [2] and Jung and Didion [3] cases.

Kattan et al. report the heat transfer coefficient in their experimental results for evaporation of R134a. The evaporation occurs at 10 $^oC$ of saturated temperature inside a 12 $mm$ diameter tube and a mass flux of 200 $kg/m^2s$. A constant heat flux of 10000 $W/m^2$ is applied to the tube.

The comparison between the numerical simulation and the experimental of heat transfer coefficient is depicted in Figure 3.3. The numerical results display the correct trend in the heat transfer coefficient, even though the transition between the boiling zone and the dry-out zone is difficult to model, due to the sharp decrease of the heat transfer coefficient. However, using the Kattan correlation and employing the differentiation between regions, the post-dryout zone is predicted correctly.

Jung and Didion reported experimental data of the wall temperature, fluid temperature and pressure. The wall temperature reported is located on the top, bottom, right and left of the tube. A tube of 9 $mm$ of diameter is used in this experiment. The refrigerant R22 is evaporated with a constant heat flux of 10060 $W/m^2$ across the tube. The refrigerant has a mass flux of 500 $kg/m^2s$ with an inlet pressure of $4.05{\cdot}10^5$ Pa and an inlet enthalpy of 185 $kJ/kg$.

The numerical results and experimental data are depicted in Figures 3.4 and 3.5. The heat transfer coefficient has different behaviour depending on the correlations used. Figure 3.4a shows the heat transfer coefficient calculated by means of the Kandlikar correlation, and also the Shah correlation (with and without adapted treatment).

For the pressure distribution, the numerical results and the experimental data are shown in Figure 3.4b. The numerical model gives results similar to the experimental data. The measured pressure displays a large decrease at the middle of the tube, attributed to the experimental setup (see [3] for details).

The influence of the adapted and non-adapted heat transfer coefficient on the wall temperature is depicted in Figure 3.5a. The wall temperature is abruptly changed between the sub-cooled boiling and the two-phase zones if the adapted treatment is not employed. When both Kandlikar sub-cooled [6] and saturated [7] correlations are

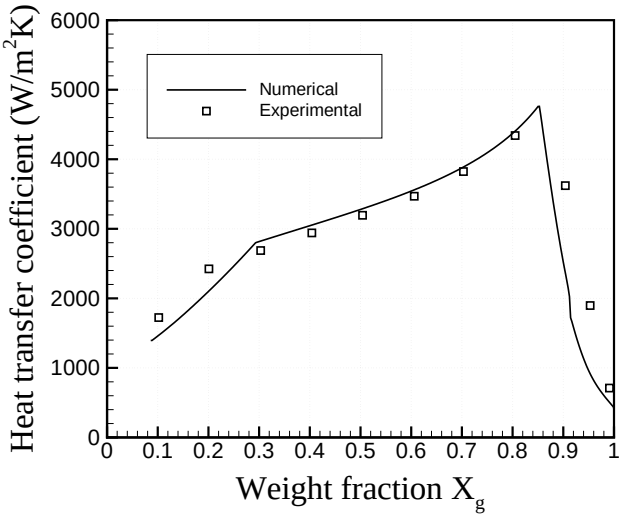


**Figure 3.3:** Numerical and experimental comparison of the heat transfer coefficient.

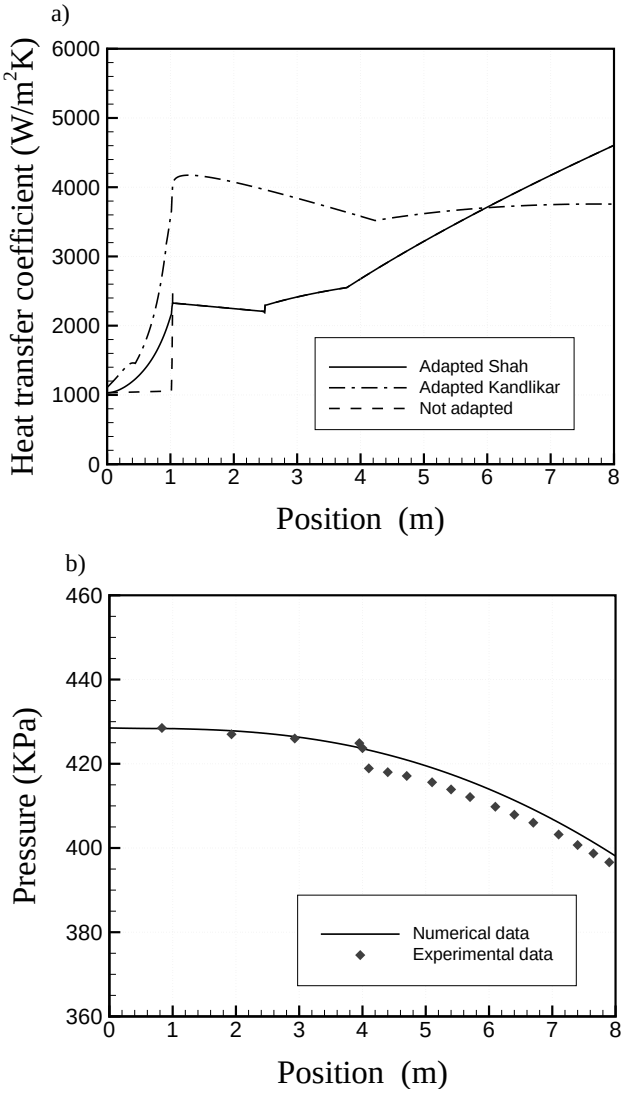


**Figure 3.4:** a)Results of the heat transfer coefficient depending on the empirical correlation used; b)Numerical and experimental pressure comparison.

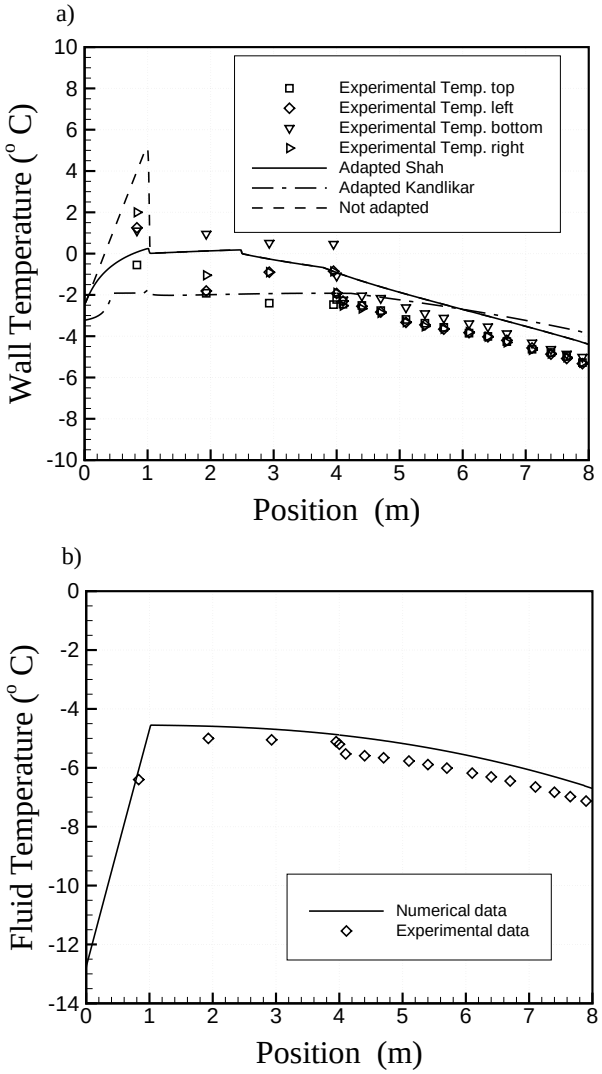


**Figure 3.5:** Numerical and experimental comparison: a)Wall temperature; b)Fluid temperature.

used, the wall temperature does not suffer the abrupt changes indicated above and a more appropriate behaviour of the wall temperature is found. The aim of the Figure 3.5a is to show the influence of the transition zones treatment in the wall temperature. In this specific test case, the adapted Shah correlation gives better results than the adapted Kandlikar correlation. Both correlations predict similar fluid temperature distributions which agrees quite well with the experimental data as shown in Figure 3.5b.

## 3.4 Evaporation case from CTTC set-up experimental data

Another source of experimental available data to validate the numerical simulation model developed has been the results published by Raush et al.[4] and Rigola et al.[8] from a particular CTTC's experimental unit used to study single stage vapour compressor refrigerant system in general and electrically heated evaporator ducts, in particular.

Although the present work has used the experimental data for validation purpose, a detailed description of the electrically heated evaporator is shown in order to understand the experimental data used.

### 3.4.1 Electrically heated evaporator

A detailed instrumented evaporator is the test section, where occur the evaporation process. The test section is a cooper tube of 6.96 m of length and 0.00965 m of external diameter. The fluid temperatures inside tube are measured with calibrated platinum resistance Pt-100 thermometer sensors. This sensors are localized at the inlet and outled sections of each element of the main and secondary circuits. In the evaporator instrument has ten thermocouples for take the refrigerant temperature measured and twenty thermocouples more to measure the external pipe wall temperature. The thermocouples have 0.25 mm of diameter and are localized along of the tube each 0.5 m.

The absolute pressure are measured by two transducers. In the evaporator is used a transducer in range of 0 - 0.6 MPa, with an accuracy within $\pm 0.1\%$ FS. The transducers are localized at the inlet and the outled of tubes, while 5 differential pressure transducers measure the pressure along of the evaporator pipe. Refrigerant mass flow rate inside main circuit is measured with a Coriolis-type mass flow meter with an accuracy of 0.0009 $kg/min$.

A detailed view of the electrically heated evaporator together with a schematic representation of the CTTC experimental set-up is depicted in Figure 3.6.

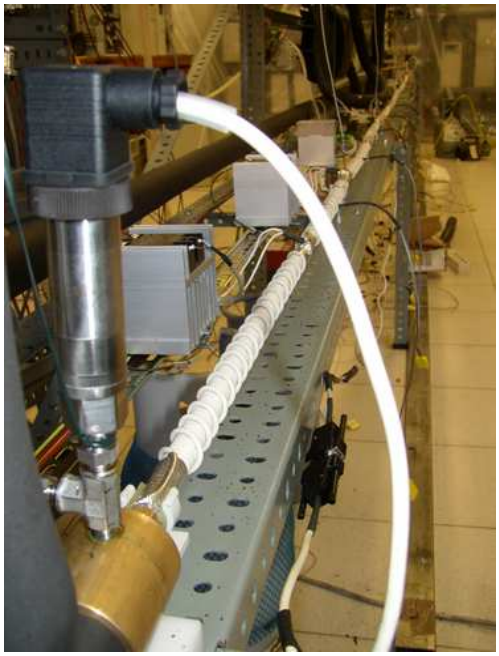

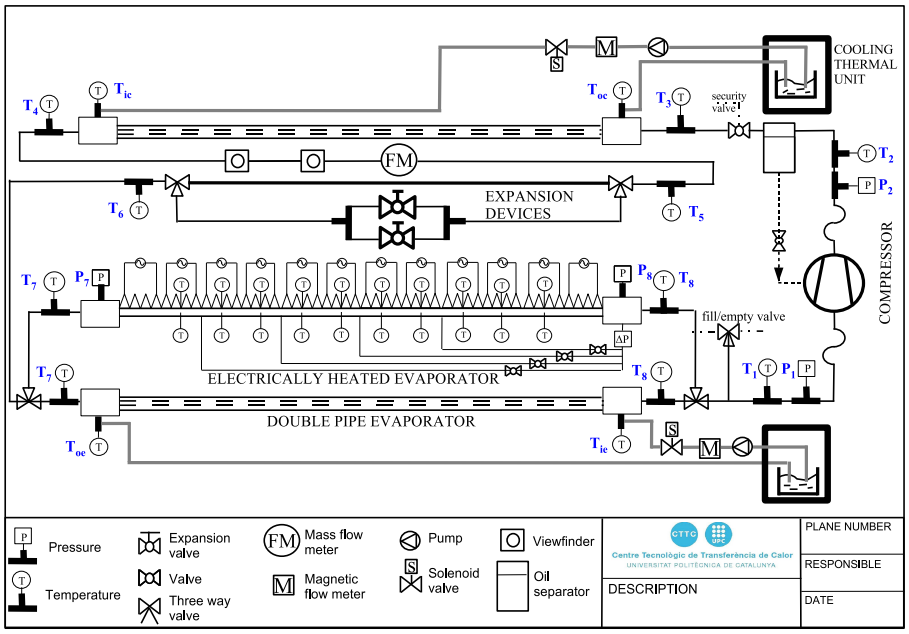


**Figure 3.6:** Detailed view of the electrically heated evaporator and schematic representation of the instrumented unit.

### 3.4.2 Experimental data

The experimental results obtained from the instrumented evaporator detailed above, under steady state conditions of the fluid flow into the evaporator for five different cases are shown in Table 3.1. Representative parameters for each test, such as swept volumes $V_{cyl}$, evaporation temperature of the fluid $T_{ev}$, evaporation pressure $p_{ev}$, mass flux per unit cross section $G$ and the heat power $q_{ev}$ applied through the wall tube are detailed.

**Table 3.1:** Evaporation cases

| Case | $V_{cyl}$ $[cm^3]$ | $T_{ev}$ $[^oC]$ | $p_{ev}$ $[kPa]$ | $G$ $[kg/m^2s]$ | $q_{ev}$ $[W]$ |
|---|---|---|---|---|---|
| 1 | 8.0 | -0.86 | 296 | 64.78 | 3573.30 |
| 2 | 8.0 | -19.73 | 139 | 21.95 | 1143.48 |
| 3 | 8.0 | 7.92 | 396 | 93.54 | 4584.91 |
| 4 | 9.0 | 0.50 | 303 | 62.21 | 3738.30 |
| 5 | 12.0 | -0.68 | 289 | 85.28 | 4409.00 |

According to the compressor swept volumes tested, 8, 9 and 12 $cm^3$, three subgroups of tests have been defined: i) cases 1-2-3, ii) case 4 and iii) case 5, respectively.

**Table 3.2:** Experimental data the electrically heated evaporator with a compressor swept volume of $8cm^3$

| Evap. | case 1 | | | case 2 | | | case 3 | | |
|---|---|---|---|---|---|---|---|---|---|
| length $[m]$ | $T_f$ $[^oC]$ | $T_{w-T}$ $[^oC]$ | $T_{w-B}$ $[^oC]$ | $T_f$ $[^oC]$ | $T_{w-T}$ $[^oC]$ | $T_{w-B}$ $[^oC]$ | $T_f$ $[^oC]$ | $T_{w-T}$ $[^oC]$ | $T_{w-B}$ $[^oC]$ |
| 0.0 | -0.86 | | | -19.72 | | | 7.92 | | |
| 0.75 | -0.44 | 2.61 | 2.18 | -19.22 | -16.24 | -16.44 | 8.05 | 11.01 | 10.42 |
| 1.25 | -0.44 | 3.45 | 3.29 | -19.22 | -16.20 | -16.19 | 8.05 | 11.92 | 11.93 |
| 1.75 | -0.27 | 2.04 | 3.30 | -19.15 | -17.00 | -16.44 | 8.09 | 10.33 | 12.17 |
| 2.25 | -0.16 | 3.81 | 5.15 | -18.90 | -16.02 | -15.49 | 8.15 | 12.57 | 14.31 |
| 2.75 | -0.16 | 2.24 | 6.42 | -18.90 | -16.43 | -14.67 | 8.15 | 10.27 | 15.68 |
| 3.25 | -0.21 | 4.03 | 3.54 | -18.93 | -16.03 | -16.42 | 8.20 | 12.78 | 12.52 |
| 3.75 | 1.04 | 3.77 | 1.96 | -18.72 | -14.55 | -15.57 | 8.23 | 12.14 | 10.20 |
| 4.25 | 1.45 | 4.93 | 4.66 | -8.22 | 9.75 | 9.800 | 9.13 | 13.18 | 13.16 |
| 4.75 | 1.77 | 4.71 | 4.50 | 4.48 | 19.77 | 19.85 | 9.54 | 11.25 | 11.41 |
| 5.25 | 9.04 | 32.99 | 31.10 | 15.44 | 27.08 | 26.53 | 10.60 | 29.43 | 27.072 |
| 6.00 | 29.22 | | | 28.48 | | | 25.42 | | |

Experimental data of the temperatures over the evaporator instrumented are detailed in Table 3.2 for case 1, case 2 and case 3, with a compressor swept volume of $8cm^3$, and Table 3.2 for case 4 and case 5, with a compressor swept volume of $9cm^3$

**Table 3.3:** Experimental data the electrically heated evaporator with a compressor swept volume of $9cm^3$ and $12cm^3$

| Evap. length $[m]$ | case 4 $T_f$ $[^oC]$ | case 4 $T_{w-T}$ $[^oC]$ | case 4 $T_{w-B}$ $[^oC]$ | case 5 $T_f$ $[^oC]$ | case 5 $T_{w-T}$ $[^oC]$ | case 5 $T_{w-B}$ $[^oC]$ |
|---|---|---|---|---|---|---|
| 0.0 | 0.49 | | | -0.68 | | |
| 0.75 | 0.68 | 3.21 | 2.77 | -0.51 | 2.25 | 1.99 |
| 1.25 | 0.68 | 4.19 | 4.58 | -0.51 | 3.21 | 4.08 |
| 1.75 | 0.60 | 2.72 | 4.33 | -0.67 | 1.60 | 3.35 |
| 2.25 | 0.69 | 4.72 | 5.96 | -0.59 | 3.42 | 5.12 |
| 2.75 | 0.70 | 2.86 | 7.20 | -0.59 | 1.31 | 6.49 |
| 3.25 | 0.78 | 4.89 | 4.61 | -0.64 | 3.69 | 3.56 |
| 3.75 | 1.58 | 4.64 | 2.73 | -0.55 | 3.17 | 1.32 |
| 4.25 | 2.05 | 5.57 | 5.29 | 0.35 | 4.57 | 4.20 |
| 4.75 | 2.40 | 4.95 | 4.73 | 0.91 | 3.35 | 3.29 |
| 5.25 | 8.62 | 29.25 | 27.52 | 7.56 | 28.57 | 26.58 |
| 6.00 | 25.82 | | | 24.01 | | |

and $12cm^3$, where fluid temperature $T_f$, top wall temperature $T_{w-T}$ and bottom wall temperature $T_{w-B}$ in evaporator to different length are showed.

The pressure distribution along the instrumented evaporator for all case is summarised in Table 3.4. These data helps to contrast the pressure drop of the fluid flow into the tube.

**Table 3.4:** Experimental pressure distribution through the electrically heated evaporator

| Evap. length $[m]$ | case 1 $p[bar]$ | case 2 $p[bar]$ | case 3 $p[bar]$ | case 4 $p[bar]$ | case 5 $p[bar]$ |
|---|---|---|---|---|---|
| 0.0 | 2.965 | 1.387 | 3.958 | 3.026 | 2.889 |
| 2.0 | 2.948 | 1.377 | 3.938 | 3.008 | 2.864 |
| 3.0 | 2.943 | 1.375 | 3.930 | 3.003 | 2.855 |
| 4.0 | 2.937 | 1.373 | 3.921 | 2.996 | 2.845 |
| 5.0 | 2.931 | 1.371 | 3.912 | 2.990 | 2.835 |
| 6.0 | 2.926 | 1.369 | 3.905 | 2.985 | 2.827 |

The experimental results show how the evolution of the fluid temperature is constant until the dry out point, after that the single phase fluid flow quickly increase. The wall temperature evolution has no abrupt changes, and it has the same evolution as the fluid flow temperature. Finally, the fluid pressure evolution is almost linear along all evaporator pipe.

### 3.4.3 Detailed comparison

The experimental data of the case 1 is used to carry out a numerical comparison with the results obtained from model presented in Chapter 2. This case has been chosen as a reference case and a detailed analysis is developed in this section. The numerical results obtained with three different correlations to evaluate the heat transfer coefficient for evaporation phenomenon are numerically compared with experimental data. Furthermore, three different empirical expressions to define the friction factor are also used in this detailed comparison.

The reference test case was obtained to $-0.8^oC$ approximately of evaporation temperature with a compressor swept volume of $8cm^3$ and presented a mass flux per unit cross section of 64.78 $kg/m^2s^1$. Different empirical correlation were used on this case to evaluate the heat transfer coefficient along of the boiling process such as: Kattan et al. correlation [2], Kandlikar correlation [7], Shah correlation [9], Groeneveld correlation [10] and combination of them.

Shah correlation [9] and Kandlikar correlation [7] are defined to work in the saturated boiling zone, when the dry-out appear in the evaporation process these correlations give bad heat transfer coefficient values. Then, a combination with other correlation must be carry out to determinate the heat transfer coefficient in the post-dry-out. Groeneveld correlation [10] is a well known empirical correlation that make an evaluation of the heat transfer coefficient in the dry-out boiling zone and can be used together with the first correlations to covert all boiling process.

On the other hand, Kattan et al. correlation [2] can evaluate the heat transfer coefficient value along saturated boiling and post-dry-out boiling zones. However, this correlation present some limitations, one of them is the mass flux supported, from 100 to 500 $kgm^{-2}s^{-1}$. When this empirical correlation is applied out of this limit an over-prediction of the wall temperature appear in the numerical results.

The wall temperature distribution is shown in Figure 3.7. The influence of use different empirical correlation is presented and the comparison with the experimental data help us to determinate which of them describe with more approximation the real behaviour of the wall temperature.

Although the combination of Shah and Groeneveld correlation give a good behaviour of the wall temperature in the saturated zone, the wall temperature predicted in the post-dry-out zone is higher than experimental data. An abrupt change of the wall temperature is not agree with the experimental data obtained. Similar results have been obtained with Kandlikar and Groeneveld correlation combination. Both of them present the same behaviour in the post-dry-out zone, then an overlap of the numerical wall temperature distribution can be seen.

Kattan et al. correlation gives an upper-estimation of the wall temperature near to the inlet, while a good agreement is described after the middle of the length when the post-dry-out boiling appear. This correlation is able to evaluate a well heat transfer

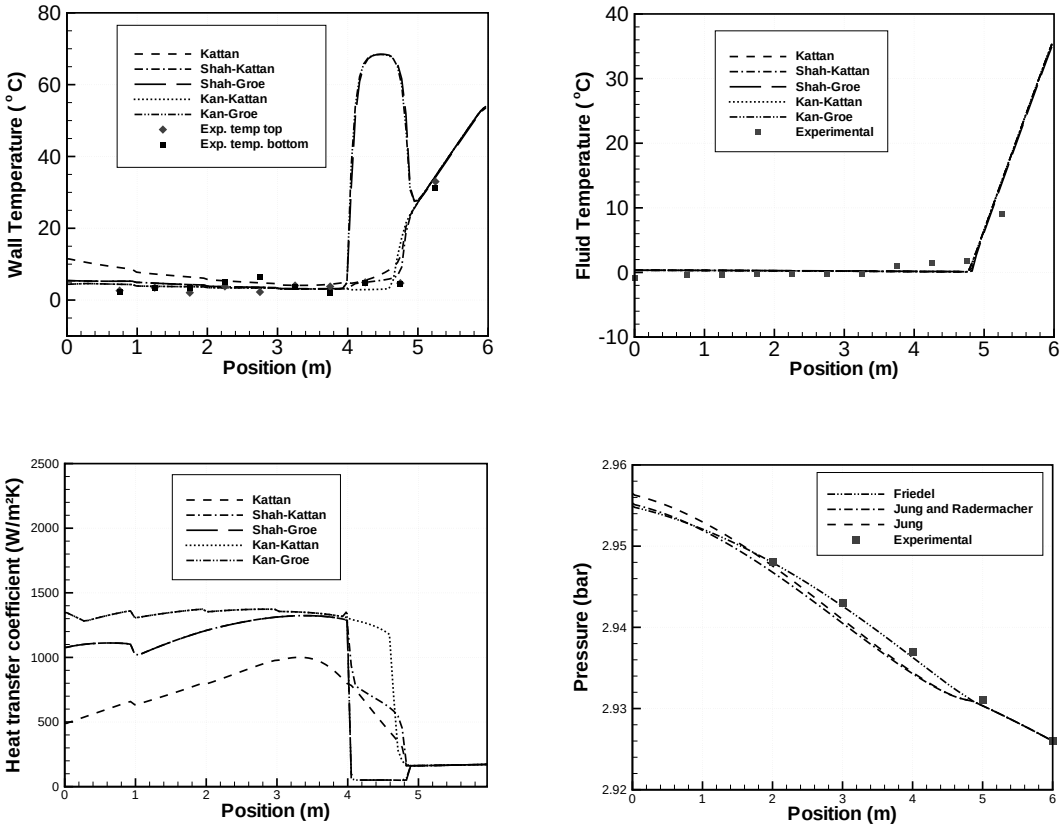


**Figure 3.7:** Reference case 1. Wall and fluid temperature, heat transfer coefficient and pressure drop

coefficient in the post-dry-out zone and give us a wall temperature distribution similar to the experimental data.

The combination of Shah correlation together with Kattan et al. correlation have been used and a good results have been obtained. In the same way, Kandlikar correlation and Kattan et al. correlation have given a good agreement with experimental data.

The Figure 3.7 shows the heat transfer coefficient of the different empirical correlation and the combination of them. An abrupt change of the value of heat transfer coefficient appear in the dry-out zone when Groeneveld correlation is used. While, Kattan et al. correlation assume a smooth change of the heat transfer coefficient between zones. The same effects are presented in the combination with the others correlations.

The fluid temperature is not affected by the heat transfer coefficient obtained from different empirical correlation. This is shown in Figure 3.7, where all of the fluid temperature distribution evaluated have the same values.

The pressure drop along the evaporator has been evaluated by means of three different correlations, Friedel [11], Jung and Radermacher [12] and Jung [13]. The comparison with the experimental data help us to define Friedel correlation as a better empirical correlation. However, all of them give us good results.

Finally, the best evaluation of the heat transfer coefficient can be obtained by means of the combination of Kandlikar and Kattan et al. correlations, and the pressure drop predicted by means of the Friedel correlation is better than the results obtained with others empirical correlation. Then, along of the paper these empirical correlation have been applied in the simulation of the test cases.

The most important difference between the three correlations is in the wall temperature comparison. The Kattan correlation clearly shows the most agreement comparison. The other correlations do not take into account the real transition evolution of the heat transfer coefficient from the two-phase flow and dry-out to a single vapour phase. The experimental data of the wall temperature shows that there are no abrupt changes, and the fluid flow and wall temperature have the same evolution along the evaporator pipe. In conclusion, the Kattan correlation is the heat transfer model that shows the best agreement between the numerical results and experimental data.

After to show the comparison between numerical results and experimental data of the evaporation case chosen as a reference case, a numerical study of the influence of the empirical correlation applied on the heat transfer coefficient is shown.

## 3.5 Influence of the empirical correlation

A group of five experimental cases have been presented in section 3.4, together with the experimental data. Some parameters of the refrigeration system such as the

pressure, the heat flux applied on the wall tube and the compression swept volume have been modified to obtain these cases, Table 3.1 shows details of each case.

These cases has been simulated using the quasi-homogeneous model proposed in this work to analyse the influence of the evaporation temperature and the mass flux in the thermical behaviour of the evaporator.

Three different test cases are presented in Figure 3.8, where different evaporation temperatures are analysed, maintaining the same compressor swept volume 8 $cm^3$. The case 1 is presented as a reference case with an evaporation temperature of $-0.8^oC$ approximately, while case 2 and case 3 with an evaporation temperatures lower and higher than case 1, $-19^oC$ and $8^oC$ approximately, are studied.

The fluid temperature of the test case 1, case 2, and case 3, together with the experimental data from the experimental facility explained about are depicted in Figure 3.8. The numerical results shows a good prediction of the transition between two-phase flow and single phase gas. In general, a good agreement between numerical results and experimental data can be see for the three cases.

The wall temperature of the test case 1, case 2, and case 3, together with the experimental data are shown in Figure 3.8. Using the combination above mentioned, Kandlikar and Kattan et al. correlations, to define the heat transfer coefficient, the numerical results obtained shown a good agreement with the experimental data. The experimental data gives wall temperature at the top and at the bottom of the wall tube, both of them are included in the comparison. Although, the numerical prediction of the wall temperature in case 3 is over-predicted in the last meter of tube, the rest of results along of tube present a well concordance with the experimental data. The case 1 and case 2 resent a quit good agreement with the experimental temperatures.

The pressure drop of the case 1, case 2, and case 3 are presented in Figure 3.8. The comparison between numerical results and experimental data shown as the prediction is quit good at different levels of pressure.

The influence of the compressor swept volume is studied by means of three different cases. Test case 1, case 4 and case 5 present a similar evaporation temperature around $1^oC$, but each of them have worked with different mass flux per unit cross section, 64.78, 68.21 and 85.28 $kgm^{-2}s^{-1}$ respectively.

The evaporation temperature of each case is depicted in figure 3.9, together with the experimental data. The numerical result of case 1 predict the transition between two-phase and single-phase gas occur earlier than case 4 and case 5. This is the reason because a little difference between numerical result and experimental data appear in the fluid temperature of case 1 in the last meter of tube. However, the rest of numerical results along the tube shows a good agreement with the experimental points.

The wall temperature of the case 1, case 4, and case 5 are presented in Figure 3.9,

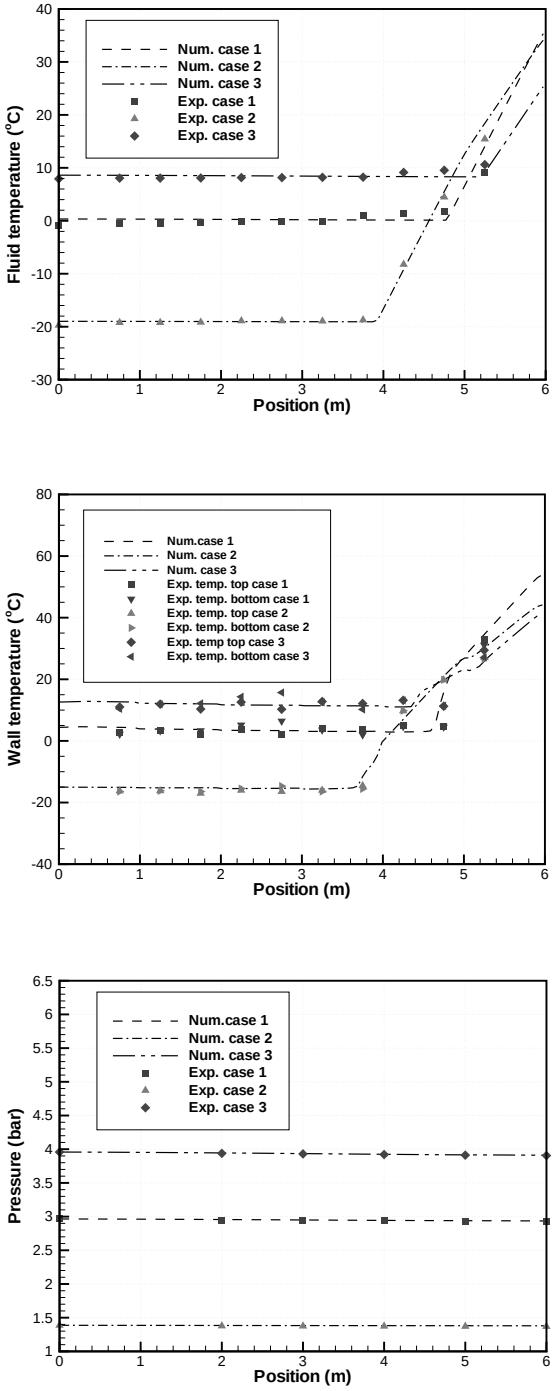


**Figure 3.8:** Comparison between tree different cases with the same compressor at different evaporation temperature

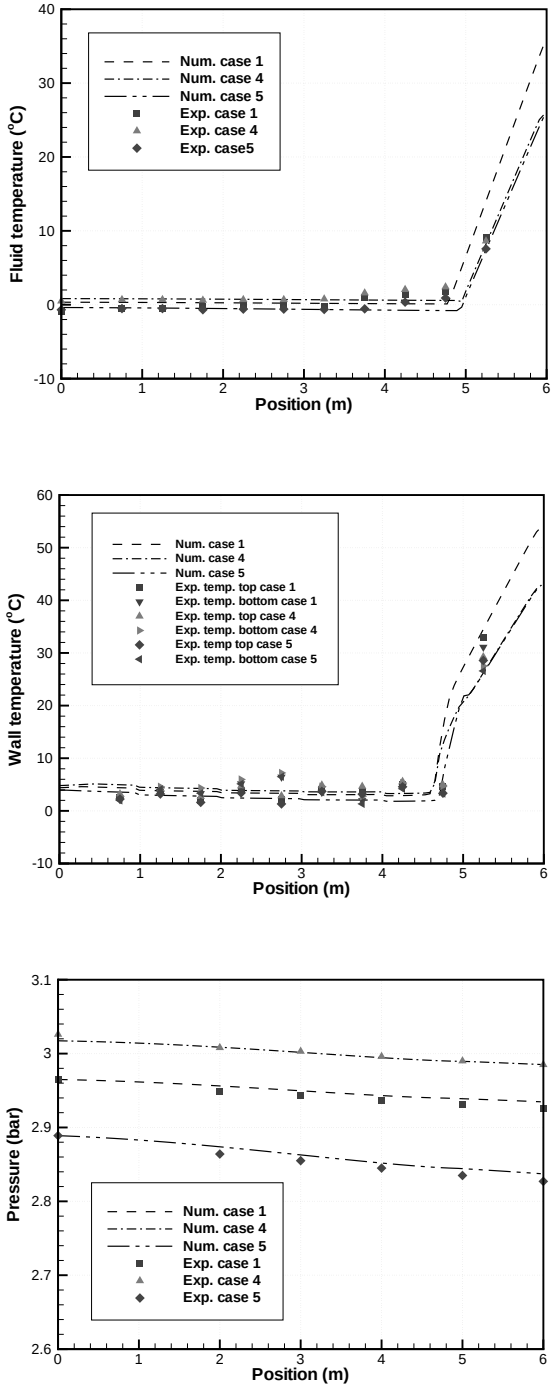


**Figure 3.9:** Comparison between tree different cases with different compressors at the same evaporation temperature

where the experimental wall temperature at the top and at the bottom are considered. The comparison of the numerical results and experimental points in the three cases give an idea that the prediction are not far of the real behaviour of the evaporation phenomena into the tube. The pressure drop of these cases are also shown in Figure 3.9, together with the experimental data. All cases present a good agreement with the experimental points along the tube.

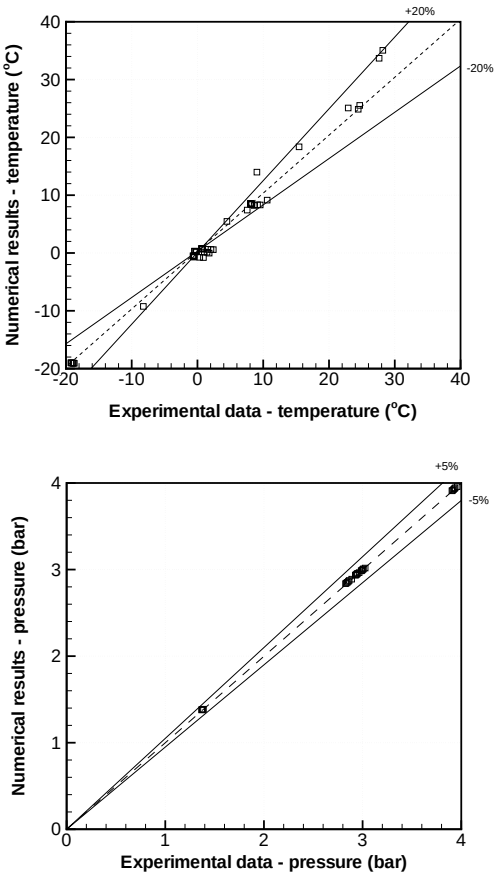


**Figure 3.10:** Numerical results vs. experimental data for the group of cases

The numerical results obtained with the quasi-homogeneous model for the group of cases presented above are contrasted with the experimental data and the error

between both values are summarised in Figure 3.10 for the fluid temperature and the pressure drop along the evaporator. The comparison shows how the numerical results have a good agreement with the experimental data, presenting discrepancies lower than ±20% for the fluid temperature and ±5% for the pressure drop in all cases.

## 3.6 Conclusions

Using a experimental data obtained from technical literature and experimental set-up, a validation of the numerical model proposed in Chapter 2 have been carried out.

An experimental validation is also performed for different condensation and evaporation cases inside tubes. The comparative results between numerical model and experimental data present a reasonable good agreement. This agreement is also improved when the adapted treatment for the heat transfer coefficient correlation in the transition zones is considered. Furthermore, a more realistic behaviour of the wall temperature distribution is obtained by means of these criteria in comparison with non-adapted treatment in both condensation and evaporation phenomena.

The detailed instrumentation in evaporator has allowed to compare the fluid flow and pressure drop distribution, together with the wall pipe temperature evolution along the tube. Comparative results have shown the good agreement in the pressure drop and fluid flow distribution. Altough the most important discrepancies are presented in the wall tube temperature and heat transfer coefficient evolution, the Kattan correlation gives numerical results similar to experimental data. The Kattan correlation, the only one which takes into account the evolution from two-phase to dry-out and single phase, shows a more realistic wall temperature distribution. However, this correlation gives overprediction when the mass flux is lower than 100 $kgm^{-2}s^{-1}$. For this reason a numerical study have been developed to find a combination of empirical correlations that give a more suitable numerical results.

Finally, a good agreement between numerical results and experimental data of the five cases proposed is presented using the fluid temperature and the pressure drop as values to contrast.

## References

[1] A. Cavallini, D. Del Col, L. Doretti, G.A. Longo, and L. Rossetto. Heat transfer and pressure drop during condensation of refrigeration inside horizontal enhanced tubes. *International Journal of Refrigeration*, 23:4–25, 2000.

[2] N. Kattan, J.R. Thome, and D. Favrat. Flow boiling in horizontal tubes: part 3 - development of a new heat transfer model based on flow pattern. *Journal of Heat Transfer - Transactions of Asme*, 120(1):156–165, 1998.

[3] D. S. Jung and A. Didion. Electrical Power Research Institute (EPRI) ER-6364, Research Project 8006-2, 1989.

[4] G. Raush, J. Rigola, S. Morales, C.D. Pérez-Segarra, and A. Oliva. Experimental analysis of two-phase flow in evaporators with special emphasis on single phase - two phase transition zones. In *Proceedings of the 3rd International Symposium on Two-Phase Modelling and Experimentation*, 2004.

[5] NIST. Thermodynamic properties of refrigerants and refrigerant mixtures database (REFPROP). Version 6.0, 1998.

[6] S.G. Kandlikar. Heat Transfer Characteristics in Partial Boiling, Fully Developed Boiling, and Significant Void Flow Regions of Subcooled Flow Boiling. *ASME J. Heat Transfer*, 244:141–150, 1997.

[7] S.G. Kandlikar. A general correlation for saturated two-phase flow boiling heat transfer inside horizontal and vertical tubes. *Journal of Heat Transfer - Transactions of Asme*, 112(1):219–228, 1990.

[8] J. Rigola, S. Morales, G. Raush, and C. D. Pérez-Segarra. Analysis of two-phase flow in double-pipe condensers and evaporators with special emphasis on transition zones: Numerical model and experimental comparison. In *Proceedings of the 2004 International Refrigeration and Air Conditioning Conference at Purdue*, pages 1–10, 2004.

[9] M.M. Shah. Chart correlation for saturated boiling heat transfer: equations and further study. *ASHRAE Transactions*, 88(1):185–196, 1982.

[10] D.C. Groeneveld. Post-Dryout Heat Transfer at Reactor Operating Conditions, 1973.

[11] L. Friedel. Improved Friction Pressure Drop Correlation for Horizontal and Vertical Two-Phase Pipe Flow. European Two-Phase Flow Group Meeting, Ispra, Italy. Paper E2., 1979.

[12] D. Jung and R. Radermacher. Prediction of Pressure Drop During Horitzontal Annular Flow Boiling of Pure and Mixed Refrigerants. *International Journal of Heat and Mass Transfer*, 32(12):2435–2446, 1989.

[13] D. Jung and R. Radermacher. Prediction of Evaporation Heat Transfer Coefficient and Pressure Drop of Refrigerant Mixtures. *International Journal of Refrigeration*, 16(5):330–338, 1993.

# Chapter 4

# Liquid-vapour two-phase flow model applied on thermal systems and equipments

**Abstract.**

The applicability of the numerical simulation method developed in Chapter 2 is shown under different cases where the two-phase flow phenomena occur. Three different cases are studied: i) double-pipe heat exchangers; ii) fin-and-tube heat exchangers; and iii) solar receivers, the numerical illustrative results are presented.

## 4.1 Introduction

The application of the numerical method presented in Chapter 2 can be used in different industrial applications where two-phase flow phenomena is found. The heat exchangers are one of the most common industrial devices where a change of phase in the fluid flow can be found.

The constant search for improving the efficiency and reducing the energy consumption of the thermal devices has had an important role in their design. The heat flux transfered from the working fluid to any other fluid is one of the most important variables to quantify, together with the external power supplied to the device.

Different kind of geometries, initial and boundary conditions have an important influence on the normal operation of the thermal machines as air-conditioning or refrigerant systems. All of these parameters can be studied to find the best design as function of the operation conditions of the system. The influence of each parameter can be studied easily by means of the proposed numerical method, which has been validated by means of experimental data. The simulation of the thermal and fluid dynamic behaviour of the heat exchanger with numerical methods helps to carry out the study of different configurations of the thermal device without the necessity to build a new experimental facility with the new configuration.

In this chapter a group of different applications where two-phase flow is present are studied. Firstly, a double-pipe heat exchanger is shown, different parameters have been changed and the influences of these on the thermal devices as evaporator and condenser are studied. Secondly, a fin-and-tube heat exchanger with two-phase flow in-tube is presented, while out the air flow is in contact with the fins and tubes. Thirdly, a solar receiver where evaporation process occur into the tube and a critical heat flux phenomena can appear due to the application of a high source of heating is studied.

## 4.2 Double-pipe heat exchanger

A double-pipe heat exchanger is used due to it has a relatively simple geometry and several aspects can be studied easily. This kind of heat exchanger has been studied extensively as a starting point to the design of more complex heat exchangers, e.g. shell-and-tube heat exchangers, fin-and-tube heat exchangers, dual heat transfer coils, etc. Evaporation and condensation process have been considered to study the two-phase flow into the inner tube while single-phase flow is present in the annulus. Different parameters have been modified and their influence on the heat exchanger behaviour is shown. The numerical method explained above in Chapter 2 is used to study several aspects as the influence of the mass flow, the configuration of the secondary fluid flow, the thickness of the heat insulation, the heat loss and the transient

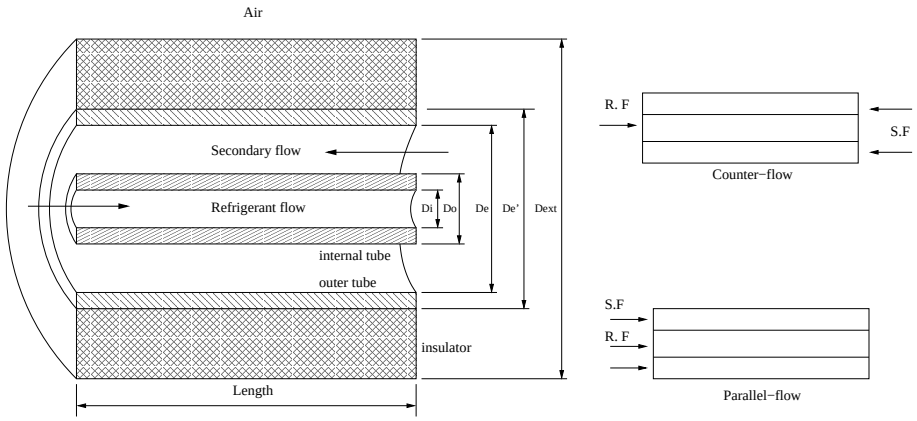


**Figure 4.1:** Representation of the double-pipe heat exchanger and configurations

behaviour of the fluid flow.

An scheme of the double-pipe heat exchanger is shown in Figure 4.1. Assuming natural convection between the air and the heat insulation on the external boundary condition, conduction into and between solid elements (tubes and insulator), adiabatic condition on the edges of the solid elements and forced convection between fluid flows and tubes wall, the double-pipe heat exchanger is solved for evaporation and condensation processes.

The double-pipe heat exchanger considered in this section consists of two concentric tubes of copper and a fiberglass insulator. The thermal conductivity value of the solid elements have been taken from literature [1]. The geometry and boundary conditions are specified in each case.

### 4.2.1 Secondary flow configuration

A first illustrative results are presented with the aim to show the local behaviour of the fluids and wall tubes temperatures, and to present the secondary flow influence on the whole system.

Two different configuration of the secondary fluid flow have been considered in the evaporation and the condensation processes into the inner tube. A counter-flow and a parallel-flow configuration between the refrigerant and the secondary fluid flows have been carried out. The numerical results of temperatures and heat flux of each case are shown.

## Evaporator

A double-pipe evaporator is analysed, the geometry description of the heat exchanger is summarised in Table 4.1 and the inlet conditions of the refrigerant (R134a), the secondary fluid flows (water) and the external fluid (air) are detailed in Table 4.2.

**Table 4.1:** Geometry description of the evaporator

| $Length$ | $D_i$ | $D_o$ | $D_e$ | $D_{e'}$ | $D_{ext}$ | $Angle$ |
|---|---|---|---|---|---|---|
| $[m]$ | $[m]$ | $[m]$ | $[m]$ | $[m]$ | $[m]$ | |
| 6.0 | 0.00815 | 0.00965 | 0.018 | 0.020 | 0.060 | 0.0 |

**Table 4.2:** Inlet conditions on the evaporator

| refrigerant (R134a) | | | secondary flow (water) | | | air | |
|---|---|---|---|---|---|---|---|
| $pressure$ | $weight\ fraction$ | $mass\ flux$ | $pressure$ | $mass\ flow$ | $temperature$ | $pressure$ | $temperature$ |
| $[bar]$ | [%] | $[kg/sm^2]$ | $[bar]$ | $[kg/sm^2]$ | $[^oC]$ | $[bar]$ | $[^oC]$ |
| 3.852 | 0.16 | 100 | 1.081 | 183 | 25.8 | 1.01 | 30.0 |

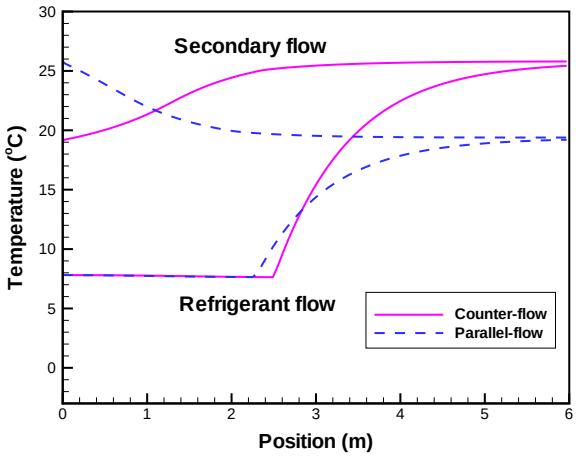


**Figure 4.2:** Temperature distribution in a double-pipe evaporator.

The temperature distribution of the refrigerant and secondary fluid flow are shown

in the Figure 4.2, the difference between both kind of configurations and their influence on the refrigerant flow can be seen in it.

**Table 4.3:** Numerical results of the evaporator in function of configuration

| Configuration | refrigerant (R134a) | | secondary flow (water) | | |
|---|---|---|---|---|---|
| | $T_{in}$ | $T_{out}$ | $T_{in}$ | $T_{out}$ | $Heat$ |
| | $[^oC]$ | $[^oC]$ | $[^oC]$ | $[^oC]$ | $[W]$ |
| counter-flow | 7.81 | 25.41 | 25.80 | 19.14 | 928.62 |
| parallel-flow | 7.81 | 19.20 | 25.80 | 19.38 | 894.33 |

The numerical results of the counter-flow and the parallel-flow are presented in Table 4.3. Temperatures at the inlet and at the outlet of the refrigerant and secondary fluid flow are given, together with the heat flux transfered from the secondary fluid flow to the refrigerant fluid.

As expect, the counter-flow configuration presents a behaviour more efficient than the parallel-flow, this effect can be seen in the comparison of the heat flux and the temperatures of the fluid flows at the outlet. The counter-flow configuration gives a heat flux higher than parallel-flow, due to the temperature of the secondary fluid at the outlet is smaller than the temperature at the outlet in the parallel-flow configuration.

## Condenser

The same analysis has been carried out with a double-pipe condenser. It has a new geometry configuration that is summarised in the Table 4.4.

**Table 4.4:** Geometry description of the condenser

| $Length$ | $D_i$ | $D_o$ | $D_e$ | $D_{e'}$ | $D_{ext}$ | $Angle$ |
|---|---|---|---|---|---|---|
| $[m]$ | $[m]$ | $[m]$ | $[m]$ | $[m]$ | $[m]$ | |
| 2.2 | 0.006 | 0.008 | 0.016 | 0.020 | 0.058 | 0.0 |

The inlet condition of the refrigerant flow (R134a), the secondary flow (water) and the external fluid (air) are detailed in Table 4.5.

**Table 4.5:** Inlet condition of the condenser

| refrigerant (R134a) | | | secondary flow (water) | | | air | |
|---|---|---|---|---|---|---|---|
| $pressure$ | $mass\ flux$ | $temperature$ | $pressure$ | $mass\ flow$ | $temperature$ | $pressure$ | $temperature$ |
| $[bar]$ | $[kg/sm^2]$ | $[^oC]$ | $[bar]$ | $[kg/sm^2]$ | $[^oC]$ | $[bar]$ | $[^oC]$ |
| 14.995 | 100 | 89.6 | 1.581 | 164 | 25.49 | 1.01 | 20 |

The temperature distribution along the double-pipe heat exchanger of the refrigerant and the secondary fluid flow are shown in the Figure 4.3, where the difference between both kind of configurations of the secondary fluid flow can be seen. The temperature distribution of the fluid flows present a different behaviour between both configurations, the refrigerant fluid temperature at the outlet shows a difference approx. of $3^oC$.

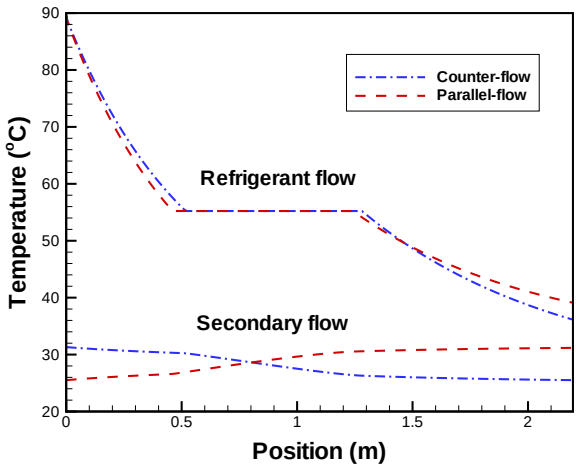


**Figure 4.3:** Temperature distribution in a double-pipe condenser.

The numerical results of the double-pipe condenser are presented in Table 4.6, where temperature of the refrigerant and secondary fluid at the inlet and at the outlet are described, together with the heat flux transfered from the refrigerant fluid to the secondary fluid.

**Table 4.6:** Numerical results of the condenser in function of configuration

| Configuration | refrigerant (R134a) | | secondary flow (water) | | |
|---|---|---|---|---|---|
| | $T_{in}$ $[^oC]$ | $T_{out}$ $[^oC]$ | $T_{in}$ $[^oC]$ | $T_{out}$ $[^oC]$ | $Heat$ $[W]$ |
| counter-flow | 89.63 | 36.25 | 25.49 | 31,32 | 605.13 |
| parallel-flow | 89.63 | 39.19 | 25.49 | 31.19 | 592.37 |

As observed in the heat flux comparison, a similar behaviour of the double-pipe evaporator can be seen in the double-pipe condenser, the counter-flow gives more

efficient results than the parallel-flow.

Analysing the evaporation and condensation process into the double-pipe heat exchanger and the influence of the kind of configuration, is possible to note that the refrigerant flow change of phase before in the parallel-flow than counter-flow configuration. It occurs due to the heat transfered between the fluid flows at the inlet of the double-pipe in parallel-flow is higher than the counter-flow configuration. The difference between temperatures of the fluid flows can be seen in the Figures 4.2 and 4.3.

### 4.2.2 Mass flow influence

Using the geometry configuration of the double-pipe heat exchangers explained in last section, a numerical analysis of the thermal behaviour of the heat exchanger has been done changing the value of the refrigerant mass flow, and after changing the secondary mass flow in evaporation and condensation process.

#### Evaporator

The double-pipe evaporator described in Tables 4.1 and 4.2 has been simulated changing the refrigerant mass flow value and maintaining the rest of the parameters. The influence of the refrigerant mass flow on the refrigerant and secondary fluid flow temperature distribution is shown for counter-flow and parallel-flow configurations in Figure 4.4 and Figure 4.5, respectively. Furthermore, the influence of this parameter on the point where the change phase occurs can be seen in the same Figures.

Four different refrigerant mass flux per cross section have been considered from 80 $kg/sm^2$ to 150 $kg/sm^2$.

**Table 4.7:** Numerical results of the evaporator in function of the refrigerant mass flux per cross section

| | counter-flow | | parallel-flow | |
|---|---|---|---|---|
| *refri. mass flux* | *heat transfered* | *water temperature* | *heat transfered* | *water temperature* |
| $[kg/sm^2]$ | $[W]$ | $[^oC]$ | $[W]$ | $[^oC]$ |
| 80.0 | 743.72 | 20.48 | 720.49 | 20.62 |
| 100.0 | 928.62 | 19.16 | 894.33 | 19.38 |
| 120.0 | 1112.56 | 17.84 | 1065.69 | 18.15 |
| 150.0 | 1384.61 | 15.89 | 1318.51 | 16.33 |

The heat flux and the secondary fluid temperature at the outlet are summarised in the numerical results of the double-pipe evaporator show in Table 4.7. There is an indirect relation between the secondary fluid temperature and the refrigerant mass flow. If the refrigerant flow is increased, the secondary fluid temperature at the outlet

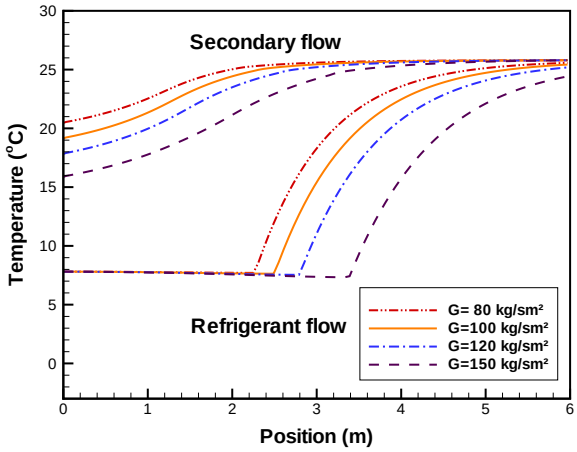


**Figure 4.4:** Temperature distribution in function of the refrigerant mass flux per cross section used in a double-pipe counter-flow evaporator.

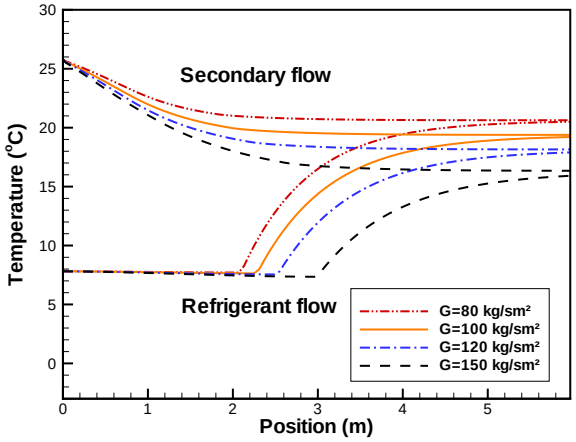


**Figure 4.5:** Temperature distribution in function of the refrigerant mass flux per cross section used in the double-pipe parallel-flow evaporator.

of the double-pipe heat exchanger will be decreased, due to the heat flux transfered between fluids is increased.

**Table 4.8:** Numerical results of the evaporator in function of secondary mass flux per cross section

| *water mass flux* $[kg/sm^2]$ | *volumetricflow* $[l/min]$ | *heat transfered* $[W]$ | *water temperature* $[^oC]$ |
|---|---|---|---|
| 91.0 | 1.0 | 910.50 | 12.76 |
| 137.0 | 1.5 | 926.30 | 16.97 |
| 183.0 | 2.0 | 928.62 | 19.17 |
| 275.0 | 3.0 | 931.06 | 21.39 |

Now, the double-pipe counter-flow evaporator is analysed maintaining the refrigerant mass flux per cross section area in 100 $kg/sm^2$ and changing the secondary mass flow. Four different mass flux per cross section values (91.0, 137.0, 183.0 and 275.0 $kg/m^2s$) correspond with four different volumetric flow values (1.0, 1.5, 2.0 and 3.0 $l/min$) of the secondary fluid flow in the annulus have been carried out.

The secondary mass flux, the volumetric flow, the heat flux and the secondary fluid temperature at the outlet of the double-pipe evaporator are summarised in Table 4.8. Furthermore, illustrative results of the temperatures are depicted in Figure 4.6.

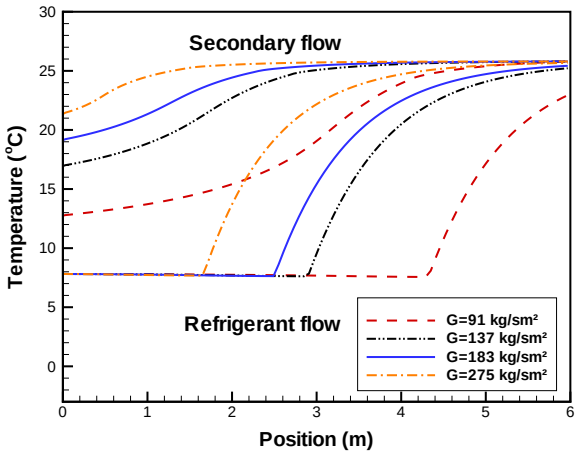


**Figure 4.6:** Temperature distribution in function of the secondary mass flow used in the double-pipe counter-flow evaporator.

The point where the change of phase in the double-pipe evaporator occurs has a direct relation with the secondary mass flow used in the heat exchanger. If the secondary mass flow is reduced, the tube should be extended to allow a complete refrigerant evaporation. Using a secondary volumetric flow of 3.0 $l/min$, 2.0 $m$ of pipe are required to evaporate the refrigerant fluid, while 5.0 $m$ of pipe are required if a secondary volumetric flow of 1.0 $l/min$ has been supplied into the annulus.

### Condenser

Now, the influence of the refrigerant mass flow on the double-pipe condenser is analysed using a counter-flow and a parallel-flow configuration, following the same methodology applied to the double-pipe evaporator. The geometry and inlet conditions described in Tables 4.4 and 4.5 are used in these cases. Following the same criteria of the double-pipe evaporator, the refrigerant mass flow has been changed, while the rest of parameters are maintained. Four different values of refrigerant mass flux per cross section have been used and the numerical results are depicted in Figure 4.7 to counter-flow and Figure 4.8 to parallel-flow.

The refrigerant mass flux, the heat flux and the secondary fluid temperature at the outlet of the double-pipe heat exchanger for the two flow configurations are summarised in Table 4.9.

**Table 4.9:** Numerical Results of the condenser in function of the refrigerant mass flux per cross section

| | counter-flow | | parallel-flow | |
|---|---|---|---|---|
| *refri. mass flux* | *heat transfered* | *water temperature* | *heat transfered* | *water temperature* |
| $[kg/sm^2]$ | $[W]$ | $[^oC]$ | $[W]$ | $[^oC]$ |
| 80.0 | 497.66 | 30.28 | 485.20 | 30.16 |
| 100.0 | 605.43 | 31.32 | 592.37 | 31.19 |
| 120.0 | 716.43 | 32.39 | 700.30 | 32.24 |
| 150.0 | 870.58 | 33.89 | 853.61 | 33.71 |

The refrigerant mass flow has a direct relation with the secondary fluid temperature at the outlet of the double-pipe. If the refrigerant mass flow is increased the secondary fluid temperature will be increased and the same aspect can be seen in the heat flux.

### 4.2.3 The thermal insulation in the double-pipe heat exchanger

The refrigerant and secondary fluid flow have been analysed in last subsections, now the insulator around the double-pipe heat exchanger, together with the heat losses will be analysed. The insulator and the outer tube are defined as a solid element and

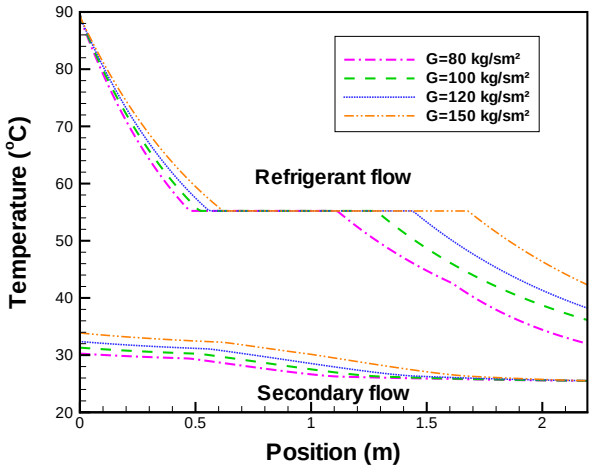


**Figure 4.7:** Temperature distribution in function of the refrigerant mass flux per cross section in the double-pipe counter-flow condenser.

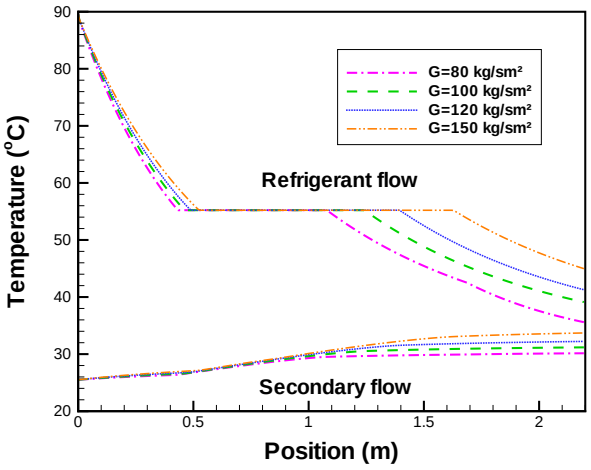


**Figure 4.8:** Temperature distribution in function of the refrigerant mass flux per cross section in the double-pipe parallel-flow condenser.

the solution of these elements is based on the formulation explained in Chapter 2. The double-pipe evaporator and condenser have been considered in this analysis.

## Evaporator

The geometry description and inlet conditions of flows in the double-pipe heat exchanger are presented in Tables 4.1 and 4.2.

An illustrative results of the fluid flows and wall tubes temperature distribution is depicted in Figure 4.9, for a case with an insulator thickness of 0.030 $m$. This Figure shows how the evaporation of the refrigerant fluid takes place in the first 2 meters of length.

Along the first 2 meters of length the internal and external wall temperature distribution suffer an important change in the profile in contrast with the change shown after 3 meters of length. The same behaviour in the insulation temperature occurs in the first part of the length, when the strongest change is noticed.

On the other hand, the internal wall temperature profile present a strong change near to 1.2 meters of length, where the dry-out phenomena occurs and the wall temperature value begin to increase quickly. Is important to notice that adiabatic condition has been imposed at the inlet and at the outlet in the wall tubes and the insulator material as boundary conditions. This is a hypothetic conditions because the solid elements are always connected to other element.

The thickness of the heat insulation is changed to analyse the thermal behaviour of the temperature in the double-pipe heat exchanger, while the other parameters are maintained. The numerical results obtained with different thickness of insulator are summarised in Table 4.10.

**Table 4.10:** Heat fluxes and heat losses of the evaporator

| *thickness* | *refrigerant heat flux* | *water heat flux* | *total heat loss* | *global heat loss* | *heat loss ratio* |
|---|---|---|---|---|---|
| $[m]$ | $[W]$ | $[W]$ | $[W]$ | $[W]$ | [%] |
| 0.005 | 869.33 | 861.61 | 7.72 | 7.30 | 0.89 |
| 0.010 | 869.32 | 863.01 | 6.31 | 6.12 | 0.73 |
| 0.020 | 869.32 | 864.43 | 4.89 | 4.89 | 0.57 |
| 0.030 | 869.32 | 865.07 | 4.25 | 4.24 | 0.49 |
| 0.040 | 869.32 | 865.34 | 3.98 | 3.84 | 0.46 |
| 0.050 | 869.32 | 865.54 | 3.78 | 3.55 | 0.43 |
| 0.060 | 869.32 | 865.76 | 3.56 | 3.33 | 0.41 |
| 0.100 | 869.31 | 866.60 | 2.71 | 2.81 | 0.31 |

The refrigerant heat flux is evaluated as the sum of the heat transfered in each control volume between the fluid and the internal tube. Applying the similar criteria, the water heat flux is obtained from the sum of the heat transfered between it and the internal and external tubes in each control volume. Using the hypothesis of adiabatic

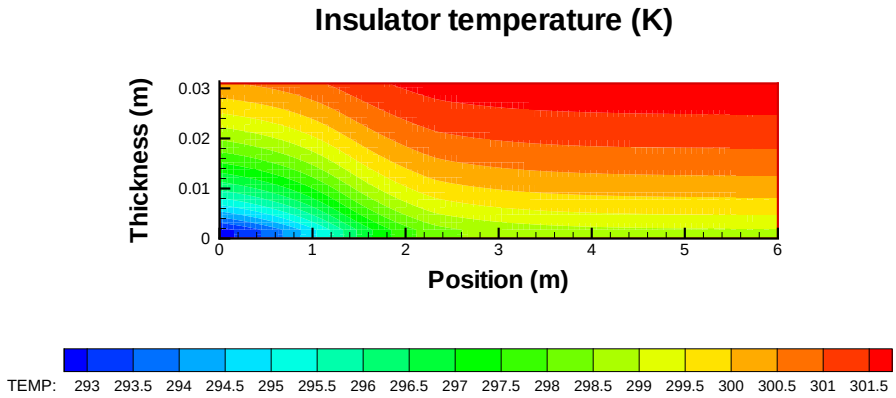


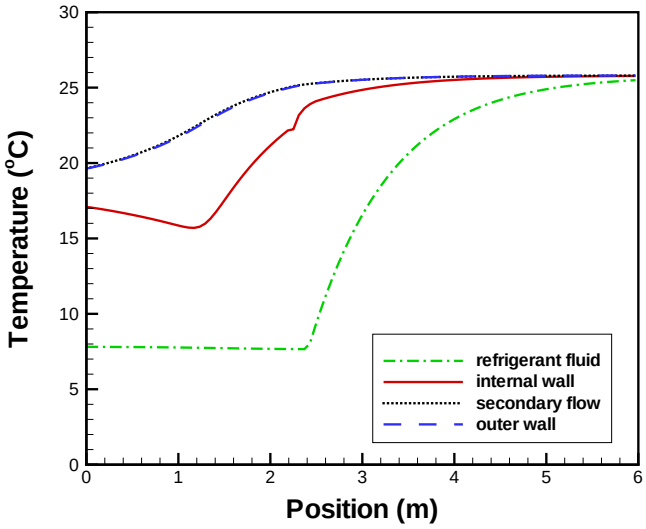


**Figure 4.9:** Temperature distribution of fluids and solids

conditions on the edges of the all solid elements, the total heat loss can be expressed as the difference between the refrigerant and water heat fluxes. On the other hand, a global heat loss through the external tube and the insulator can be evaluated from the difference of the average external wall temperature and the average insulator temperature at the surface divided by a thermal resistance. This value is compared with the total heat loss. Finally, the heat loss ratio is evaluated as the relation between the heat loss and the heat flux of the water. The number of mesh in the insulator has been chosen to maintain the same value of the radial increment $\triangle$r=0.00005, and 100 CV has been used along the axial direction.

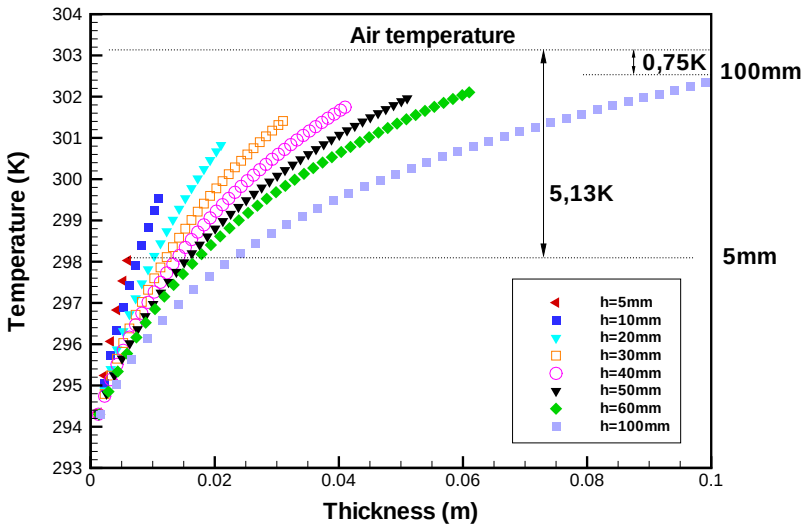


**Figure 4.10:** Temperature vs. thickness in the insulator.

The temperature distribution into the insulator is depicted in Figure 4.10. This graphic shows the direct relation between the thickness and the insulator temperature. If the thickness value is increased, the temperature on the external face of the insulator will be near to the air temperature, and the heat loss value will be low. This effect has been quantified and summarised in Table 4.10. The relation between the heat loss through the insulator and the economic cost of it, is an important factor to decide which insulation thickness uses in any installation.

The numerical results of the temperature distribution in the heat insulation are depicted in Figure 4.11. Differences on the temperatures distribution in function of

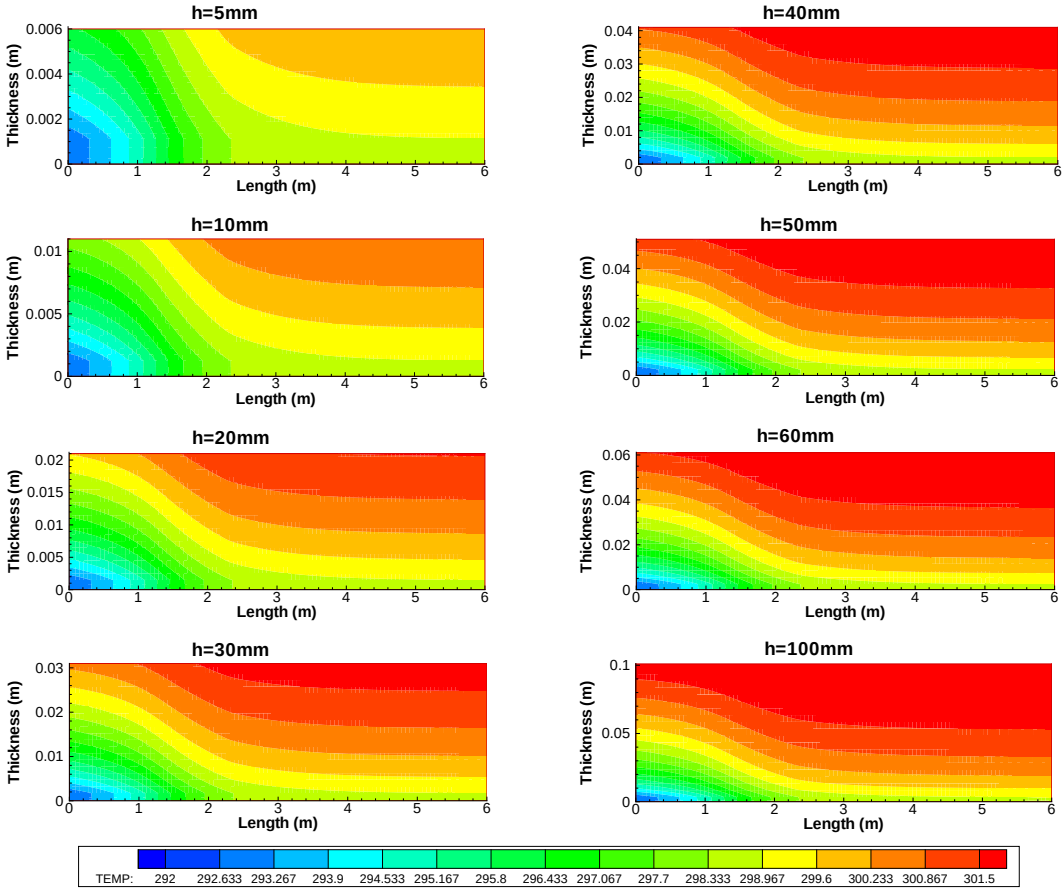


**Figure 4.11:** Illustrative maps of temperature distribution in the heat insulation.

the heat insulation thickness are shown. If a small heat insulation thickness is used, the temperature of the insulator on the external face will be lower than external fluid and it produce higher heat losses through the solid element. Increasing the insulator thickness the difference between insulator and external fluid on the surface is lower and the heat losses decrease.

All illustrative figures show the influence of the evaporation phenomena on the thermal behaviour of the heat insulation. A high heat flux through the fluid flows and solids elements take place in the first part of the double-pipe evaporator when the evaporation occur, while a smooth heat flux should occur when the single-phase flow takes place into the inner tube.

## Condenser

A similar analysis developed with the evaporator has been carried out with the double-pipe condenser. The geometry configuration of the condenser has been described in Table 4.4 and inlet conditions are described in Table 4.11. A different inlet temperature in the secondary flow has been changed in comparison with Table 4.5 to show the thermal behaviour of the insulator when the secondary flow temperature value is higher than the external fluid. The diameter of the heat insulator has been changed to study their influence on the heat flux and the heat loss.

**Table 4.11:** Inlet conditions of the condenser

| refrigerant (R134a) | | | secondary flow (water) | | | air | |
|---|---|---|---|---|---|---|---|
| *pressure* | *mass flux* | *temperature* | *pressure* | *mass flow* | *temperature* | *pressure* | *temperature* |
| $[bar]$ | $[kg/sm^2]$ | $[^oC]$ | $[bar]$ | $[kg/sm^2]$ | $[^oC]$ | $[bar]$ | $[^oC]$ |
| 14.995 | 100 | 89.6 | 1.581 | 164 | 30.0 | 1.01 | 20 |

The numerical results obtained with different thickness of the heat insulation in the double-pipe condenser are summarised in Table 4.12, where the total heat flux of the refrigerant and secondary fluid flow, the total heat loss through the heat insulator, the global heat loss and the heat loss ratio have been quantified.

The fluid flows and the wall tubes temperatures are depicted in Figure 4.12, together with the temperature distribution of the heat insulation of the double-pipe condenser, using an insulator thickness of 0.02 m. The highest value of the insulator temperature is reached when the refrigerant fluid is in single-phase gas and the temperature difference between refrigerant and secondary fluid flow is maximum. The internal wall temperature profile shows abrupt changes near to 0.6 $m$ and near to 1.4 $m$, where the change of phase occur and the evaluation of the heat transfer coefficient value go up considerably. This aspect was commented above in Chapter 3.

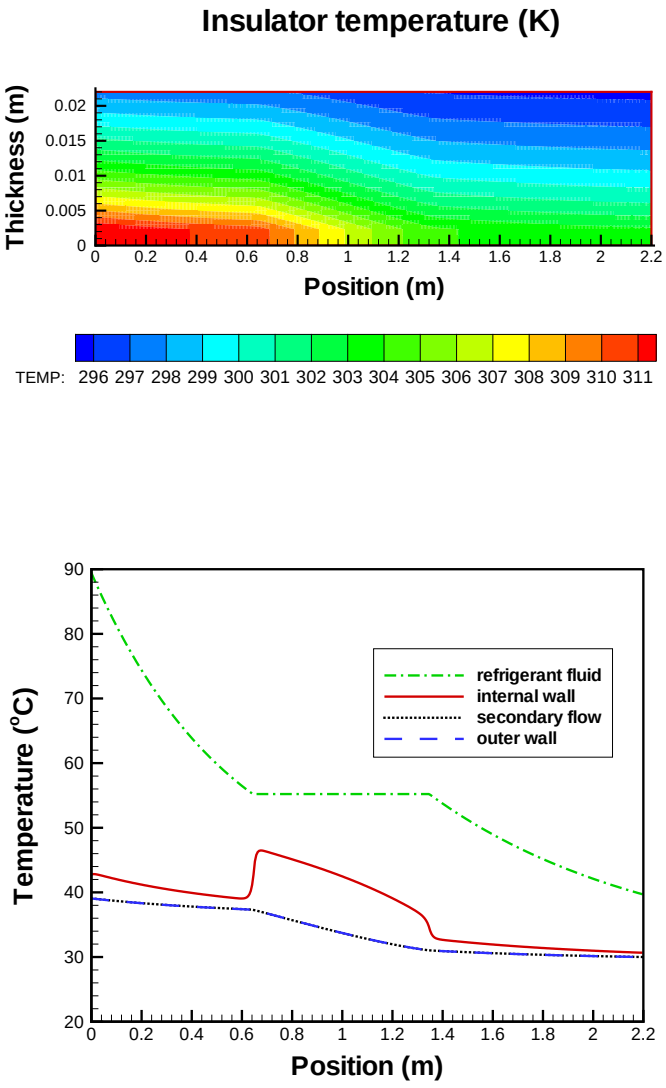


**Figure 4.12:** Temperature distribution in the fluid flows and wall tubes.

**Table 4.12:** Heat fluxes and heat losses of the condenser

| *thickness* | *refrigerant heat flux* | *water heat flux* | *total heat loss* | *global heat loss* | *heat loss ratio* |
|---|---|---|---|---|---|
| $[m]$ | $[W]$ | $[W]$ | $[W]$ | $[W]$ | [%] |
| 0.010 | 567.13 | 561.00 | 6.13 | 5.91 | 1.09 |
| 0.020 | 567.10 | 562.38 | 4.72 | 4.58 | 0.83 |
| 0.030 | 567.08 | 563.04 | 4.04 | 3.93 | 0.71 |
| 0.040 | 567.07 | 563.43 | 3.64 | 3.53 | 0.64 |
| 0.050 | 567.06 | 563.71 | 3.35 | 3.26 | 0.59 |
| 0.060 | 567.06 | 563.92 | 3.14 | 3.06 | 0.55 |
| 0.100 | 567.05 | 564.41 | 2.64 | 2.58 | 0.46 |

The insulator temperature profile at the middle length is depicted in Figure 4.13. This graphic shows the direct relation between the thickness and the insulator temperature. If the thickness value is increased, the temperature on the external face of the insulator will be near to the external fluid temperature. A difference of 5K approximately can be seen between the thickness insulation of 10 mm and 100 mm.

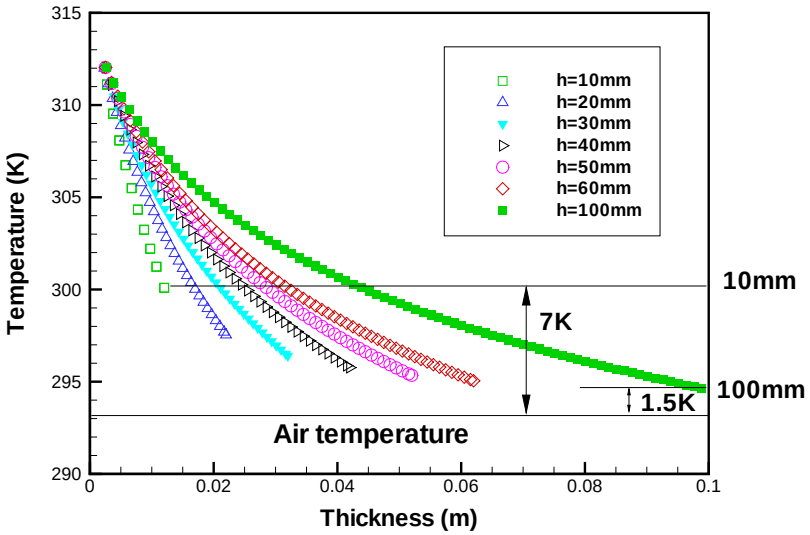


**Figure 4.13:** Temperature vs. thickness in the insulator.

The temperature map distribution in the heat insulation is depicted in Figure 4.14 for different insulator thickness of the double-pipe condenser, the thermal behaviour

of the insulator can be see. A small value of insulator thickness produce a high difference between temperature at the surface of the insulator and the external fluid, so a high heat loss is generated. When a enough thickness is used this heat loss can decrease.

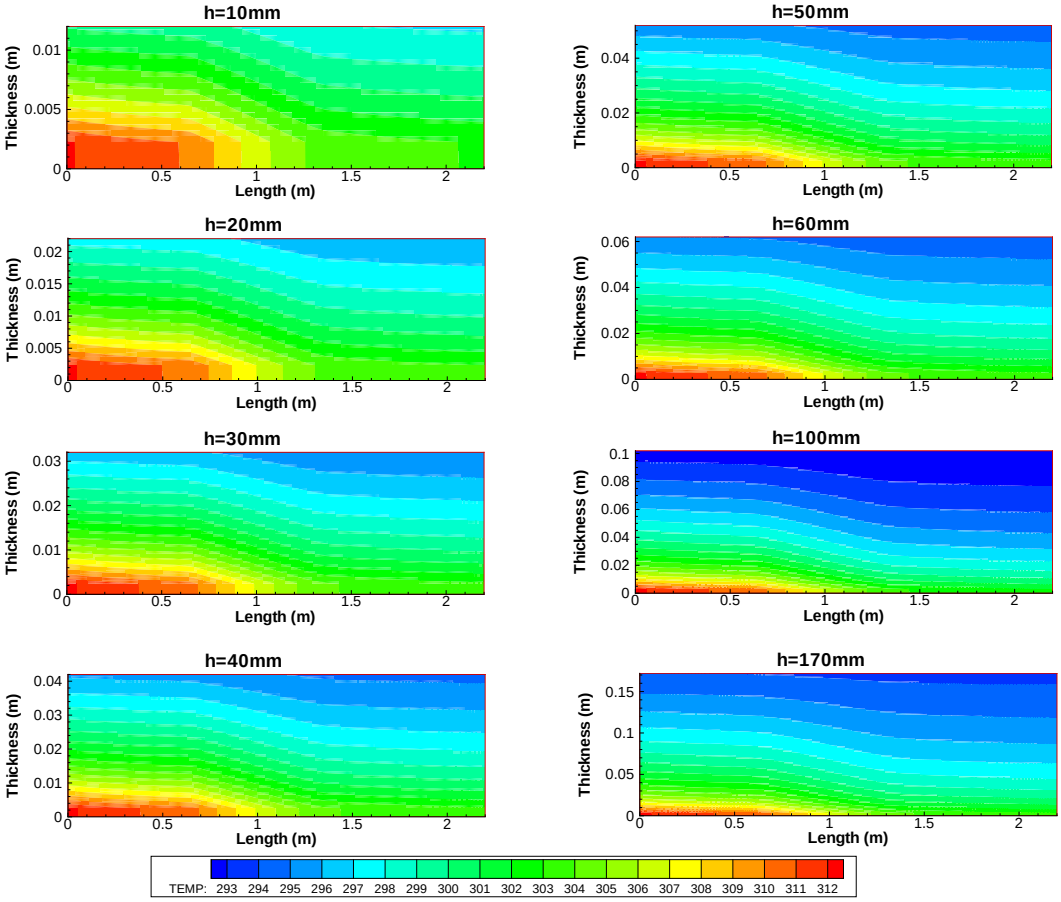


**Figure 4.14:** Illustrative maps of temperature distribution in the heat insulation.

### 4.2.4 The transient analysis of the double-pipe heat exchanger

The double-pipe heat exchanger has been studied in transient conditions. The influence of the transient initial condition of some parameters in the evaporator and the condenser cases are presented in this subsection.

## Evaporator

A double-pipe evaporator in counter-flow configuration has been analysed in transient conditions. The geometry description of the heat exchanger is equal to data of Table 4.1. The inlet conditions are presented in Table 4.13.

**Table 4.13:** Inlet conditions of the transient evaporator

| refrigerant (R134a) | | | secondary flow (water) | | | air | |
|---|---|---|---|---|---|---|---|
| *pressure* | *weight fraction* | *mass flux* | *pressure* | *mass flow* | *temperature* | *pressure* | *temperature* |
| $[bar]$ | [%] | $[kg/sm^2]$ | $[bar]$ | $[kg/sm^2]$ | $[^oC]$ | $[bar]$ | $[^oC]$ |
| 2.5 | 0.1 | 100 | 1.03 | 183 | 20.0 | 1.01 | 25.0 |

Once the solution reaches the steady-state condition a variation of refrigerant pressure at the inlet and the secondary fluid temperature at the inlet is applied to the heat exchanger simultaneously by means of the next expressions, that is function of the time $t$:

$$\begin{aligned} p_{i,refri}(t) &= p_\infty + (p_o - p_\infty)exp(-t/t_o) \\ T_{i,water}(t) &= T_\infty + (T_o - T_\infty)exp(-t/t_o) \end{aligned} \tag{4.1}$$

where $p_\infty = 2.0\ bar$, $p_o = 2.5\ bar$, $T_\infty = 15.0^oC$, $T_o = 20.0^oC$ and $t_o = 2000s$.

The temperature distribution of the fluid flows into the double-pipe evaporator are shown in Figure 4.15. Different temperature profiles are represented in function of the time, from the initial steady-state condition (t=0s) to a large time (t=2000s) when the initial condition on the refrigerant fluid and secondary fluid temperature are unchanged as function on time.

These results show how the variation in the inlet conditions of the refrigerant pressure and secondary fluid flow produce a general change in the thermal behaviour of the double-pipe evaporator. The point where the refrigerant fluid change of phase suffer a small variation of the length in function of time, i.e., the single-phase gas takes place at 0s after 1.18 m, while the same change occur after 1.08 m at 2000s.

The strong change on the evolution of the secondary fluid temperature occur while the refrigerant fluid is in two-phase flow, after this point the secondary fluid temperature is maintained a smooth change along the double-pipe heat exchanger.

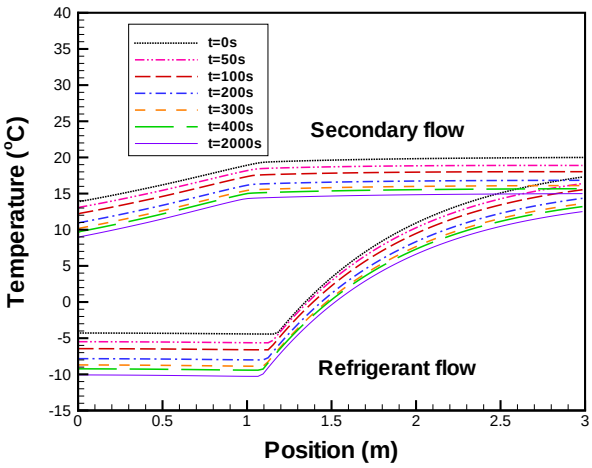


**Figure 4.15:** Temperature distribution in transient evaporator case.

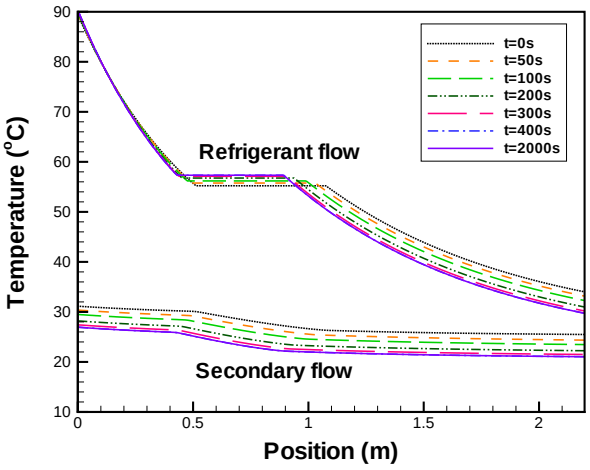


**Figure 4.16:** Temperature distribution in transient condenser case.

### Condenser

A similar analysis has been carried out with a double-pipe condenser. Once the solution of the condenser reaches the steady-state condition, the inlet conditions have been modified in function of the time, then transient solutions of the heat exchange are studied.

The geometry and boundary conditions are the same of the Tables 4.4 and 4.5. In the double-pipe condenser a new initial conditions of pressure and temperature are applied from equation 4.1. The parameter values that define new initial conditions are: $p_\infty = 15.8\ bar$, $p_o = 15.0\ bar$, $T_\infty = 21.0^oC$, $T_o = 25.5^oC$ and $t_o = 2000s$.

The temperature profiles from initial condition (t=0s) to the final conditions (t= 2000s), when the initial conditions of the refrigerant pressure and the secondary flow temperature are unchanged as function on time, are depicted in Figure 4.16.

## 4.3 Fin-and-tube heat exchanger

The heat exchangers used in heating, ventilating, and air conditioning (HVAC) systems are important due to their extended use in commercial, residential and industrial buildings. Most HVAC heat exchangers are designed to exchange energy between a refrigerant and an air stream that is in turn used to condition an indoor space. Typical heat exchangers consist of horizontal refrigerant tubes with attached thin vertical fins to increase heat transfer.

The CTTC laboratory has developed a numerical code (CHESS) capable to solve the fin-and-tube heat exchangers. The principal characteristics of the code are:

1. Discretization of the heat exchanger domain into a set of control volumes.
2. Steady and unsteady analysis.
3. Flexible geometry.
4. Accurate evaluation of the heat conduction in the solids.
5. Internal flow distribution through the headers and coil

A detailed explanation of the CHESS code and the applicability of this numerical model are found in [2] and [3], respectively.

The fin-and-tube heat exchanger is selected due to the evaporation and condensation processes into the inner tubes occur and a numerical study of the two-phase flow is needed to solve this kind of thermal devices. A schematic drawing of the fin-and-tubes heat exchanger is presented in Figure 4.17. The refrigerant fluid flow and the air stream are simulated by means of the mathematical formulation based

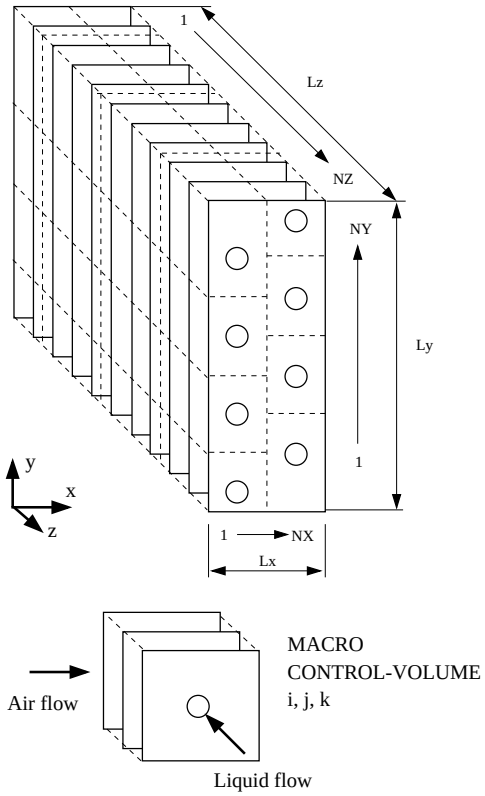


**Figure 4.17:** Schematic representation of the fin-and-tubes heat exchanger.

on the conservation equations of mass, momentum and energy, while the solids are solving by means of the energy equation. All of these equations are expressed as a set of algebraic equations and solved to find a thermo-hydraulic solution of the system.

The mathematical method explained in Chapter 2 is used to study the two-phase flow phenomena present into the inner tubes of the fin-and-tube heat exchanger. This method has been implemented into the CHESS code, which can describe the thermal-dynamics behaviour of the fluid flows, refrigerant and air, together with the thermal evolution of the fin-and-tubes.

The air fluid flow resolution method will not explained here, because the main aim of this thesis is the study of the two-phase flow phenomena into the pipes. However, the influence of the two-phase flow on the air flow in contact with the surface of the tube and the vertical fins is analysed for evaporation and condensation processes.

An important fact is that the numerical method detailed in this thesis to solve the two-phase flow into the pipes has been used and coupled in the numerical model to simulate fin-and-tube heat exchangers CHESS code.

Evaporation and condensation processes will be studied in this section. A short explanation of the geometry and a comparison between numerical and experimental data of two fin-and-tube heat exchanger working as evaporator and condenser will be presented. The main intention with these both cases is to show how the two-phase flow study can help to carry out a coupled thermo-hydraulic study of the complex air-conditioning or refrigeration systems. The mathematical method proposed by Morales, et al. [4] and detailed in this thesis to solve the two-phase flow together with some others can help to find accurate numerical results in comparison with the experimental data.

### 4.3.1 Evaporator

The evaporation process in a fin-and-tube heat exchanger has been simulated and a comparison with experimental data is presented. The numerical results obtained with CHESS code have shown a good agreement with the experimental data, specially in the cooling capacity $\dot{Q}$. The super-heating temperature $T_{sh}$ is reasonably predicted by the numerical model, although a small difference between these values is obtained. A set of numerical results and experimental data comparison has been carried out into the work developed by other CTTC researcher (Oliet [2]), where the predictions are assumed remarkably good considering the wide spectrum of evaporating conditions.

The evaporation case reported in this section has been simulated using the next empirical correlations to evaluate the heat transfer coefficient, the friction factor and the void fraction. The heat transfer coefficient of the two-phase flow has been evaluated from the Shah correlation [5], the Premoli expression from Rice correlation [6] is used to determine the void fraction and the friction factor on two-phase has been obtained from Friedel correlation [7]. On the other hand, the heat transfer coefficient

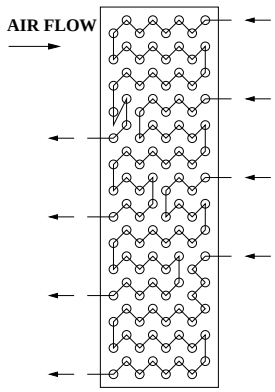


**Figure 4.18:** Schematic representation of the heat exchanger circuit.

| | |
|---|---|
| Tube arrangement | Staggered |
| Rows (depth) | 8 |
| Columns (height) | 14 |
| Circuits | 4 |
| Coil depth X[mm] | 264 |
| Coil height Y[mm] | 533.4 |
| Coil length Z[mm] | 650 |
| $P_l$ [mm] | 33.0 |
| $P_t$ [mm] | 38.1 |
| Fin material | Al |
| $F_p$ [mm] | 4.2 |
| $F_t$ [mm] | 0.19 |
| Enhancement | Wavy |
| Tube material | Cu, Smooth |
| $D_o$ [mm] | 13.20 |
| $T_t$ [mm] | 0.42 |

**Table 4.14:** Geometry of the tested evaporator.

and the friction factor of the air stream has been evaluated from Kim et al. correlation [8].

The geometry of the tested evaporator are detailed in Table 4.14 and a schematic representation of the fin-and-tube heat exchanger circuit is shown in Figure 4.18. A grid size of 30 control volume and an convergence criteria of $1.0e^{-6}$ has been used to solve the seudo-transient resolution process.

The fin conduction effects in this case have been considered negligible due to the difference between the evaporating temperature and the super-heated outlet is low (about $5^oC$), then the heat conduction has been solved by means of the analytical expressions.

The comparison between numerical results and experimental data of the evaporator are detailed in Table 4.15.

**Table 4.15:** Evaporator: numerical and experimental comparison.

| $\dot{m}_r$(R22) | $x_g$ | $T_{ev}$ | $\dot{V}_a$ | $T_a$ | $RH_a$ | $\dot{Q}^{exp}$ | $\dot{Q}^{num}$ | $T_{sh}^{exp}$ | $T_{sh}^{num}$ |
|---|---|---|---|---|---|---|---|---|---|
| $[kg/h]$ | [%] | $[^oC]$ | $[m^3/h]$ | $[^oC]$ | [%] | $[kW]$ | $[kW]$ | $[^oC]$ | $[^oC]$ |
| 130.5 | 19.29 | 0.0 | 2800 | 10.1 | 41 | 6.05 | 6.09 | 5.5 | 6.31 |

The developed model is able to give us detailed information of the refrigerant fluid flow evolution into the fin-and tube heat exchanger as temperature, pressure drop, mass weight and void fraction distribution along the circuits. The numerical results of the two-phase flow into the pipes of the tested evaporator are depicted in Figure 4.19. In this case, the mass weight fraction value of 0.96 was used as criteria to define the point where the liquid vanish of the wall tube and the dry-out phenomena appear.

The heat transferred and the pressure drop are affected in this point, so the small change of the slope in the pressure drop, near to 15 meters of length, can be explained as an influence of the dry-out.

The evaporation temperature decreases as a function of the pressure drop during the evaporation process. Once the refrigerant change from two-phase to super-heated vapour condition the temperature value begins to increase. The point where the refrigerant fluid changes of phase and the refrigerant fluid temperature at the outlet in each circuit follows a similar behaviour, although circuits 1 and 2 give higher temperature at the outlet than circuits 3 and 4. The change of phase along the tubes take place at different length in each circuit due to the mass weight fraction value of 0.96 used as criteria to define the point where the dry-out occurs.

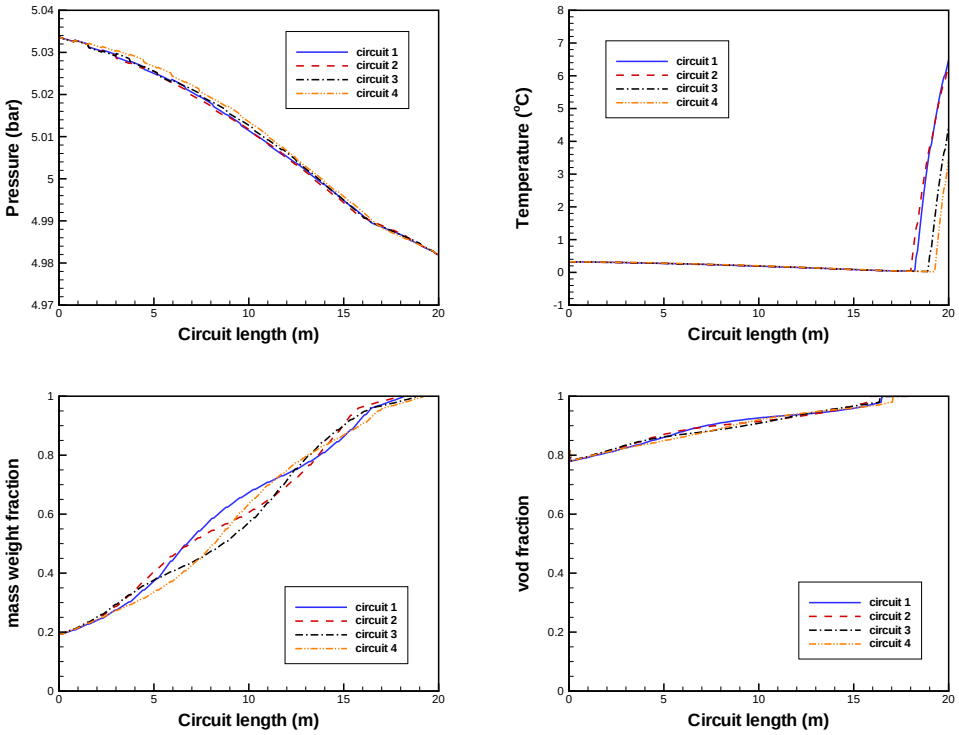


**Figure 4.19:** Refrigerant temperature and pressure distribution, mass weight fraction and void fraction along the fin-and-tube heat exchanger evaporator.

### 4.3.2 Condenser

The fin-and-tube heat exchanger condenser has been simulated with CHESS code and a comparison with experimental data has been carried out in a similar way of the evaporator case. The geometry description of the fin-and-tube heat exchanger is presented in Table 4.16.

| | |
|---|---|
| Tube arrangement | Staggered |
| Rows (depth) | 4 |
| Columns (height) | 24 |
| Circuits | 4 |
| Coil depth X[mm] | 132 |
| Coil height Y[mm] | 914.4 |
| Coil length Z[mm] | 980 |
| $P_l$ [mm] | 33.0 |
| $P_t$ [mm] | 38.1 |
| Fin material | Al |
| $F_p$ [mm] | 2.1 |
| $F_t$ [mm] | 0.12 |
| Enhancement | Wavy |
| Tube material | Cu, Smooth |
| $D_o$ [mm] | 13.20 |
| $T_t$ [mm] | 0.42 |

**Table 4.16:** Geometry of the tested condenser.

The empirical correlations used to evaluate the heat transfer coefficient, the friction factor and the void fraction in the two-phase flow are: Dobson and Chato [9] correlation, Friedel [7] correlation and the expression of Premoli, cited by Rice [6], respectively. The air stream was evaluated by means of the Kim et al. [8] correlation to define the heat transfer coefficient and the friction factor.

The numerical feature as grid size and convergence criteria are equal than the evaporator case, 30 control volume and $1.0e^{-6}$.

The numerical results and experimental data are shown in Table 4.17. The comparison has shown a good agreement with the experimental data. The numerical heat flux transferred $\dot{Q}$ and the sub-cooling temperature $T_{sc}$ of the fin-and-tube heat exchanger condenser present similar values with the experimental data.

| $\dot{m}_r$(R22) | $T_{sh}$ | $T_{cd}$ | $\dot{V}_a$ | $T_a$ | $RH_a$ | $\dot{Q}^{exp}$ | $\dot{Q}^{num}$ | $T_{sc}^{exp}$ | $T_{sc}^{num}$ |
|---|---|---|---|---|---|---|---|---|---|
| $[kg/h]$ | $[^oC]$ | $[^oC]$ | $[m^3/h]$ | $[^oC]$ | [%] | $[kW]$ | $[kW]$ | [°C] | [°C] |
| 489.3 | 61.5 | 39.9 | 7830 | 25.2 | 75 | 25.6 | 25.93 | 36.7 | 35.60 |

**Table 4.17:** Condensers: numerical and experimental comparison.

The temperature distribution and pressure drop of the refrigerant along the circuit length are depicted in Figure 4.20.

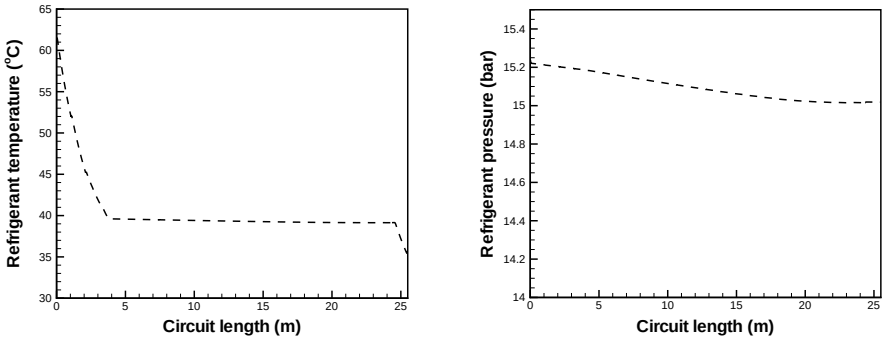


**Figure 4.20:** Refrigerant temperature and pressure distribution in the fin-and-tube heat exchanger condenser.

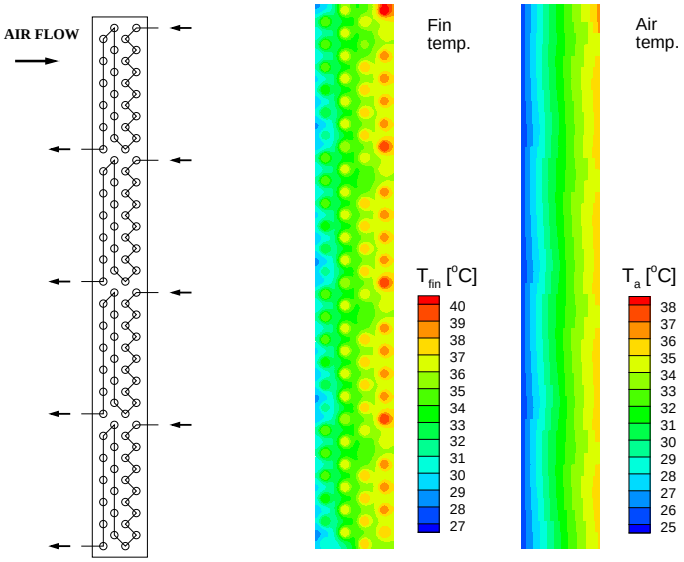


**Figure 4.21:** Schematic representation of the circuits and numerical temperatures results of the fins and the air for the central slice of the condenser.

The refrigerant fluid flow temperature is detailed from super-heating vapour zone to sub-cooling liquid zone, passing through the two-phase zone, together with the pressure behaviour along into the fin-and-tube heat exchanger.

This case present a high temperature difference between the super-heating inlet and the condensation temperature (about 20 $^{o}$C). Then an alternative and more accurate method than the analytical method used in the fin-and-tube heat exchanger evaporator has been used to calculate the heat conduction through the fins. The numerical results of the fin and air temperature in a cross section of the fin-and-tubes heat exchanger condenser is depicted in Figure 4.21, together with a schematic representation of the heat exchanger condenser circuit.

After show the good results obtained with the CTTC's CHESS code, which include the model to solve the two-phase flow explained in this thesis, it is a fact that the applicability of the CTTC code has been extended to the study of the heat exchanger with phase change.

## 4.4 Solar receiver with critical heat flux

The CTTC laboratory has collaborate in the development of a numerical code (TermoFluids) [10] capable to solve numerically the thermo-hydraulic behaviour of the fluid flow and the thermal evolution of the solid elements that make up a solar receiver. A short description of the way to solve the thermal system is enumerated:

1. The heat conduction and the thermal radiation in the solid elements are solved using a specific code to generate the 3D mesh for the solar receiver and a method to calculate the view factors in 3D.

2. The two-phase flow inside the horizontal ducts is evaluated by means the model developed in this thesis and detailed in Chapter 2. The two phase flow has been solved with the quasi-homogeneous model [11] and a special empirical method to predict the possible appearance of the critical heat flux.

3. The convection in the chamber is solved by means of LES simulations model. There are important difficulties with this part because a high value of the Rayleigh number is used, this part is in development.

The models for conduction, two phase flow and thermal radiation are coupled and run on parallel computers. The total and coupled solution of the solar receiver is still in study and some improvements should be implemented. However, this case helps to show the importance of the numerical study of the two-phase flow inside of tubes and the influence in the wall tubes in different applications.

Before to continue with the numerical results of the solar receiver obtained with the model explained in this work to solve the two-phase flow, the critical heat flux

phenomenon is defined, together with an explanation of the empirical correlations applied to obtain the numerical results presented. The method proposed in Chapter 2 is applied to compare the numerical results with numerical results obtained from literature [12] for a direct steam generation solar collector. Furthermore, numerical results of two different solar receivers are shown. The operation conditions of the first case produce that critical heat flux appear in the fluid flow and the consequences on the wall tubes are presented. The second case works on normal conditions and a critical heat flux not appear, working into desirable operation conditions.

### 4.4.1 Critical heat flux

The meaning of the critical heat flux (CHF) is an abrupt rise of wall temperature, due to a slight change in one of the flow variables. This point is clearly of crucial importance because the temperature rise may be of two or three orders of magnitude, which most likely will cause a failure of the heated surface.

The prediction of CHF is complex, since there are many parameters involved and since experiments and frequently ill defined [13]. Since 1982 there are more than 500 methods or correlations available and all attempts to standardize them have failed. The majority deal with water-cooled tubes and have relatively narrow range of validity.

There are different forms to identify the phenomenon - the occurrence of CHF has been denoted as: burnout, dryout, boiling crisis, and departure from nucleate boiling (DNB) [14]. The latter has been mostly reserved for the cases where the bulk fluid is either saturated or subcooled - as distinguished from the case at which a dryout of the wall is caused by dryout of the liquid film.

The prediction of CHF in water pipes has been studied over time and several empirical expressions have been proposed. These correlations try to find the point where the CHF appears, depending on the conditions at the entry of the fluid such as pressure, mass flow, temperature and geometry.

It has been found that the results obtained with correlations based on the conditions at the entrance largely differ with the experimental results. It is suggested to use correlations to evaluate the phenomenon locally. Thus, correlations that consider local data such as pressure, mass flow, quality and geometry were found giving values similar to the experimental results.

The empirical correlations that determine the appearance of the CHF locally are highly dependent on the geometry of the pipe, especially on the diameter. So, it must be taken into account that the correlations are valid within certain geometrical parameters.

Some authors have tried to define an empirical correlation based on experimental studies with refrigerant fluids such as R134a or R113 [15] [16]. Comparison between

vertical and horizontal tubes in the CHF prediction has been carried out by Wong, L., et. al [17].

Another proposal that is shown in the literature are a group of data tables known as CHF Look-up tables [18]. These tables are an extensive database that extend the range of use and improve the results compared with those obtained from the empirical correlations. Doroshchuk proposes the first tables towards 1975. Subsequently improvements and extensions have been proposed by Groeneveld et. al [13] [19].

The effect of axial heat flux distribution on the critical heat flux has been studied and experimental measurements over a vertical tube with R134a refrigerant has been presented with good prediction of the CHF location [20]

In this section the CHF location and their implementation in the quasi-homogeneous model for the evaluation of the two-phase flow inside the pipes is presented. Finally, an illustrative two-phase flow inside the tubes with CHF case is shown.

## CHF Look-up tables

CHF Look-up tables as a method of prediction has been widely accepted and has a number of advantages over empirical correlations. These advantages are: a more precise prediction, a wide range of application, easy to use because it does not requires physical properties, easy modification and finally a parametric, asymptotic and correct trend.

This technique has been widely used in numerical codes in the field of nuclear engineering, such as: CATHARE, CATHENA, RELAP3, ASSERT and THERMOHYDRAULIK which employ AECL-UO look-up tables of Groeneveld [19] to determine the CHF, which is an undesired condition in the applications of nuclear reactors.

The database consists of approximately 30000 CHF data that were obtained in 48 different studies The range of application is defined in function of the diameter, length, pressure, mass flow and weight mass fraction, for details see [13].

The database has been obtained on the basis of vertical water/steam pipes with uniform heat flux and 8mm of diameter. This database can be used for different situations, using correction factors that take into account the effect of change the original conditions.

## Correction factor of diameter and orientation

As noted earlier the values of the Look-up tables have been obtained for tubes with a 8mm diameter, so if we want to use this method of prediction for pipes with different diameter will be necessary to make a correction in the prediction obtained. Different approaches have been suggested for the correction factor of the diameter. The following is the most used equation to compute it:

$$\frac{CHF_D}{CHF_{D=8mm}} = \left(\frac{D}{8}\right)^n \tag{4.2}$$

where D is the diameter of the pipe, $CHF_D$ is the desired value, $CHF_{D=8mm}$ is the value obtained from the database for the specific conditions of pressure, mass flow and quality. There have been proposed different values for the exponent n (-1/2, 1/3, -1/4) depending on the diameter, but it has been found that the best overall results are obtained by taking the value of -1/3.

Different authors claim that by increasing the diameter of the pipe the value of CHF decreases. On the other hand, there is not enough information to ensure what happens with small diameter (2 or 3mm) pipes. Finally it is proposed that the ratio between the value of $CHF_D$ and $CHF_{D=8mm}$ has a value of 0.6 or 0.63 for pipes with diameters greater than 25mm.

A prediction of the CHF value for vertical pipes can be extrapolated to horizontal pipes by means of the correction parameter defined by Pioro, I. et. al [15]. The proposal consists in to assume that the value obtained for vertical pipes, can be applied to horizontal pipes because similar regimen flow appear in both kind of positions. In addition to that, it is imposed that for a stratified flow the CHF is considered to be zero. The relationship between the heat flux in vertical and horizontal pipes can be established from the following equation:

$$CHF_{hor} = K(CHF_{ver}) \tag{4.3}$$

where the value of K depends on the following parameters:

$$K = 1 - exp\left[ - \left(\frac{\gamma}{C_1}\right)^{0.5}\right] \tag{4.4}$$

$$\gamma = C_2 Re^{-0.2}\left(\frac{1 - X_a}{1 - \epsilon_g}\right)^2 \frac{G^2}{gD\rho_l(\rho_l - \rho_g)\epsilon_g^{0.5}}$$

where $C_1$ y $C_2$ are constants and have the values 3 and 0.046 respectively, the Reynolds number is rated as $Re = (GD/\mu_l)(1 - X_a)$, $X_a$ is the quality of the current steam and $\epsilon_g$ is the volumetric fraction of steam.

There are different methods proposed to obtain the value of the CHF in horizontal pipes, some depending on the minimum mass flow that there should be to have an stratified flow. This method defines the value of K depending on the mass flows as follows:

$$\begin{aligned} K = &\quad 0.0 \quad G \leq G_{min} \\ K = &\quad \left[\frac{G - G_{min}}{G_{max} - G}\right] \quad G_{min} < G < G_{max} \\ K = &\quad 1.0 \quad G \geq G_{max} \end{aligned} \tag{4.5}$$

where $G_{min}$ and $G_{max}$ are calculated by Wong [17] as :

$$G_{min} = \frac{(gD\rho_g(\rho_l - \rho_g))^{0.5}}{X}\left(\frac{1}{0.65 + 1.11X_{tt}}\right)^2 \tag{4.6}$$

$$G_{max} = \left[\frac{gD^{1.2}\rho_l(\rho_l - \rho_g)}{0.092(1 - X_{tt})^{1.8}\mu_l^{0.2}}(-0.3470 + 0.2920[ln(X_{tt})] - 0.0556[ln(X_{tt})]^2)\right]^{0.556}$$

The thickness and material of the tube are two parameters to be taken into account in the calculation of the CHF. Thus, variations between 0.5 to 3mm, and/or changes in the thermal conductivity of the material (15 for steel and 400 for copper) can vary the value of the CHF more than 2 times.

### 4.4.2 The CHF in a solar collector

A steam generator absorber tube with 54 mm of internal diameter and 600 m of length has been solved by means of the quasi-homogeneous model. The wall and fluid flow temperature distribution along the tube have been obtained, together with an evaluation of the heat transfer coefficient in single and two-phase flow.

The initial conditions of the fluid flow are: 120 *bar* of pressure, 0.8 $kg/m^2$ of mass flux and fluid temperature of 190 $^oC$. A heat flux of 18000 $W/m^2$ is applied on the external wall, this heat transferred to the fluid flow is able to produce the change of phase of the fluid flow from single phase subcooled liquid to single phase gas. The heat flux around the tube is produced by the concentration of the radiation heat of $1000W/m^2$ on a parabolic reflector.

The results of the wall temperature distribution along the tube presented by Odeh et al. [12] are presented together with the numerical results obtained with the model developed in this thesis. The empirical correlations used to find the heat transfer coefficient are Gungor and Winterton correlation [21] during two-phase flow and Dittus-Boelter in the single-phase flow region, using the same empirical correlations reported by Odeh et al.[12]. The numerical comparison are depicted in Figure 4.22.

The comparison present a little difference in the temperature distribution in the single phase gas region. The model developed in this thesis predict the change of phase between two-phase and single phase gas occur more later than the results presented in

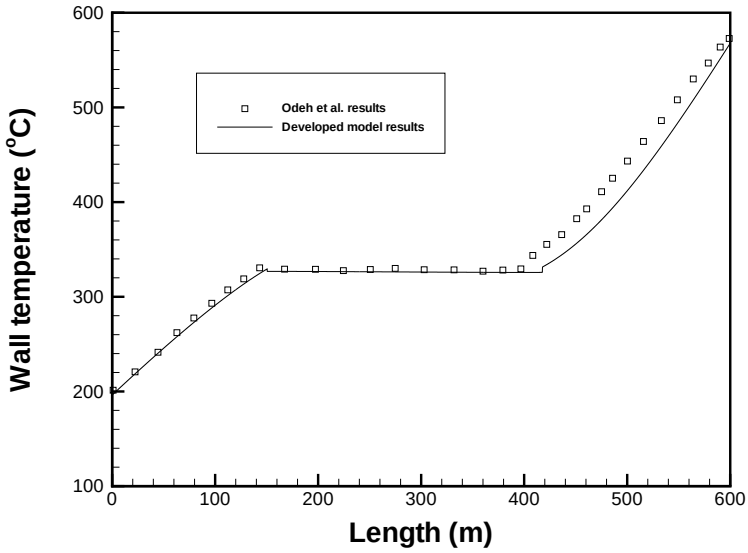


**Figure 4.22:** Wall temperature distribution along the tube. Numerical results obtained from model developed vs. numerical Odeh's results

Odeh's study. However, at the end of the tube the wall temperature are quite similar between both results.

Two different empirical correlations have been used to show the influence of the heat transfer coefficient in the wall and the fluid flow temperature distribution. Shah correlation [22] and Kandlikar correlation [23] are applied along saturated boiling region, while Groeneveld correlation [24] is used in the post-dry-out region.

The methodology to find the dry-out point is based on the critical heat flux criteria proposed by Groeneveld [18] and the CHF look-up-tables [19]. In Figure 4.23 the value of the three different heat transfer coefficient in function of the steam quality is shown. Furthermore, in Figure 4.24 the heat transfer coefficients evaluated along the tube is presented.

The case when the Gungor-Winterton correlation is used not critical heat flux criteria is applied, it can see in Figure 4.23, where the value of the heat transfer coefficient does not suffer any strong drop in contrast with the other two results depicted.

The heat transfer coefficient value presents a strong drop when the dry-out point

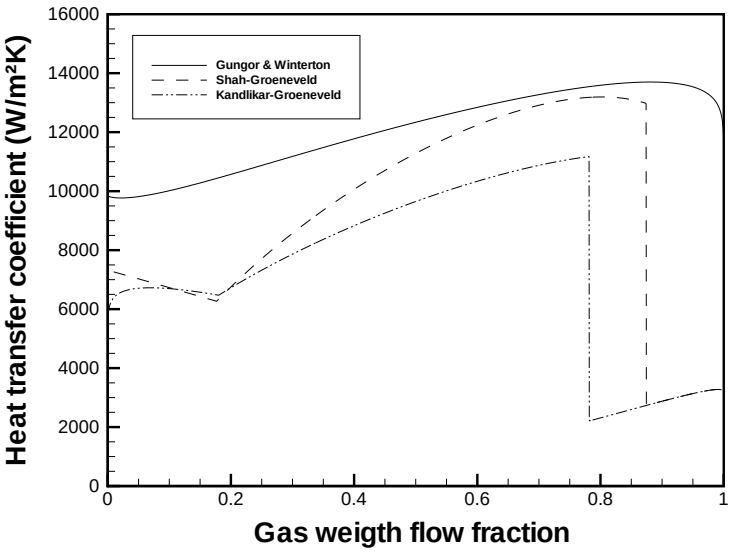


**Figure 4.23:** Heat transfer coefficient in function of the steam quality

is detected into the tube. It phenomena is a consequence of the drop of the contact between liquid film and the wall. It produce a change in the wall temperature distribution. The wall temperature suffer an abrupt change and the difference between wall and fluid temperature can be increased. It phenomena can be see in Figure 4.25, where the difference between wall and fluid flow is bigger in Shah-Groeneveld and Kandlikar-Groeneveld than Gungor-Winterton, because in last evaluation of the heat transfer coefficient the critical heat flux criteria is not used in the simulation.

In Figure 4.25 the difference between wall and fluid flow is shown for the same case using three different correlations, together with the result obtained from Odeh's study. Altought, the behaviour of the difference is quite similar in all results, the quasi-homogeneous model predict less difference in single-phase liquid and single-phase gas than results presented by Odeh et al. [12]. In the two-phase flow a local increase of the difference between wall and fluid flow temperature occur when the critical heat flux is found along the tube. This phenomenon does not appear in Odeh's study because it does not consider the critical heat flux into the solution of phase change.

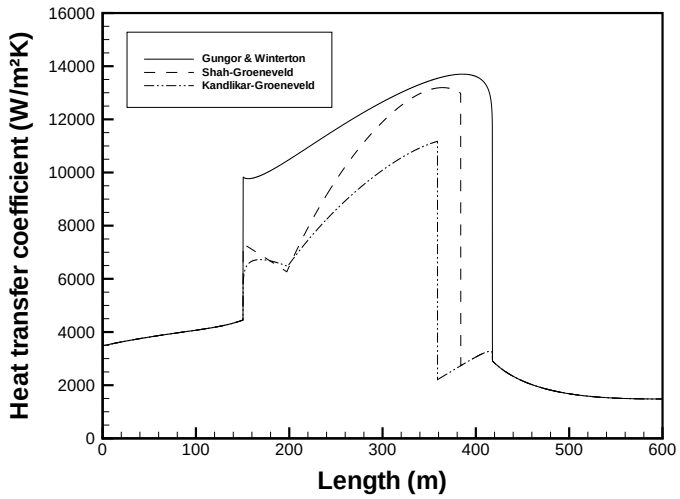


**Figure 4.24:** Heat transfer coefficient in function of the length

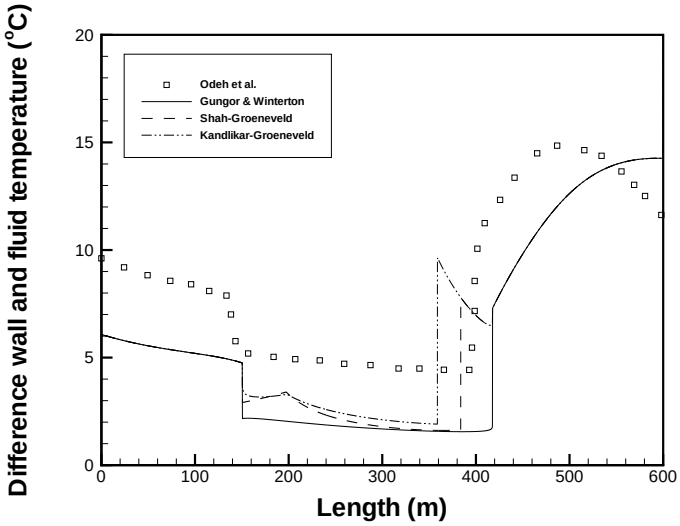


**Figure 4.25:** Difference between wall and fluid temperature along the tube

### 4.4.3 Illustrative cases of a solar receiver

Now, two illustrative cases are shown applying the CTTC code to solve conduction, radiation and two-phase flow in a solar receiver. The first case is a panel with a high incident heat flux that produce the occurrence of the critical heat flux phenomena. The second case is a solar receiver where the steam generation occurs as consequence of the incident heat flux applied. However, the critical heat flux in this case does not occur and the operation conditions will not produce damages in this thermal device. In both cases, results show how the numerical method to solve the two-phase flow phenomena studied in this work has been implemented with other methods to simulate a complex thermal device.

#### Solar panel with CHF

The first case consists of two horizontal tubes linked for a fin making up a panel, on this device a high incident heat flux is applied. The geometry of tubes is 0.055 meters of internal diameter and 5.4 meters of length. The inlet conditions of the water flow are: mass flow rate = 2.0 $kg/s$, temperature = 210 $^oC$ and pressure = 25.0 $bar$. The incident heat flux is about $1.0 MW/m^2$ on a projected surface of 0.822 $m^2$.

Showing the effect produced for the high heat flux on the wall temperature surface is the main aim of this case, where the critical heat flux condition explained above occurs. Furthermore, the evolution of the average wall and fluid flow temperature, heat transfer coefficient, weight mass fraction and void fraction along the tubes are shown.

The heat transfer coefficient profile is shown in Figure 4.26. An abrupt change of the heat transfer coefficient value between 3.0 and 4.0 meters can be seen in the profile due to the appearence of the critical heat flux. The heat transfer coefficient has been evaluated by means of the Kandlikar correlation on boiling saturation region and Groeneveld correlation on post dry-out region. The criteria explained above to define where occurs the critical heat flux phenomena into the tubes has been used.

The critical heat flux occurs at low gas weight flow fraction value (less than 0.1), it can be seen in Figure 4.27. After this point the gas weight flow fraction profile suffer a quickly increase, from 0.08 to 0.64 approximately, next a slowly change in the gas weight flow fraction value is obtained. This slow change in the weight flow fraction after the CHF appearance is a consequence of the poor heat transfer mechanism present in this region, due to a low heat transfer coefficient value evaluated from the correlation to post dry-out. The effect of the poor heat transfer mechanism on the void fraction can be see after 3.4 m of length, where the value of this parameter is almost constant. If a total evaporation of the fluid flow is required, the length of tube will be increased.

The abrupt change in the heat transfer coefficient and the gas weight flow fraction

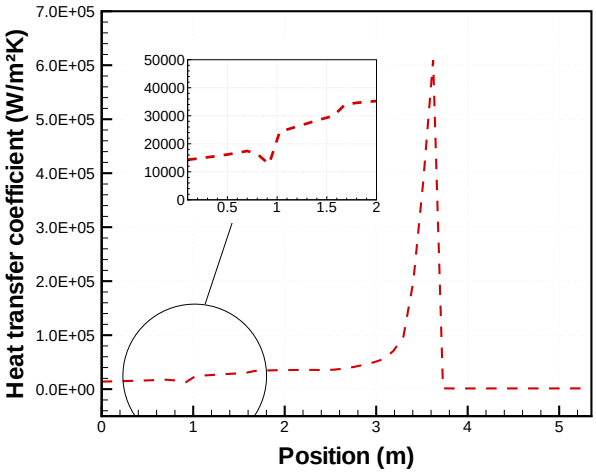


**Figure 4.26:** Heat transfer coefficient along the tube

values of the water flow have been found when CHF condition appear, as a consequence a high jump in the wall temperature value can be detected. A strong increase in the wall temperature profile is found at 3.4 meters of length, this change is shown in Figure 4.28, where the average wall temperature and water flow temperature profiles are depicted. Although the average wall temperature value is increased about $250^oC$, the local wall temperature value at the top on the surface of the tube is higher than the average value.

Illustrative results of the local wall temperature are presented in Figure 4.29. The effect of the CHF phenomena on the tube can be seen when a local analysis of the wall temperature is carried out. The numerical results of the local analysis show with more detail the change on the wall temperature at the top of the tubes. The local results of the wall temperature predict a higher jump of the wall temperature than the predicted value from average result. A jump of 500 $^oC$ approximately, appear in less than 1 meter of length, between 3.0 and 3.6 meters, in comparison with only $250^oC$ obtained from average analysis.

A high incident heat flux into contact with the surface of the panel favour the appearance of the critical heat flux at low mass weight fraction. This thermal mechanism can produce damages in the tubes of the solar receiver due to the high temperature generated in the wall tubes. To avoid reach a similar critical operation condition the analysis of the two-phase flow phenomena and the influence of different parameters

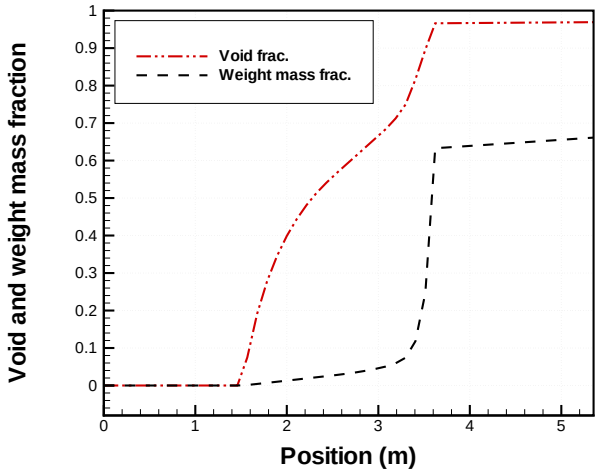


**Figure 4.27:** Weight mass fraction and void fraction

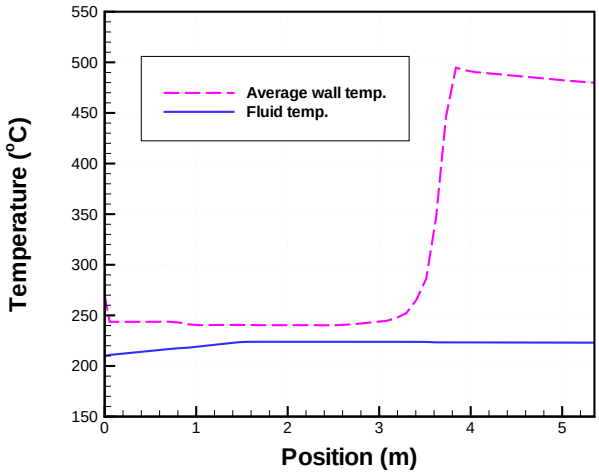


**Figure 4.28:** Average wall and fluid flow temperature distribution

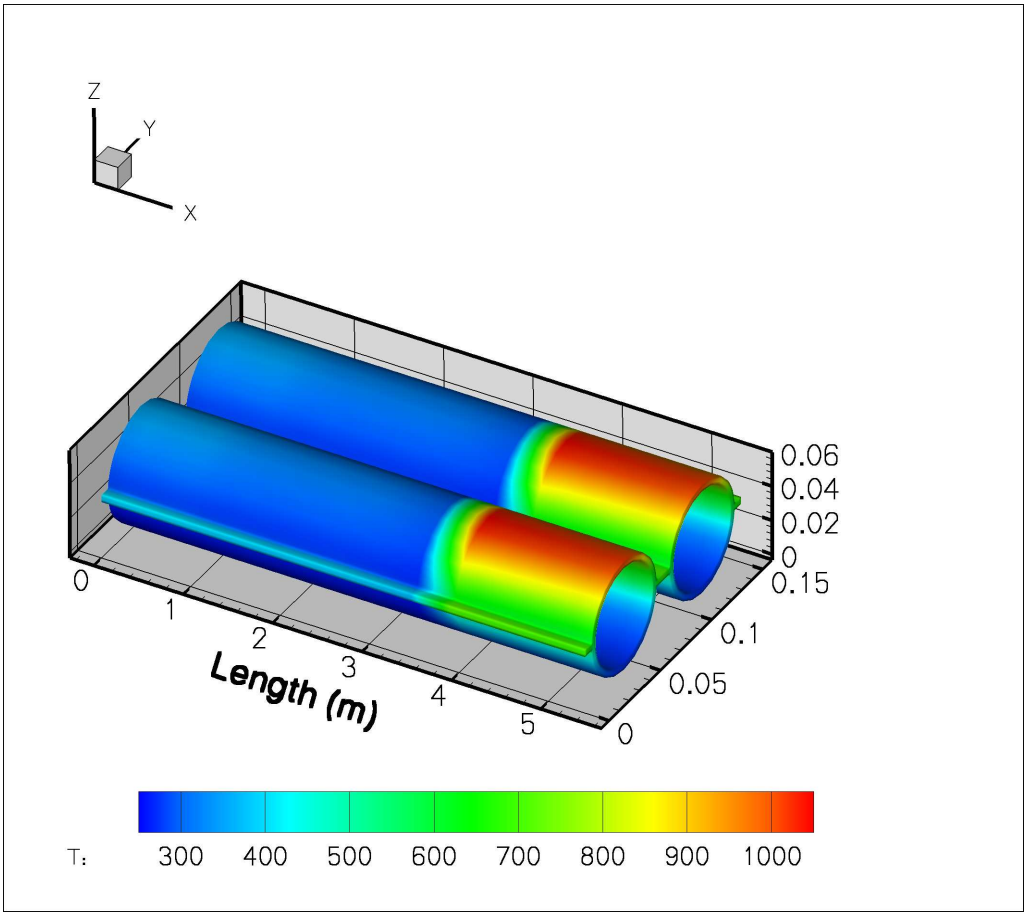


**Figure 4.29:** Temperature distribution on the wall with critical heat flux inside of tubes

as the mass flow, the heat transferred, and the geometry on the critical heat flux are more important in the design of this thermal device.

## Solar receiver with steam generation

The second case consists of a rectangular panel built with an array of circular tubes linked between them by means of fins, making up a solar receiver. A water flow is heated by action of the solar incident heat flux on the panel and steam generation occurs inside of tubes. A schematic representation of the solar receiver is depicted in Figure 4.30.

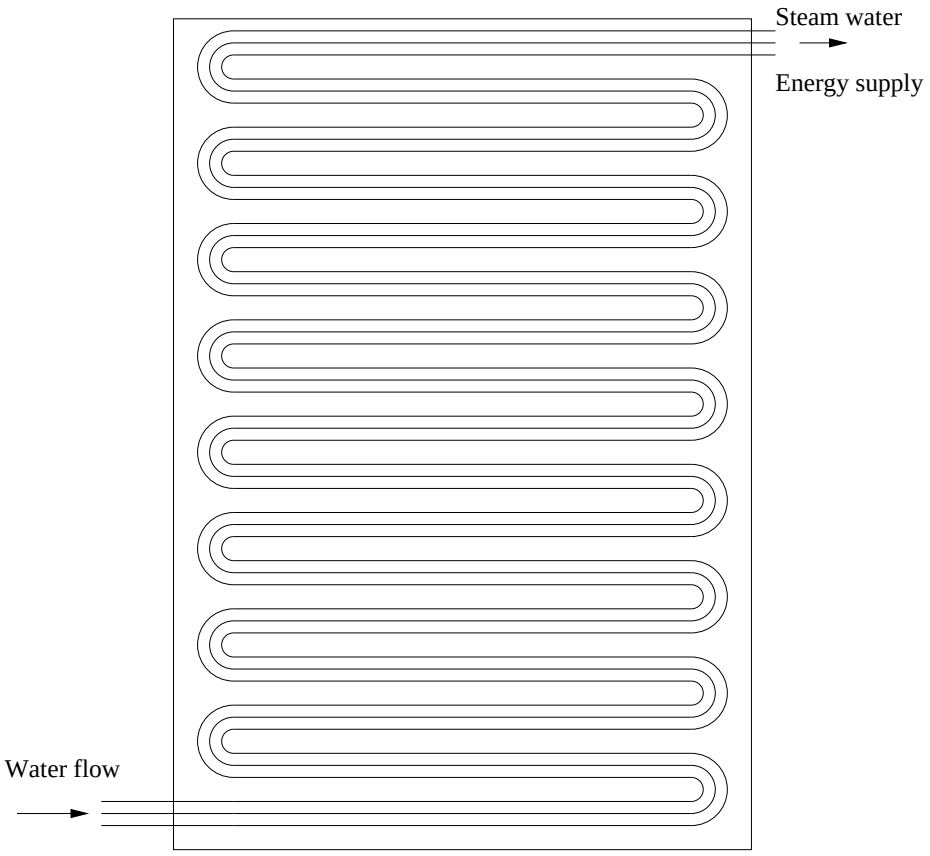


**Figure 4.30:** Schematic representation of the solar receiver.

The numerical results of the steady state solar receiver have been obtained using 1000 CV for each tube and near to 600.000 CV for all panel. The code developed by CTTC laboratory is able to solve the receiver panel considering the two-phase flow inside the tubes, the heat conduction in the solid elements and the thermal radiation. A pararell computational technique is used to run the solar receiver case. The solar panel is divided in horizontal rectangles, to avoid cutting the tubes. In each rectangle the two-phase flow and the conduction are evaluated by a processor, while the thermal radiation is solved by all of the processors, simultaneously.

The solar receiver is a rectangular panel make up for a group of tubes properly configured. The geometric description of the rectangular panel is 12.0 $m$ by 5.5 $m$ approximately. The internal diameter of the tubes is 0.0055 $m$, each tube is configured as a heating coil with several loops along the length of the rectangular panel.

The inlet conditions of the fluid flow (water) is presented in Table 4.18.

**Table 4.18:** Inlet conditions of the water on the solar receiver.

| *pressure* | *mass flow* | *temperature* |
|---|---|---|
| $[bar]$ | $[kg/s]$ | $[^oC]$ |
| 53.7 | 7.7 | 258 |

An illustrative numerical results of the whole panel and a detailed on some wall tubes are shown in Figures 4.31 4.32 4.33 and 4.34.

The incident heat flux for unit area on the solar receiver is depicted in Figure 4.31, the highest value of the incident heat flux is applied between 5 and 7 meters in Y direction and 4 and 5 in X direction. The temperature of the panel in this zone present higher values than temperature in other zones of the solar receiver. This effect can be see in Figure 4.32.

A detailed temperature distribution on the surface of the panel is depicted in Figure 4.33. The highest wall temperature is to reach on the top surface of the wall tubes where a high incident heat flux is applied, while the bottom surface of the wall tubes have a temperature near to the saturation temperature of the fluid flow.

The gas weight flow fraction of the water into the solar receiver is shown in Figure 4.34, where the influence of the incident heat flux is clearly seen. The two-phase flow occur when a high value of the incident heat flux is applied on the panel. Before this zone, the water fluid is single-phase flow.

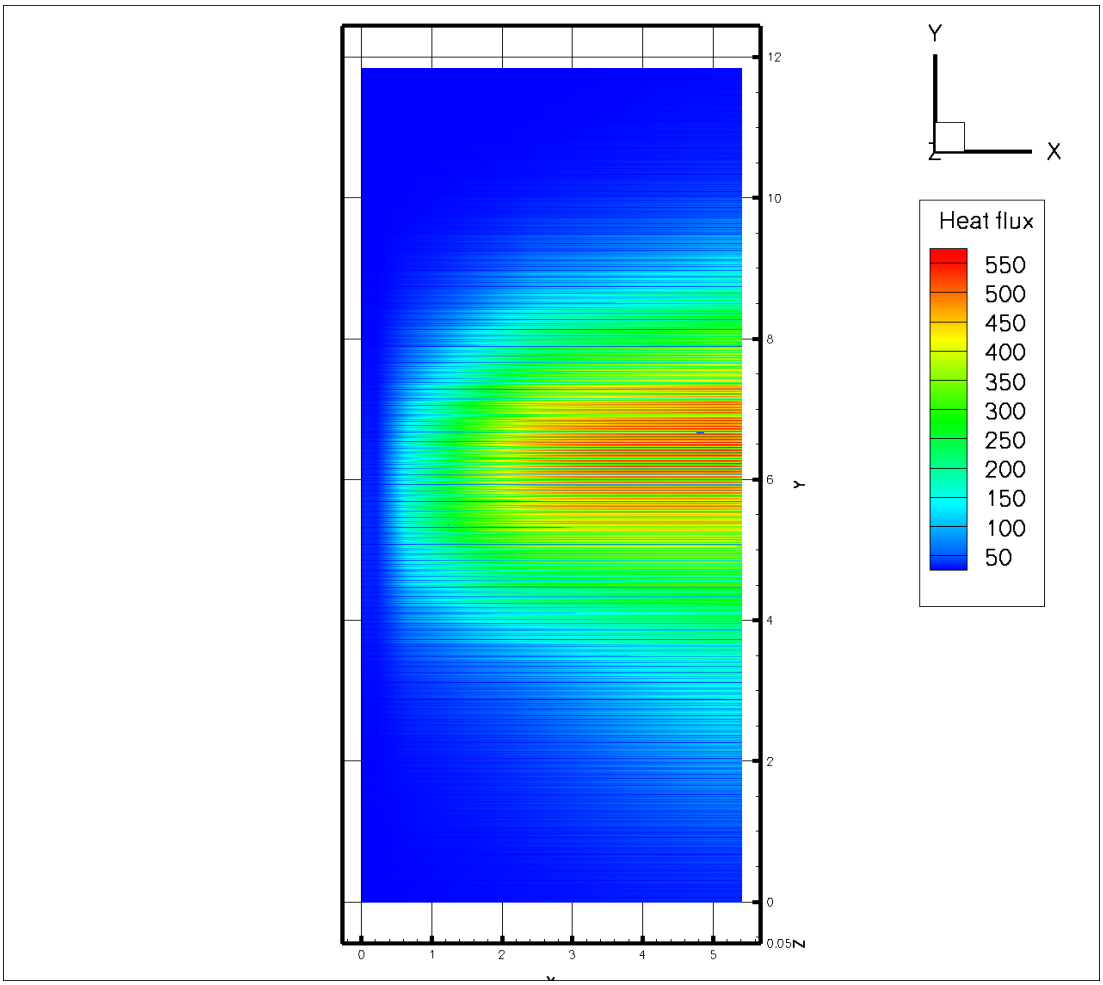


**Figure 4.31:** Incident heat flux ($kW/m^2$) on the panel

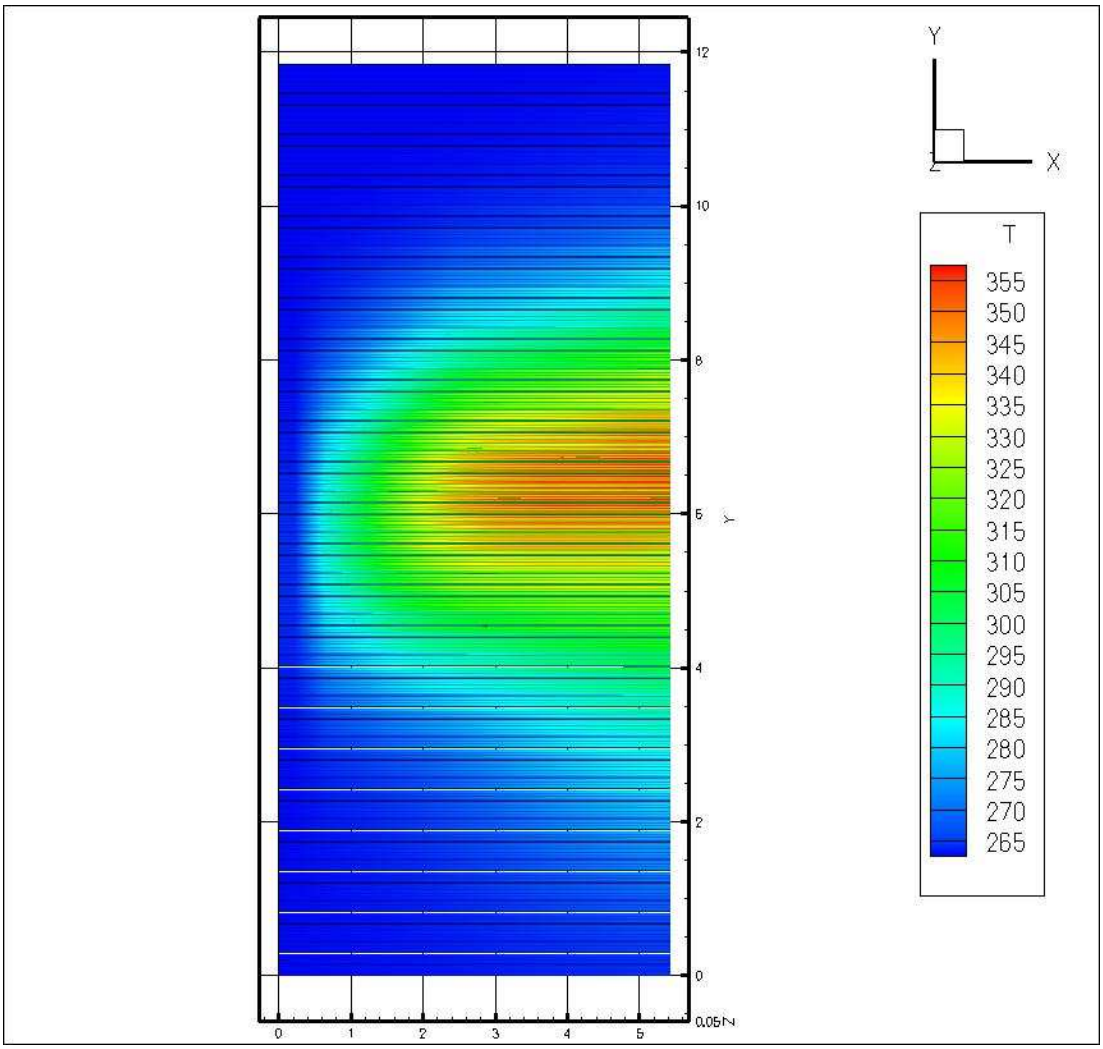


**Figure 4.32:** The solid temperature distribution of the total panel ($^oC$)

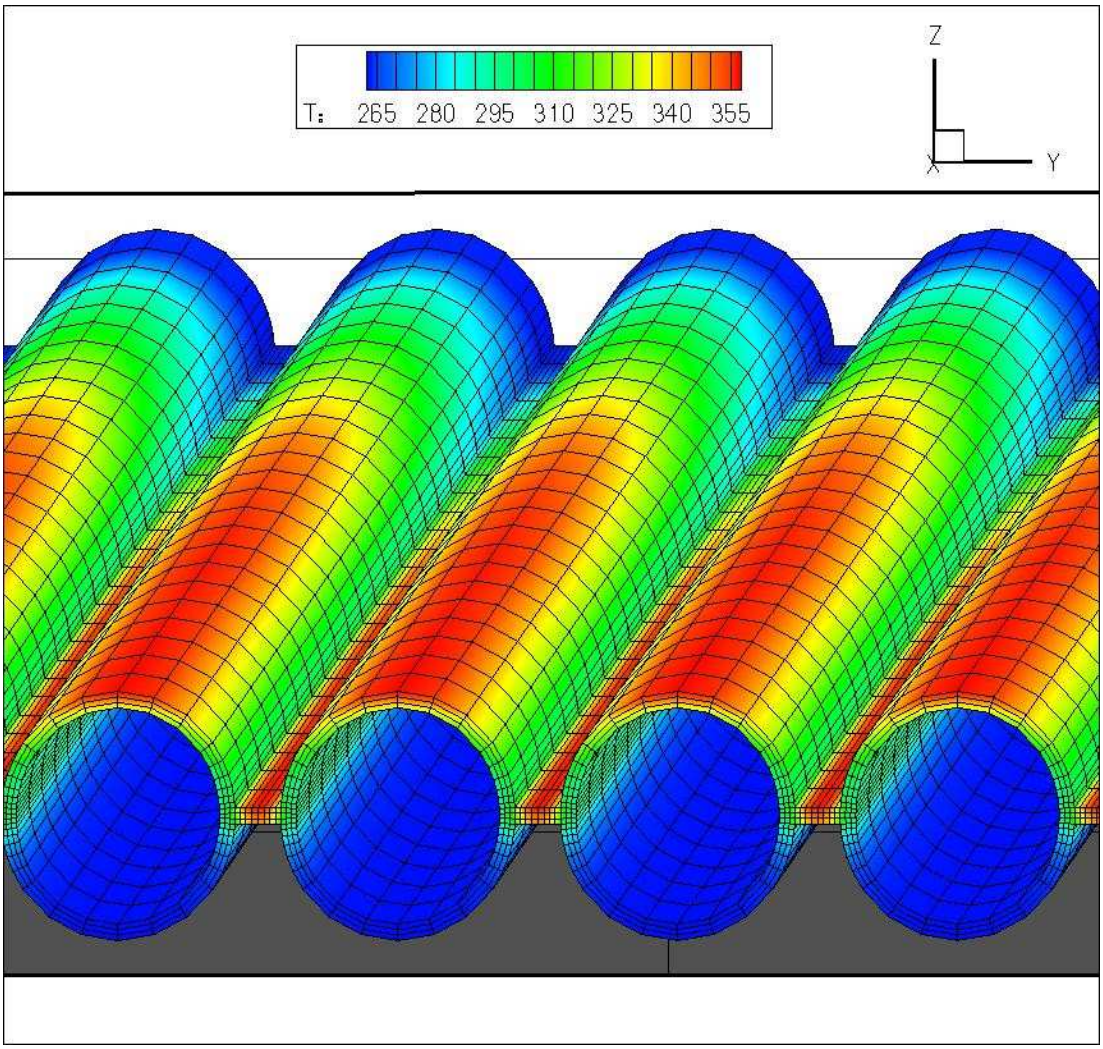


**Figure 4.33:** The wall temperature distribution of some tubes ($^oC$)

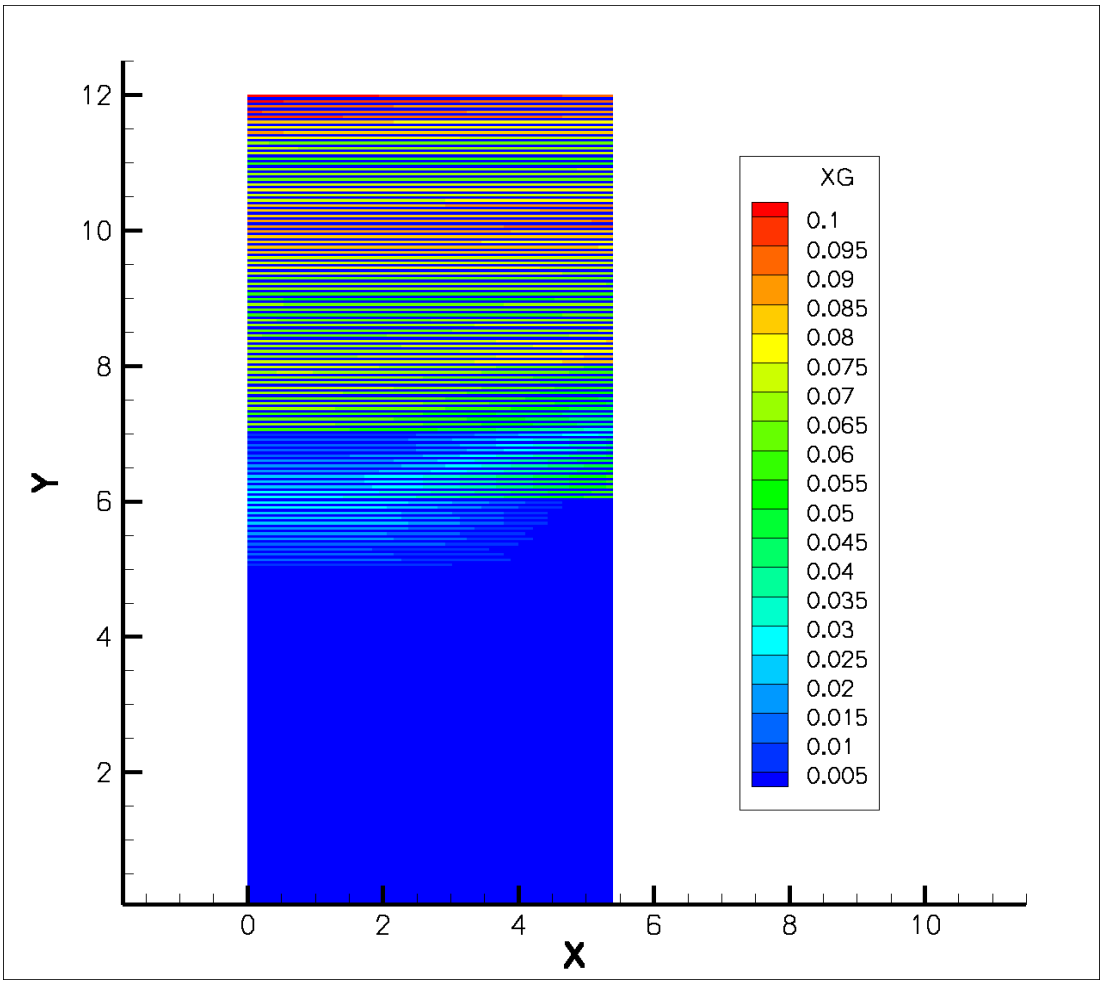


**Figure 4.34:** The gas weight flow fraction distribution inside of tubes on the panel

## 4.5 Conclusions

The method proposed in the Chapter 2 has been used to simulate different kind of thermal heat systems, the numerical results are shown in this Chapter.

The influence of different parameters have been studied on the Double-pipe heat exchanger working as an evaporator or a condenser. The fluid flow configuration, the quantity of mass flow, the insulation thickness and the initial conditions of the fluid flows have been analysed on this kind of heat exchanger. The Double-pipe heat exchanger has been chosen because it has a simple geometry configuration and several aspects can be studied.

The numerical analysis of the Fin-and-tube heat exchanger working as an evaporator or a condenser is shown. The numerical results of different parameters such as temperature, pressure, void fraction and weight mass fraction have been described in each channel along of the heat exchanger. The numerical analysis of the two-phase flow into the tubes of the heat exchanger helps to evaluate the thermal behaviour of the air flow and the influence on the solid parts (fin-and-tube).

The solar receiver with steam generation is studied as application of the method proposed in this work, because the two-phase flow occurs into the tubes. Sometimes the critical heat flux phenomena can appear into this kind of thermal devices with undesirable consequences to the solid elements that make up the thermal system.

Finding the CHF in terms of saturated evaporation is not an easy task. There is a wide variety of correlations that try to predict this condition and the corresponding location of the point of dry-out inside pipes. However, there is not a correlation that provides satisfactory results under different geometries and working conditions of the fluid. So far, the LUT method seems to be one that can give similar results to the experiments. Moreover, this method allows to extend this application to different situations in a manner not too complicated.

The implementation of this method in the code for evaluation of the heat exchangers was made using the LUT [19]. These tables are a function of pressure, mass flow and quality of steam. It is necessary to make a process of linear interpolation between the various tables to find the CHF corresponding to the working conditions of the fluid.

Finally, the use of the method proposed in this work to solve the two-phase flow has been evaluated with different cases. The numerical method works alone to resolve the two-phase flow into the pipe or linked with two different codes to solve a complex thermal devices.

# References

[1] F. P. Incropera and D. P. DeWitt. *Fundamentals of Heat and Mass Transfer, 4th ed.* John Wiley and Sons Inc., 1999.

[2] C. Oliet. *Numerical Simulation and Experimental Validation of Fin-and-Tube Heat Exchangers.* PhD thesis, Universitat Politècnica de Catalunya, 2006.

[3] C. Oliet, C. D. Pérez-Segarra, S. Danov, and A. Oliva. Numerical Simulation of Dehumidifying Fin-and-Tube Heat Exchangers. Semi-Analytical Modelling and Experimental Comparison. *International Journal of Refrigeration*, 30(7):1266–1277, 2007.

[4] S. Morales, J. Rigola, C. D. Pérez-Segarra, and A. Oliva. Numerical analysis of two-phase flow in condensers and evaporators with special emphasis on single phase - two phase transition zones. In *Proceedings of the 3rd International Symposium on Two-Phase Modelling and Experimentation*, pages 321–328, 2004.

[5] M.M. Shah. A new correlation for heat transfer during boiling flow through pipes. *ASHRAE Transactions*, 82(2):66–86, 1976.

[6] C.K. Rice. The Effect of Void Fraction Correlation and Heat Flux Assumption on Refrigerant Charge Inventory Predictions. *ASHRAE Transactions*, 93(1):341–367, 1987.

[7] L. Friedel. Improved Friction Pressure Drop Correlation for Horizontal and Vertical Two-Phase Pipe Flow. European Two-Phase Flow Group Meeting, Ispra, Italy. Paper E2., 1979.

[8] N. H. Kim, J. H. Yun, and R. L. Webb. Heat transfer and friction correlations for wavy plate fin-and-tube heat exchangers. *Journal of Heat Transfer - Transactions of Asme*, 119(3):560–567, 1997.

[9] M.K. Dobson and J.C. Chato. Condensation in Smooth Horizontal Tubes. *Journal of Heat Transfer - Transactions of Asme*, 120(1):193–213, 1998.

[10] O. Lehmkuhl, C. D. Perez-Segarra, R. Borrell, M. Soria, and A. Oliva. TERMOFLUIDS: A new Parallel unstructured CFD code for the simulation of turbulent industrial problems on low cost PC Cluster. In *Proceedings of the Parallel CFD 2007 Conference*, pages 1–8, 2007.

[11] S. Morales-Ruiz, J. Rigola, C. D. Pérez-Segarra, and O. García-Valladares. Numerical analysis of two-phase flow in condensers and evaporators with special emphasis on single-phase / two-phase transition zones. *Applied Thermal Engineering*, 2008.

[12] S. D. Odeh, G. L. Morrison, and M. Behnia. Modelling of parabolic trough direct steam generation solar collectors. *Solar Energy*, 62(6):395–406, 1998.

[13] D. C. Groeneveld. On the definition of critical heat flux margin. *Nuclear Engineering and Design*, 163:245–247, 1996.

[14] J. G. Collier. "Boiling and evaporation", chapter in Heat Exchanger Design Handbook, Hemisphere Publishing Corporation (Chapter 2.7), 1983.

[15] I. Pioro, D. Groeneveld, L. Leung, S. Doerffer, S. Cheng, Y. Antoshko, Y. Guo, and A. Vasic. Comparison of CHF measurements in horizontal and vertical tubes cooled with R-134a. *International Journal of Heat and Mass Transfer*, 45:4435–4450, 2002.

[16] S. J. Yoon and D. M. France. Post-CHF heat transfer with water and refrigerants. *Nuclear Engineering and Design*, 163:163–175, 1996.

[17] Y. L. Wong, D. C. Groeneveld, and S. C. Cheng. CHF prediction for horizontal tubes. *International Journal of Multiphase Flow*, 16(1):123–138, 1990.

[18] D. C. Groeneveld, L. Leung, P. Kirillov, V. Bobkov, I. Smogalev, V. Vinogradov, X. Huang, and E. Royer. The 1995 look-up table for critical heat flux in tubes. *Nuclear Engineering and Design*, 163:1–23, 1996.

[19] D. C. Groeneveld, J. Q. Shan, A. Z. Vasíc, L. K. H. Leung, A. Durmayaz, J. Jang, S. C. Cheng, and A. Tanase. The 2006 CHF look-up-table. *Nuclear Engineering and Design*, 237:1909–1922, 2006.

[20] J. Yang, D. C. Groeneveld, L. K. H. Leung, S. C. Cheng, and M. A. El Nakla. An experimental and analytical study of the effect of axial power profile on. *Nuclear Engineering and Design*, 236:1384–1395, 2006.

[21] K.E. Gungor and R.H.S. Winterton. A general correlation for flow boiling in tubes and annuli. *International Journal of Heat and Mass Transfer*, 29(3):351–358, 1986.

[22] M.M. Shah. Chart correlation for saturated boiling heat transfer: equations and further study. *ASHRAE Transactions*, 88(1):185–196, 1982.

[23] S.G. Kandlikar. A general correlation for saturated two-phase flow boiling heat transfer inside horizontal and vertical tubes. *Journal of Heat Transfer - Transactions of Asme*, 112(1):219–228, 1990.

[24] D.C. Groeneveld. Post-Dryout Heat Transfer at Reactor Operating Conditions, 1973.

# Chapter 5

# Numerical analysis of two-phase flow using Two-fluid models. One dimensional case.

**Abstract.**

A numerical study based on two-fluid model has been developed to describes the thermal and fluid-dynamic behaviour of the two-phase flow inside ducts. The discretization of the governing equations has been carried out by means of the finite volume technique, based on an one-dimensional in this Chapter and bi-dimensional in the next Chapter transient integration of the conservative equations using a staggered mesh. A semi-implicit pressure based method is used to solve the pressure distribution of the flow, the liquid and vapour velocities, and the liquid and vapour temperatures distribution. Different empirical correlations have been used to evaluate the mass, momentum and energy exchanged through the interface, geometric conditions, gas and liquid distribution into the tube and other terms that appear in the conservation equations as the convective heat transfer and shear stresses. These correlations are known depending on the flow regimen map, which is function of the gas volume fraction and velocities. A simplified flow pattern map is expressed in function of the gas volume fraction and the liquid and gas velocities. A comparison between the numerical simulation data obtained with quasi-homogeneous model and the one-dimensional two-fluid model in contrast with experimental data are illustrated.

## 5.1 Introduction

In different industrial applications the two-phase flow phenomena is very common, it can be described as the flow of two different kind of matter, e.g. solid particles in a gas or liquid, gas bubbles in a liquid or droplets in a gas stream. Two-phase flow is present along the different manufacturing process and a variety of fluids can be working at the same time, e.g., air-water, oil-water, carbon particles-steam, etc [1]. The high number of applications where the two-phase flow phenomena is present has increased the motivation to study the multiphase flow in multi-component fluids along the last forty years.

A deeper undertanding of the two-phase flow phenomena (boiling or condensation) helps to find new solutions and improve the design of the refrigerant and air-conditioning system. Usually, this task uses a resolution of a mathematical model as a power tool to predict the thermo hydraulic behaviour of the fluid flow, looking for a realistic description of the phenomena.

Different models to simulate the two-phase flow phenomena have been used to describe the two phase flow, from a simplified homogeneous equilibrium model HEM to a complex two-fluid model TFM. The homogeneous model assume the two-phase flow as a mixture, then non interface exchange is considered and only one pressure, one velocity and one temperature are using to describe the thermo hydraulic behaviour of the fluid flow [2]. The separated two-phase flow model with no interface exchange assume one pressure, different gas and liquid velocities and equal gas and liquid temperature. Inside this model group is the drift-flux model [3] [4], which define a relative motion between phases, due to only a mixture momentum equation is used and a simplified formulation is obtained. The two-fluid model propose a separated model considering the interface exchange, this permit obtain different gas and liquid velocities and temperatures. A group of conservative equations are proposed by each phase, then a more complex set of equations than the model presented above should be resolve to find the pressure distribution, void fraction, velocities and temperatures of the liquid and gas, respectively [5] [6].

All models commented above need a set of empirical information, depending on type of model and hypothesis assumed by each one, the number of empirical expressions required can change. The two-fluid model require a big number or empirical expressions to define different effects on the fluid flow along the interface and between each phase and the wall in comparison with other models. The empirical information used in the simulation of the thermo hydraulics behaviour of the nuclear systems [7] [8] [9] have been applied to our case. Important parameters such as geometric conditions, heat transfer coefficients and shear stresses at the interface and with the wall are defined by means of these expressions. All of these parameters depend on the flow regimen map, which is defined as function of the void fraction and velocities of the flow. A combination of flow regimen maps has been used in this paper, a flow

regimen map proposed to steam-water system [7] and a flow regimen map proposed to boiling in refrigeration system [10] have been implemented to find a criteria to evaporation process in a refrigeration system. A specific information obtained from science literature have been studied with the propose to define the most adequate empirical expression in function of regimen flow and heat conditions [11] [12] [13].

There are enough information in the science literature about the mathematical formulation of the one-dimensional two-fluid model [14] [15], the resolution methodology and numerical strategies [16] [17] [18] and the instability problem [19] [20]. In general the two-fluid model applied to the study of the thermo hydraulic behaviour and damage effects on nuclear systems is the topic more reported in literature, together with the use of this model and improvements in different commercial codes as RELAP, CATHARE, TRACE and others. In contrast with the application of the two-fluid model to nuclear systems, less information are found about the use of two-fluid model to refrigerant systems.

Some numerical studies of two-phase flow in refrigeration reported in literature have used a steady-state one-dimensional two-fluid model. One of them is a two-phase critical flow through short tube orifice, it uses a two-fluid model six equations to predict the mass flow rate, the velocities and temperatures of each phases [21], including a comparison between TFM and HEM with different kind of refrigerant fluids. A double-pipe evaporator [22] and a double-pipe condenser [23] have been studied assuming non-equilibrium and applying a two-fluid model four equation to find the velocities of each phase and the fluid temperature. Both of last papers have tried to define the influence of friction and heat flux on the two-phase fluid flow.

The one-dimensional two-fluid model solution by means of a pressure based method is reported by M. Darwish and F. Moukalled[24] and M. R. Ansari and V. Shokri[25] and modifications of this method have proposed by W.H. Lee and R.W. Lyczkowski[26] and T.F. Miller and D.J. Miller[27]. Some of these papers only solve the continuity and momentum equation, non assuming the effect of the energy equations on the physical properties (e.g. density) and their influence on the pressure correction equation [25][27]. An extension to two-dimensional two-fluid model applying a pressure based method can be find in [28].

This chapter is focused on detailed one-dimensional numerical simulation of phase change phenomena gas-liquid flow into pipes, assuming a only one fluid. The basic field equation following the transient two-fluid model consists of two continuity equations, two momentum equations and two energy equations, one equation for each phase. The six governing equations have been organized in a set of algebraic equations that is solved using the three diagonal matrix algorithm TDMA. The coupling between momentum and continuity equations is solve with a semi-implicit pressure based method like SIMPLE method [29]. This method is very usual and robust in the single-phase flow finite volume simulation technique. However, some difficulties

should be take into account in two-phase flow due to the strong coupling between two momentum and two continuity equations, together with the effect of the interphase drag and mass transfer [27]. The strong coupling makes the algorithm depend more on the velocities of previous solution iteration producing an instabilities along the simulation process. The solution to this effect is written explicitly the interfacial terms in continuity, momentum and energy equation and solve to obtain a pseudo-solution that resolves the interphase coupling [24].

Transient and steady-state have been considered in this study and two different cases are presented. Different numerical aspects have been evaluated with the aim of verifying the quality of the numerical solution. The difference between the numerical simulation results obtained with quasi-homogeneous QHM [30] model and two-fluid model TFM [31] into the tube are illustrated. Finally, a comparison between numerical results and experimental data of the evaporation into the tube using R134a as a refrigerant fluid is shown.

## 5.2 Mathematical Formulation

The mathematical formulation of the two-fluid model is based on the conceptual models for single-phase flow of a gas or a liquid, which are formulated in terms of field equations describing the conservation laws of mass, momentum and energy. Furthermore, the appropriate constitutive equations, interfacial balance and boundary conditions should be considered to find a model capable to predict the two-phase flow behaviour.

The derivation of the field and constitutive equations for the flow of structured media is more complicated than homogeneous media such as single phase flow. The difficulties encountered in deriving the equations are due to the interface and the fact of the two-phase flow depend on the interfacial structure of the flow.

In order to differentiate the field and constitutive equations in concordance with the two-phase flow structure, it is necessary to describe the local characteristic of the flow, together with the appropriate macroscopic properties definition. An appropriate averaging procedure should be used to solve the macroscopic aspect of the two-phase flow, these are much more important than microscopic details.

There are different kind of averaging that can be applied to thermo-fluid dynamics in general and to two-phase flow in particular. The Eulerian averaging, the Lagrangian averaging and the Boltzmann statical averaging [6].

In this thesis the two-fluid model formulation is based on a Eulerian averaging procedure, because it is the most important and widely applied in continuum mechanics and it is closely related to human observations and most instrumentations.

The basic concept of the Eulerian averaging is the time-space description of physical phenomena, then the time and space are taken as independent variables and

various dependent variables are expressed in function of these coordinates. The averaging processes are basically integral operators, thermore, these have an effect of smoothing out instant or local variations within the domain of integrations.

Being $F$ any function, the time and spatial mean value can be expressed as:

$$\begin{aligned} &F = F(t,x)\ function \\ &time\ (temporal)\ \frac{1}{\Delta t}\int_{\Delta t} F(t,x)dt \\ &spatial\ (volume)\ \frac{1}{\Delta V}\int_{\Delta V} F(t,x)dV \end{aligned} \tag{5.1}$$

To derive the volume-averaged equations is necessary to take each point of the domain $x$ contained into an average volume $V(x)$ bounded by a surface $S(x)$. Considering the case of two-phases, using the sub-indice $k$ which can be $g$ or $l$ for gas or liquid, the averaging volume $V$ can then be expressed as two portions $V_g$ and $V_l$ occupied by each phase, and bounded by $S(x) = S_g(x,t) + S_l(x,t)$. The boundary of $V_k$ will consist of $S_k(x,t)$ and of interfaces $S_i(x,t)$ contained inside of volume. Thus $S_k$ and $S_i$ is a closed surface for both $k = g$ and $l$. Figure 5.1 shows an schematic volume divided in two volumes by an interface with their respective boundaries.

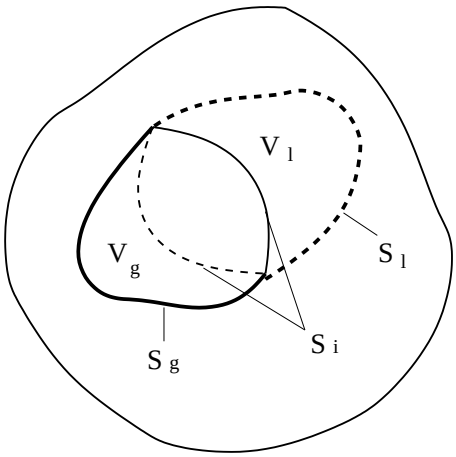


**Figure 5.1:** Control volume cut by an interface

Now, $F_k$ can be any extensive physical quantity pertaining to the matter which constitutes phases $k$ such as mass, momentum, energy, etc. The infinitesimal amount of $F_k$ in terms of the density, and $\phi_k$ per unit mass can be expressed as:

$$dF_k = \rho_k \phi_k dV_k \tag{5.2}$$

The balance of the total amount of $F_k$ in the averaging volume $V$ can be written as:

$$\frac{\partial}{\partial t}\int_{V_k} \rho_k \phi_k dV_k = \int_{S_k} (-\rho_k \phi_k u_k + \Upsilon_k) \cdot n_k dS_k + \int_{S_i} (-\rho_k \phi_k (u_k - w) + \Upsilon_k) \cdot n_k dS_i + \int_{V_k} \rho_k \theta_k dV_k \tag{5.3}$$

The first term in the right-hand is the amount of $F_k$ transported by convective or diffusive processes through the part $S_k$ of the surface of the averaging volume occupied by the phase $k$. The second terms is the same contribution by the interfacial surface $S_i$ contained inside the averaging volume. The unit normal $n_k$ is directed out the phase and $n_g = -n_l$ on $S_i$. The value $w$ is the velocity of the interfacial surface $S_i$, while the averaging volume surfaces $S_k$ are considered stationary. The last term is the source contributions $\theta_k$ of the $F_k$ inside V.

The integral balance equation 5.3 is transformed, by means of the Leibniz rule, the Green's theorem and put in the volume fraction definition of the phase $k$ as $\alpha_k = \frac{V_k}{V}$, in the general balance equation (for more details see [6] [32]):

$$\frac{\partial}{\partial t}\alpha_k \rho_k \phi_k + \bigtriangledown \cdot (\alpha_k \rho_k \phi_k u_k) = \bigtriangledown \cdot (\alpha_k \Upsilon_k) + \alpha_k \rho_k \theta_k + \frac{1}{V}\int_{S_i} [-\rho_k \phi_k (u_k - w) + \Upsilon_k] \cdot n_k dS_i \tag{5.4}$$

From equation 5.4 the mass, momentum and energy equations can be formulated for each one of the phases following the next conventions:

| Conserved Quantity | $\phi$ | $\Upsilon$ | $\theta$ |
|---|---|---|---|
| Mass | 1 | 0 | 0 |
| Momentum | $u$ | $\sigma$ | $g$ |
| Energy | $e + e_c + e_p$ | $u \cdot \sigma - q$ | $Q$ |

where $\sigma$ is the total stress tensor, $e$ is the internal energy per unit mass, $e_c$ is the kinetic energy per unit mass, $e_p$ is the potential energy per unit mass, $q$ is the heat flux transferred and $Q$ is the heat generation per unit mass.

The last term in equation 5.4 represent the gains or loses through the interface of mass, momentum or energy. Some of these quantities are more difficult to evaluate, (e.g. shear stress at the interface, the mass and heat transferred between phases), then some assumptions should be considered to simplified the solution, together with a specific constitutive laws are required to evaluate the influence of these values on the general behaviour of the fluid flow.

## 5.3 Discretized Equations

Mathematical formulation is based on the application of the conservative equations on each phase, liquid and gas. Then, six-equations are considered: two continuity, two momentum and two energy equations for each one of the phases [6]. The assumed hypotheses are: one-dimensional flow, constant cross section, and negligible axial heat conduction in fluid, and heat radiation. An schematic representation of the two-phase flow into the pipe is depicted in Figure 5.2, where some physics aspect that affect the flow are shown.

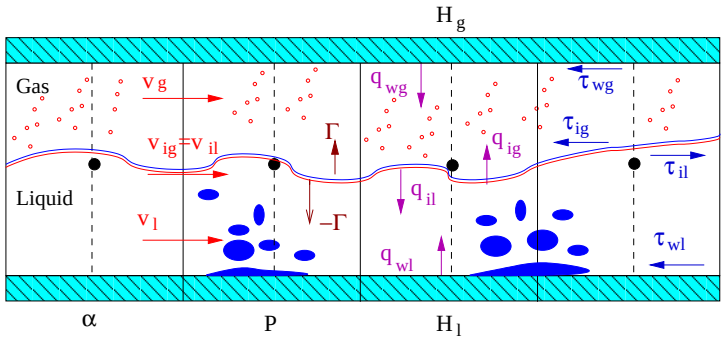


**Figure 5.2:** Schematic two-phase flow into the pipe

The mass conservation equations for liquid and gas phases are:

$$\frac{\partial}{\partial t}[\rho_l(1-\overline{\alpha})] + \frac{1}{A}\frac{\partial}{\partial z}[\rho_l(1-\overline{\alpha})\overline{v}_l A] = -\Gamma \tag{5.5}$$

$$\frac{\partial}{\partial t}[\rho_g\overline{\alpha}] + \frac{1}{A}\frac{\partial}{\partial z}[\rho_g\overline{\alpha v}_g A] = \Gamma \tag{5.6}$$

where $\alpha$ is the void fraction of gas, the void fraction of liquid is expressed as $(1-\alpha)$ assuming the geometric conservation equation (void fractions sum to 1), $v_l$ and $v_g$ are

the liquid and gas velocities, physical aspect that affect the flow are the total cross section area is called $A$ and $\Gamma$ is the mass transfer rate per unit volume. Applying a mass balance, the mass transfer from liquid to gas should be equal to mass lost by liquid.

The momentum equations for each phase is expressed as:

$$\frac{\partial}{\partial t}[\rho_l(1-\overline{\alpha})\overline{v}_l] + \frac{1}{A}\frac{\partial}{\partial z}[\rho_l(1-\overline{\alpha})\overline{v}_l{}^2 A] = -(1-\overline{\alpha})\frac{\partial p}{\partial z} - g\rho_l(1-\overline{\alpha})sin\theta - \frac{P_{wl}\tau_{wl}}{A} + \frac{P_i\tau_i}{A} - \Gamma\overline{v}_{il} + C\overline{\alpha\rho}(1-\overline{\alpha})\frac{\partial(\overline{v}_g - \overline{v}_l)}{\partial t} \tag{5.7}$$

$$\frac{\partial}{\partial t}[\rho_g\overline{\alpha v}_g] + \frac{1}{A}\frac{\partial}{\partial z}[\rho_g\overline{\alpha v}_g{}^2 A] = -\overline{\alpha}\frac{\partial p}{\partial z} - g\rho_g\overline{\alpha}sin\theta - \frac{P_{wg}\tau_{wg}}{A} - \frac{P_i\tau_i}{A} + \Gamma\overline{v}_{ig} - C\overline{\alpha\rho}(1-\overline{\alpha})\frac{\partial(\overline{v}_g - \overline{v}_l)}{\partial t} \tag{5.8}$$

Where $p$ is the total pressure, $\theta$ is the inclination angle of the pipe, $\tau_{wg}$ and $\tau_{wl}$ are the shear stresses acting on the gas and liquid phase at the wall respectively, and $\tau_i$ is the shear stress between phases at the interface. The wall perimeter wetted by liquid and gas are denoted as $P_{wl}$ and $P_{wg}$, $v_{il}$ and $v_{ig}$ are the interfacial velocities and $C$ is the virtual mass coefficient. The virtual mass coefficient depends on regimen present in the flow (C=0 in stratified regimen flow).

The energy equations are expressed in function of the internal, kinetic and potential energy $e = (H - p/\rho) + e_c + e_p$ as:

$$\frac{\partial}{\partial t}[\rho_l(1-\overline{\alpha})\overline{H}_l] + \frac{\partial}{\partial t}\left[\rho_l(1-\overline{\alpha})\frac{\overline{v}_l{}^2}{2} - \rho_l(1-\overline{\alpha})gzsin\theta\right] + \frac{1}{A}\frac{\partial}{\partial z}\left[\rho_l(1-\overline{\alpha})\overline{H}_l\overline{v}_l A\right] + \frac{1}{A}\frac{\partial}{\partial z}\left[\rho_l(1-\overline{\alpha})\frac{\overline{v}_l{}^3}{2}A - \rho_l(1-\overline{\alpha})\overline{v}_l Agzsin\theta\right] = \frac{q_{il}P_{il}}{A} + \frac{q_{wl}P_{wl}}{A} - \Gamma\left[\overline{H}_{il} + \frac{\overline{v}_{il}{}^2}{2} - gzsin\theta\right] + (1-\overline{\alpha})\frac{\partial p}{\partial t} \tag{5.9}$$

$$\frac{\partial}{\partial t}[\rho_g\overline{\alpha}\overline{H}_g] + \frac{\partial}{\partial t}\left[\rho_g\overline{\alpha}\frac{\overline{v}_g{}^2}{2} - \rho_g\overline{\alpha}gzsin\theta\right] + \frac{1}{A}\frac{\partial}{\partial z}\left[\rho_g\overline{\alpha}\overline{H}_g\overline{v}_g A\right] + \frac{1}{A}\frac{\partial}{\partial z}\left[\rho_g\overline{\alpha}\frac{\overline{v}_g{}^3}{2}A - \rho_g\overline{\alpha v}_g Agzsin\theta\right] = \frac{q_{ig}P_{ig}}{A} + \frac{q_{wg}P_{wg}}{A} + \Gamma\left[\overline{H}_{ig} + \frac{\overline{v}_{ig}{}^2}{2} - gzsin\theta\right] + \overline{\alpha}\frac{\partial p}{\partial t} \tag{5.10}$$

where $q_{il}$ and $q_{ig}$ are the heat transfer exchanged at the interface, while $q_{wl}$ and $q_{wg}$ are the heat transfered from the wall to the liquid and gas phase, respectively.

### 5.3.1 Discretization

The governing equations (5.5) to (5.10) can be integrated in terms of the local averaged fluid variables using the finite control volume technique. The concept of a staggered mesh has been used, therefore velocities are defined at the cell boundaries, while pressure, void fraction and enthalpy are located at the middle of the main volume. Figure 5.3 depicts a control volumes representation.

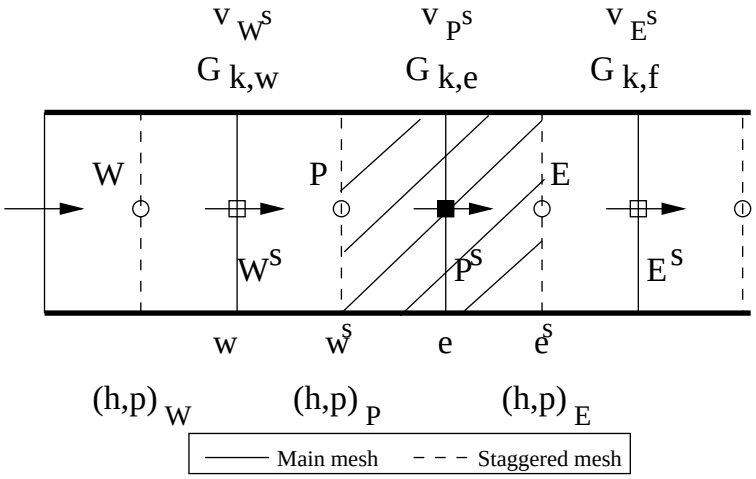


**Figure 5.3:** Schematic control volumes

Before the discretization of the governing equations, it is necessary to define two previous aspects that are important in the equations development. Firstly, the mass flow rate per unit of area is defined as: $G_{k,e} = [\rho_{k,e}\overline{\alpha}_{k,e}\overline{v}_{k,e}]$, where $k$ means the gas or liquid phases and $e$ means the position. Secondly, the void fraction is defined as the relation between the cross area occupied by the gas and the total cross area, $\alpha = S_g/S$.

Using a first order numerical scheme upwind in the convective terms and based on the parameters defined above, the momentum of the gas and liquid are discretized on the staggered mesh and the algebraic equations can be expressed as:

$$\frac{1}{\Delta t}\left[\frac{({\rho^o}_{g,P}\overline{\alpha}^o{}_P + {\rho^o}_{g,E}\overline{\alpha}^o{}_E)}{2}\right](v_{g,P^s} - {v^o}_{g,P^s}) +$$
$$\frac{1}{\Delta z}\left[-max\left(-\frac{(G_{g,e}+G_{g,f})}{2},0\right)v_{g,E^s} + max\left(-\frac{(G_{g,e}+G_{g,f})}{2},0\right)v_{g,P^s}\right] -$$
$$\frac{1}{\Delta z}\left[max\left(\frac{(G_{g,e}+G_{g,w})}{2},0\right)v_{g,W^s} - max\left(\frac{(G_{g,e}+G_{g,w})}{2},0\right)v_{g,P^s}\right] =$$
$$-\frac{1}{\Delta z}\frac{(\overline{\alpha}_P+\overline{\alpha}_E)}{2}[p_E - p_P] - g\frac{(\rho_{g,P}\overline{\alpha}_P + \rho_{g,E}\overline{\alpha}_E)}{2}sin\theta -$$
$$\frac{P_{wg}\tau_{wg}}{A} - \frac{P_i\tau_i}{A} + \Gamma[\overline{v}_{ig,P^s} + v_{g,P^s}] \tag{5.11}$$

$$\frac{1}{\Delta t}\left[\frac{{\rho^o}_{l,P}(1-\overline{\alpha}^o)_P + {\rho^o}_{l,E}(1-\overline{\alpha}^o)_E}{2}\right](v_{l,P^s} - {v^o}_{l,P^s}) +$$
$$\frac{1}{\Delta z}\left[-max\left(-\frac{(G_{l,e}+G_{l,f})}{2},0\right)v_{l,E^s} + max\left(-\frac{(G_{l,e}+G_{l,f})}{2},0\right)v_{l,P^s}\right] -$$
$$\frac{1}{\Delta z}\left[max\left(\frac{(G_{l,e}+G_{l,w})}{2},0\right)v_{l,W^s} - max\left(\frac{(G_{l,e}+G_{l,w})}{2},0\right)v_{l,P^s}\right] =$$
$$-\frac{1}{\Delta z}\frac{(1-\overline{\alpha})_P + (1-\overline{\alpha})_E}{2}[p_E - p_P] - g\frac{\rho_{l,P}(1-\overline{\alpha})_P + \rho_{l,E}(1-\overline{\alpha})_E}{2}sin\theta -$$
$$\frac{P_{wl}\tau_{wl}}{A} + \frac{P_i\tau_i}{A} - \Gamma[\overline{v}_{il,P^s} - v_{l,P^s}] \tag{5.12}$$

The interface velocities $v_{il}$ and $v_{ig}$ values are assumed to be equals and are defined as $v_{il} = v_{ig} = \lambda v_g + (1-\lambda)v_l$, where $\lambda$ is 0 or 1 depending on sign of the mass transfer rate per unit volume value $\Gamma$. Then, $\lambda$ is 0 if $\Gamma$'s value is positive or 1 if it is negative [7].

The pressure correction equation is defined from gas and liquid continuity equations. The sum of both equations is discretized on the main mesh, following the mass conservation-based algorithm (MCBA) [24]. Next relations help to develop the pressure correction equation:

$$
\begin{aligned}
&G_{g,e} = (\rho_{g,e}\overline{\alpha}_{g,e})v_{g,e} = (\rho_{g,e}\overline{\alpha}_{g,e})^* v^*{}_{g,e} + (\rho_{g,e}\overline{\alpha}_{g,e})' v^*{}_{g,e} + (\rho_{g,e}\overline{\alpha}_{g,e})^* v'{}_{g,e} \\
&G_{g,e}{}^* = (\rho_{g,e}{}^*\overline{\alpha}_{g,e}{}^*)v_{g,e}{}^* \\
&v'{}_{g,e} = v'{}_{g,P^s} = d_e{}^{v_{g,Ps}}(p'_P - p'_E) \\
&(\rho_{g,e}\overline{\alpha}_{g,e})' = \frac{1}{\rho_{g,ref}}p'_e = \frac{1}{a^2}p'_e = \frac{1}{\gamma r T_e}p'_e = \frac{\rho_{g,e}{}^*\overline{\alpha}_{g,e}{}^*}{\gamma p_e{}^*}p'_e \\
&(\rho_{g,e}\overline{\alpha}_{g,e})' v^*_{g,e} = max(G_{g,e}{}^*, 0)\frac{1}{\gamma p_P{}^*}p'_P - max(-G_{g,e}{}^*, 0)\frac{1}{\gamma p_E{}^*}p'_E
\end{aligned} \tag{5.13}
$$

Where the superscript $^*$ indicate the guess value of the variable $\phi$ and the superscript $'$ means the correction of the variable $\phi$, assuming $\phi$ as the variable value, i.e. velocity, density or pressure. Using a first order numerical scheme upwind in convective terms and the above expressions, the pressure correction equation can be written in the following form:

$$
\begin{aligned}
&\Delta z\frac{\rho^*{}_{g,P}\overline{\alpha}^*{}_P}{\Delta t} + \frac{\Delta z}{\Delta t}\frac{\rho^*{}_{g,P}\overline{\alpha}^*{}_P}{\gamma p_P{}^*}p'_P - \Delta z\frac{\rho^o{}_{g,P}\overline{\alpha}^o{}_P}{\Delta t} + \\
&\Delta z\frac{\rho^*{}_{l,P}(1-\overline{\alpha}^*)_P}{\Delta t} + \frac{\Delta z}{\Delta t}\frac{\rho^*{}_{l,P}(1-\overline{\alpha}^*)_P}{\gamma p_P{}^*}p'_P - \Delta z\frac{\rho^o{}_{l,P}(1-\overline{\alpha}^o)_P}{\Delta t} + \\
&G_{g,e}{}^* + max(G_{g,e}{}^*, 0)\frac{1}{\gamma p_P{}^*}p'_P - max(-G_{g,e}{}^*, 0)\frac{1}{\gamma p_E{}^*}p'_E + \\
&[\rho_{g,e}\overline{\alpha}_{g,e}]^* d_e{}^{v_{g,Ps}}(p'_P - p'_E) + \\
&G_{l,e}{}^* + max(G_{l,e}{}^*, 0)\frac{1}{\gamma p_P{}^*}p'_P - max(-G_{l,e}{}^*, 0)\frac{1}{\gamma p_E{}^*}p'_E + \\
&[\rho_{l,e}(1-\overline{\alpha}_{g,e})]^* d_e{}^{v_{l,Ps}}(p'_P - p'_E) - \\
&G_{g,w}{}^* - max(G_{g,w}{}^*, 0)\frac{1}{\gamma p_W{}^*}p'_W + max(-G_{g,w}{}^*, 0)\frac{1}{\gamma p_P{}^*}p'_P - \\
&[\rho_{g,w}\overline{\alpha}_{g,w}]^* d_e{}^{v_{g,Ws}}(p'_W - p'_P) - \\
&G_{l,w}{}^* - max(G_{l,w}{}^*, 0)\frac{1}{\gamma p_W{}^*}p'_W + max(-G_{l,w}{}^*, 0)\frac{1}{\gamma p_P{}^*}p'_P - \\
&[\rho_{l,w}(1-\overline{\alpha}_{g,w})]^* d_e{}^{v_{l,Ws}}(p'_W - p'_P) = 0
\end{aligned} \tag{5.14}
$$

The void fraction equation can be obtained following a similar strategy of the pressure correction equation, the difference between the gas and the liquid continuity equations is used to find a gas void fraction equation. The liquid void fraction is evaluated using the geometric conservation equation $\alpha_g + \alpha_l = 1$. Then, the gas void fraction equation is expressed as:

$$\frac{1}{\Delta t}(\rho_{g,P}+\rho_{l,P})\overline{\alpha}_P+\frac{1}{\Delta z}[max(\rho_{g,P}v_{g,e},0)\overline{\alpha}_P+max(-\rho_{g,E}v_{g,e},0)\overline{\alpha}_E-$$
$$max(\rho_{g,W}v_{g,w},0)\overline{\alpha}_W-max(-\rho_{g,P}v_{g,w},0)\overline{\alpha}_P]+$$
$$\frac{1}{\Delta z}[max(\rho_{l,P}v_{l,e},0)\overline{\alpha}_P+max(-\rho_{l,E}v_{l,e},0)\overline{\alpha}_E-$$
$$max(\rho_{l,W}v_{l,w},0)\overline{\alpha}_W-max(-\rho_{l,P}v_{l,w},0)\overline{\alpha}_P]=$$
$$2\Gamma+\frac{\rho_{l,P}}{\Delta t}+\frac{{\rho^o}_{g,P}{\overline{\alpha}^o}_P}{\Delta t}-\frac{{\rho^o}_{l,P}(1-{\overline{\alpha}^o}_P)}{\Delta t}+\frac{1}{\Delta z}[\rho_{l,e}v_{l,e}-\rho_{l,w}v_{l,w}] \tag{5.15}$$

The gas and liquid energy equations have been obtained discretazing over the main mesh and using a first order scheme upwind in the convective terms. The difference between the discretized energy equation and the continuity equation multiplied by the value of enthalpy $H_{k,P}$ in the center of the CV are expressed in the following form:

$$\frac{{\rho^o}_{g,P}{\overline{\alpha}^o}_P\overline{H}_{g,P}}{\Delta t}-\frac{{\rho^o}_{g,P}{\overline{\alpha}^o}_P{\overline{H}^o}_{g,P}}{\Delta t}+$$
$$\frac{1}{A\Delta z}\left[max(-G_{g,e},0)A_e(\overline{H}_{g,e}-\overline{H}_{g,P})-max(G_{g,w},0)A_w(\overline{H}_{g,w}-\overline{H}_{g,P})\right]=$$
$$\left[\frac{q_{ig}P_{ig}}{A}\right]_P+\left[\frac{q_{wg}P_{wg}}{A}\right]_P+\Gamma[\overline{H}_{ig}-H_{g,P}]+\overline{\alpha}_P\frac{(p-p^o)_P}{\Delta t} \tag{5.16}$$

$$\frac{{\rho^o}_{l,P}(1-\overline{\alpha}^o)_P\overline{H}_{l,P}}{\Delta t}-\frac{{\rho^o}_{l,P}(1-\overline{\alpha}^o)_P{\overline{H}^o}_{l,P}}{\Delta t}+$$
$$\frac{1}{A\Delta z}\left[max(-G_{l,e},0)A_e(\overline{H}_{l,e}-\overline{H}_{l,P})-max(G_{l,w},0)A_w(\overline{H}_{l,w}-\overline{H}_{l,P})\right]=$$
$$\left[\frac{q_{il}P_{il}}{A}\right]_P+\left[\frac{q_{wl}P_{wl}}{A}\right]_P-\Gamma\left[\overline{H}_{il}-H_{l,P}\right]+(1-\overline{\alpha})_P\frac{(p-p^o)_P}{\Delta t} \tag{5.17}$$

The value of gas and liquid interfacial enthalpy $H_{ig}$ and $H_{il}$ are assumed to be equals to the gas saturated enthalpy and liquid saturated enthalpy values, respectively.

### 5.3.2 Heat conduction in solid element

To solve the solid element that contain the fluid flow, the energy equation is applied over each CV. A general heat conduction equation can be integrated, obtaining the following generic form:

$$\rho c_p \frac{(T_P - T_P^o)}{\Delta t} V_P = \dot{Q}_w + \dot{Q}_e + \dot{Q}_n + \dot{Q}_s \tag{5.18}$$

where the left hand side indicates the internal energy increase in the CV, while the right hand represents the inlet net heat flux through the CV-faces (west, east, north, and south). For the tube the different heat fluxes through the CV-faces are the consequence of convective heat transfer with the inner fluid in both phases, liquid and gas, together with axial heat conduction through the tube itself. These fluxes can be approximated as:

$$\begin{aligned}
\dot{Q}_w &= \lambda_w^t \left( \frac{T_{t,W} - T_{t,P}}{d_{PW}} \right) A_{t,in} \\
\dot{Q}_e &= \lambda_e^t \left( \frac{T_{t,E} - T_{t,P}}{d_{PE}} \right) A_{t,in} \\
\dot{Q}_s &= HT_{wl}(T_{l,P} - T_{t,P})\alpha\pi D_{i.t}\Delta z_P + HT_{wg}(T_{g,P} - T_{t,P})(1-\alpha)\pi D_{i.t}\Delta z_P \\
\dot{Q}_n &= HT_{f.sec}(T_{f.sec,P} - T_{t,P})\pi D_{o.t}\Delta z_P
\end{aligned}$$

where $T_t$ is the wall temperature, $T_l$ and $T_g$ are the liquid and gas fluid temperatures, $d_{PW}$ and $d_{PE}$ are the distance between nodes, $A_{t,in}$ is the cross-section of the tube, and $HT_{wk}$ is the heat transfer coefficients of the liquid or gas phase. If some fluid is in contact with the external surface, a heat transfer coefficient $HT_{f.sec}$ and a temperature $T_{f.sec}$ will be defined.

The boundary conditions in the west and the east extreme nodes of the tubes can be a fix temperature or a null heat flux. The north face of the CV's tube can consider a convective heat transfer or a heat flux applied.

## 5.4 Empirical Information

Factors such as frictional coefficients, heat transfer coefficients and interfacial area are obtained by means of empirical correlations. Geometry, inclination, velocities and boundary conditions are some parameters that help to find the kind of regimen present into the pipes. A good definition of the regimen is required in order to select the most suitable empirical correlation. A simplified flow regimen map proposed to steam-water system [7] and a flow regimen map proposed to boiling in refrigeration system [10] have been combined to define a general flow regimen map which helps to define a pattern flow present in the fluid flow along the tube.

The empirical expressions of stratified and annular regimen flow have been used due to it is the regimen flow presented in the cases studied. If some other regimen has

to be taken into account, the empirical information must be changed and a validation of the new expression is required. Now, a short summary of the empirical expressions used in this work are listed.

The momentum equations require the evaluation of the frictional shear stress at the wall and at the interface. The interfacial friction is defined as:

$$\tau_{ig} = -\tau_{il} = \frac{1}{2} C_D \rho_g |v_g - v_l| (v_g - v_l) A_i \tag{5.19}$$

where the interfacial friction factor $C_D$ is defined as the maximum value between $\frac{64.0}{Re_i}$ and $\frac{0.3164}{(Re_i)^{1/4}}$ evaluated the interfacial Reynolds number as $Re_i = \frac{D_i \rho_g |v_g - v_l|}{\mu_g}$, where the equivalent wetted diameter is defined as $D_i = \frac{\alpha \pi D}{(\omega + sin\omega)}$. The interfacial area is defined as $A_i = 4sin\omega/(\pi D)$ in function of the angle $\omega$, which represents the angle between the vertical symmetry axis and the intersection of the liquid level.

The pressure drop at the wall are defined including only the wall shear effect, others as abruptly change area or loses due to elbows are not considering here. The Lockhart-Martinelli model is applied to evaluate the pressure drop in two-phase flow. Then, the pressure drop of two-phase flow is obtained from the pressure drop evaluated assuming only one phase, liquid or gas, and using the two-phase multiplier ${\Phi_l}^2$ or ${\Phi_g}^2$ in the following form:

$$\begin{aligned} \left(\frac{dp}{dz}\right)_{2\phi} &= {\Phi_l}^2 \left(\frac{dp}{dz}\right)_l = {\Phi_g}^2 \left(\frac{dp}{dz}\right)_g \\ \left(\frac{dp}{dz}\right)_k &= f_k \frac{G^2}{2\rho_k D} \end{aligned} \tag{5.20}$$

where k represents liquid or gas and $f_k$ is the friction factor and is defined in function of Reynolds number.

The two-fluid model require a partitioning of the pressure drop and the determination of related shear stress for liquid and gas [7], using a parameter $Z^2$ is possible to define the shear stresses of liquid and gas in the following manner:

$$\begin{aligned} \tau_g &= \alpha \left(\frac{dp}{dz}\right)_{2\phi} \left(\frac{1}{\alpha + (1-\alpha)Z^2}\right) \frac{A}{P_{wg}} \\ \tau_l &= (1-\alpha) \left(\frac{dp}{dz}\right)_{2\phi} \left(\frac{Z^2}{\alpha + (1-\alpha)Z^2}\right) \frac{A}{P_{wl}} \end{aligned} \tag{5.21}$$

$$Z^2 = \frac{f_l \rho_l {v_l}^2 \frac{\alpha_{lw}}{\alpha_l}}{f_g \rho_g {v_g}^2 \frac{\alpha_{gw}}{\alpha_g}} \tag{5.22}$$

where $\alpha_{gw} = \frac{\omega}{\pi}$ and $\alpha_{lw} = 1 - \alpha_{gw}$ are the liquid and gas fraction on the wall and these are defined in function of the angle $\omega$ in stratified regimen flow.

The mass flux per unit volume transfered through interface can be defined as the sum of the mass transfered at the interface $\Gamma_i$ due to the energy exchanged between phases, and the mass transfer from the wall to interface $\Gamma_w$ due to the external heat transfer, in the following form:

$$\begin{aligned}
\Gamma_w &= \frac{q_{wl} P_{wl}}{(H_{g,sat} - H_l)} \\
\Gamma_i &= -\frac{\left[\left(\frac{q_{il} P_{il}}{A}\right) - \Gamma_w (H_{g,sat} - H_l) + \left(\frac{q_{ig} P_{ig}}{A}\right)\right]}{(H_{g,sat} - H_l)} \\
\Gamma &= \Gamma_w + \Gamma_i
\end{aligned} \tag{5.23}$$

The heat transfer at the interface is evaluated by means of the heat transfer coefficient and the difference between saturated condition and liquid or gas phase temperature in the following form:

$$\begin{aligned}
\left[\frac{q_{il} P_{il}}{A}\right] &= HT_{il}(T_{sat} - T_l) + \Gamma_w (H_{g,sat} - H_l) \\
\left[\frac{q_{ig} P_{ig}}{A}\right] &= HT_{ig}(T_{sat} - T_g)
\end{aligned} \tag{5.24}$$

The interfacial heat transfer coefficients per unit volume $HT_{il}$ and $HT_{ig}$ for liquid and gas, respectively are evaluated in next form:

$$\begin{aligned}
&if \quad (T_{sat} > T_l) \\
&\quad HT_{il} = \frac{\lambda_l}{D_l}\left[(0.023 {Re_l}^{0.8} F12) - 3.81972 \frac{(T_{sat} - T_l)\rho_l cp_l}{[\rho_g H_{lg} max(4\alpha, 1)]}\right] A_i \\
&else \\
&\quad HT_{il} = \frac{\lambda_l}{D_l}(0.023 {Re_l}^{0.8}) A_i
\end{aligned} \tag{5.25}$$

$$\begin{aligned}
&if \quad (T_{sat} < T_g) \\
&\quad HT_{ig} = \frac{\lambda_g}{D_g}\left[(0.023 {Re_g}^{0.8}) + (4e^5 \; F \max[0, (0.25\alpha)])\right] A_i \\
&else \\
&\quad HT_{il} = 0.0
\end{aligned} \tag{5.26}$$

The heat transfer at the wall is calculated using the difference between wall and fluid phase temperature, the superficial area wetted by phase and the heat transfer coefficient. The heat transfer coefficients of the liquid at the wall is evaluated in function of the nucleate pool boiling $HT_{nb}$ and the convective liquid flow boiling $HT_{cb}$ with next empirical expressions:

$$\begin{aligned} HT_{cb} &= \frac{\lambda_l}{D} 0.0133 {Re_l}^{0.69} {Pr_l}^{0.4} \\ HT_{nb} &= 55 {P_r}^{0.12} [-log_{10} P_r]^{-0.55} M^{-0.5} q^{0.67} \\ HT_{wl} &= [{HT_{cb}}^3 + {HT_{nb}}^3]^{1/3} \end{aligned} \tag{5.27}$$

where $Re_l$ is the Reynolds number and $Pr_l$ is the Prandtl number of liquid, $P_r$ is the reduced pressure, $M$ is the fluid molecular weight, and $q$ is the heat flux applied.

The heat transfer coefficient of the gas at the wall is evaluated by means of the maximum value between two expressions of the form $CRe^m Pr^n$, following the Dittus-Bolter correlation.

$$HT_{wg} = \frac{\lambda_g}{D} \left[ max(0.0797 {Re_g}^{0.6774} {Pr_g}^{0.333}, 0.023 {Re_g}^{0.8} {Pr_g}^{0.4}) \right] \tag{5.28}$$

All of these expressions have been taken from the nuclear reactors literature [2][7][11] and a flow boiling model [33] [34]. Now, with the empirical expression defined to both phases and the interaction between phases and the wall, the set of algebraic equation can be resolved by means the numerical algorithm proposed above.

### 5.4.1 Thermo-physical properties

The thermo-physical properties for both fluids and the solid elements are evaluated locally at each control-volume, for each time step and iteration. All thermodynamic properties of the refrigerant are evaluated at the grid nodes by means of the REFPROP program [35], as function of the pressure and enthalpy. When the fluid used in the simulation is steam water, thermodynamic properties are obtained from the NIST-STEAM program [36]. For the solid elements, Eckert and Drake [37] values have been implemented.

## 5.5 Numerical Solution

The numerical resolution of the discretized equations described above has been obtained ordering these equations in a generic discretized form $a_P \phi_P = a_E \phi_E + a_W \phi_W + b_P$. The set of algebraic equations is solved using the three diagonal matrix algorithm

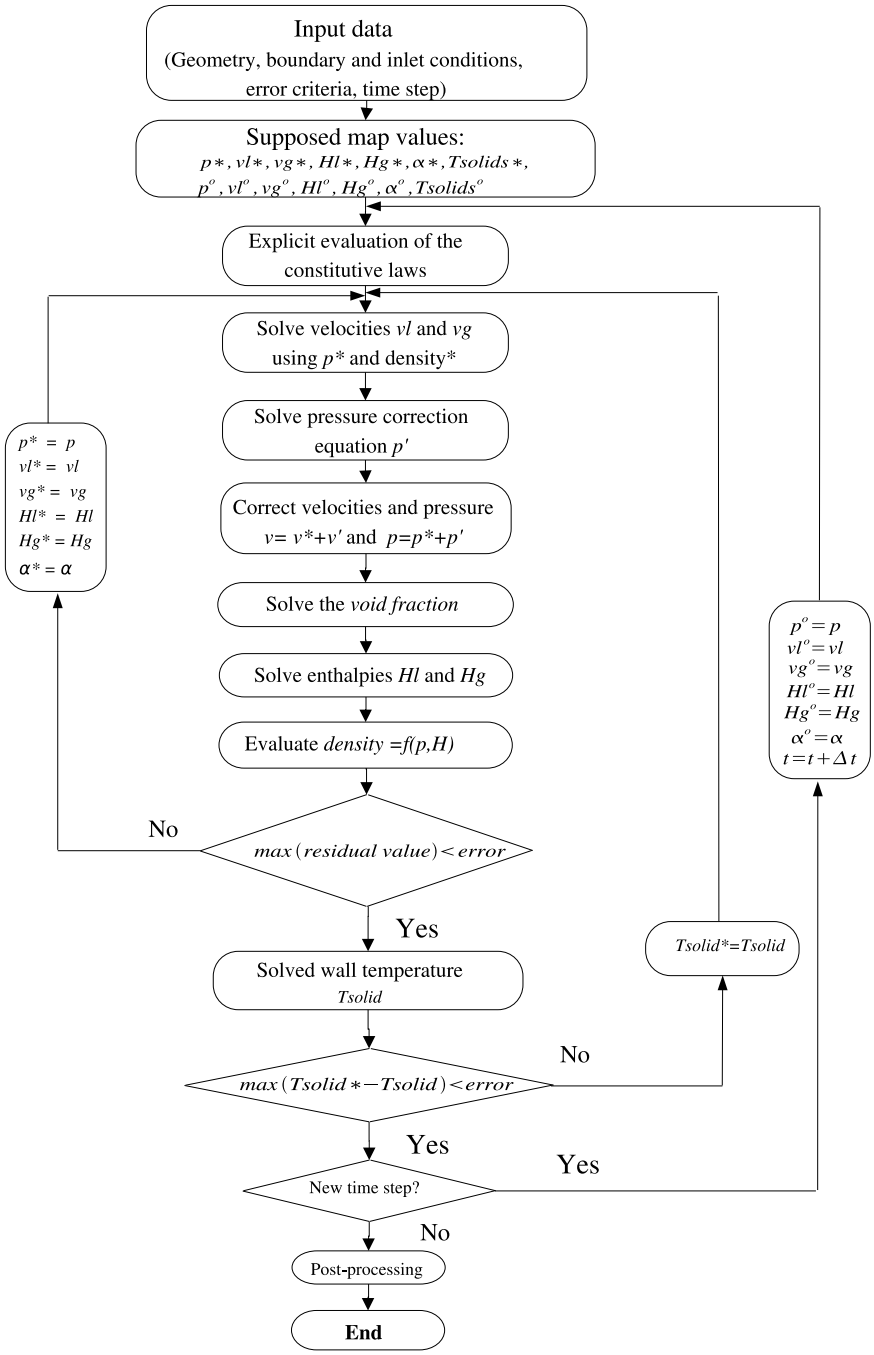


**Figure 5.4:** Numerical algorithm of the two fluid model 1D

TDMA. The coupling between momentum and continuity is solved by means of the semi-implicit pressure based method similar to SIMPLE method use in single phase flow [29]. Although this method has been commonly used in single-phase flow due to it is quite robust, when two-phase flow is present in the flux some complications can appear in the solution of the equation, due to some modifications must be considered [24]. The global algorithm consists of solving implicitly velocities $v_k$, using guess pressure $p^*$ and density ${\rho_k}^*$ fields. After that, solve the pressure correction equation to obtain the pressure correction value $p'$ and correct with it the velocities $v_k = {v_k}^* + {v_k}'$, pressure $p = p* + p'$ and densities $\rho_k = \frac{\rho_k p'}{\varphi p*}$. Next, the void fraction $\alpha$, together with the energy equations in function of enthalpy $H_k$ are solved using the updated values of pressure and velocities. Finally, the density fields must be update with the new values of pressure and enthalpy. Return to the first step and an iterative process should be make until the convergence criteria is reached. The interface momentum and energy terms have been evaluated explicitly, this criteria helps to find a solution when the interface terms are more large. The global algorithm depicted in Figure 5.4 has been used to analyse the two-phase flow into the pipes, obtaining good results [38].

## 5.6 Validation of the mathematical model

The validation of the mathematical model developed in this thesis to solve the one-dimensional two-phase flow into the pipes using a two-fluid model is carried out by means of the well-known water faucet problem.

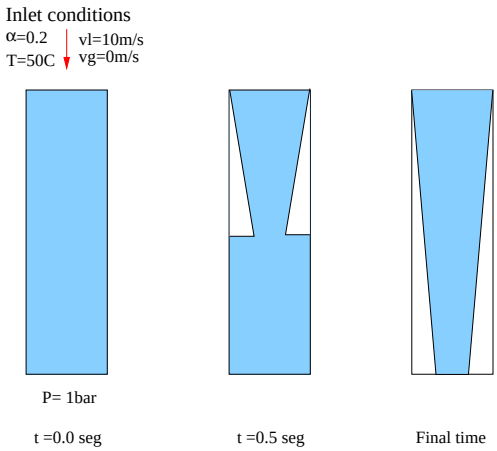


**Figure 5.5:** Water faucet representation

This is a transient case reported as benchmark proof in two-fluid models works, [39]. It consists of a vertical pipe with 12 meters of length and 1 meter of diameter. Pipe is filled with water to next conditions: inlet void fraction 0.2, gas velocity 0.0 $m/s$, liquid velocity 10 $m/s$ and temperature of fluid 50 $^oC$, and outlet pressure of 1.0 x $10e^5$ $Pa$. Figure 5.5 shows an schematic representation of this case.

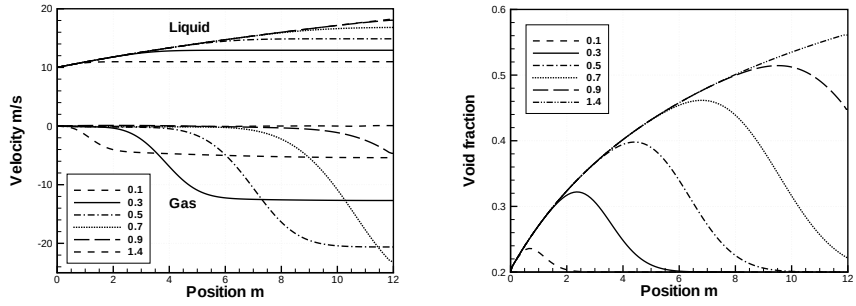


**Figure 5.6:** Water faucet results along the time

The water faucet assumes that frictional forces and thermal effects on interface are negligible, because they have a minor effect and is possible to obtain a simplification of the problem. It case helps to see the gravity effect over the acceleration of the fluid. Illustrative results of this transient case are depicted in Figure 5.6, where evolution of the void fraction, and liquid and gas velocities are shown at different times.

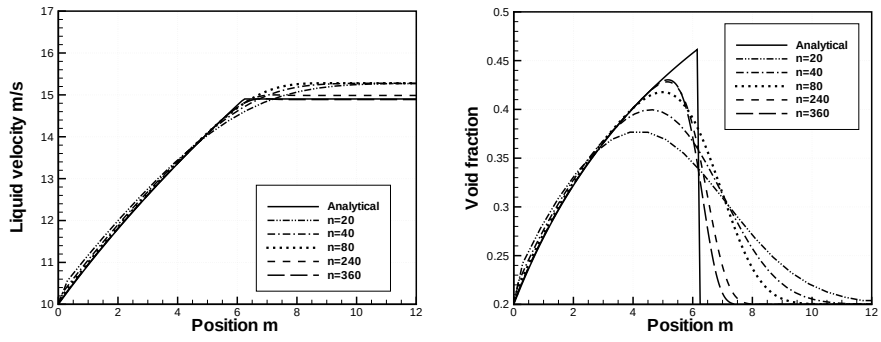


**Figure 5.7:** Analytical and numerical comparison at 0.5 seconds of water faucet case

Four meshes has been proof 20 CVs, 40 CVs, 80 CVs and 240 Cvs, with a $1.0e^{-8}$ as convergence criteria and a time rate of 0.0005 $s$ were used to solve this case. A comparison of the transient case with analytical solution at 0.5 $s$ to void fraction and liquid velocity are depicted in Figure 5.7. Results obtained with the numerical model proposed are quite similar to results reported by Cortes [40]. If the grid number is increased, the numerical solution will be more near to the analytical solution..

## 5.7 Application of TFM in a refrigerant evaporator

A horizontal evaporator, using R134a as refrigerant fluid, has been chosen to analyse the numerical solution of the two-phase flow applying the two-fluid model TFM explained in this chapter. First, the application of the TFM and a comparison with experimental data has been carried out. Next, a comparative between the numerical results obtained with the quasi-homogeneous model QHM and the two-fluid model TFM is presented.

### 5.7.1 Numerical solution using TFM

A group of four cases of a horizontal evaporator, using R134a as refrigerant fluid, in steady-state condition have been used to show quality of the numerical results obtained with the two-fluid model TFM proposed in this chapter.

Four different cases have been simulated and numerical results are compared with experimental data. The experimental data are obtained from an experimental set-up presented in Chapter 3. Measurement of the wall and fluid temperatures and the pressure along the evaporator are used to contrast the numerical results.

**Table 5.1:** Inlet conditions of the evaporation cases

| Case | $T_{ev}$ $[^oC]$ | $p_{ev}$ $[kPa]$ | $G$ $[kg/m^2s]$ | $q_{ev}$ $[W]$ |
|---|---|---|---|---|
| D1 | -0.86 | 296 | 64.78 | 3573.3 |
| D2 | -5.50 | 249 | 51.80 | 2985.1 |
| D3 | -10.13 | 208 | 39.96 | 2418.9 |
| D4 | -19.73 | 139 | 21.95 | 1143.5 |

The geometry description of the evaporator consists of a copper tube of 6 m length with an internal diameter of 8.15 $mm$, different heat flux can be applied on the external surface of the tube by means of a set of electric resistances. The conditions of the refrigerant fluid (R134a) at the inlet are detailed in Table 5.1.

All of these cases have the characteristic of a stratified flow regimen, then the empirical correlations for the heat transfer coefficient and pressure drop have been

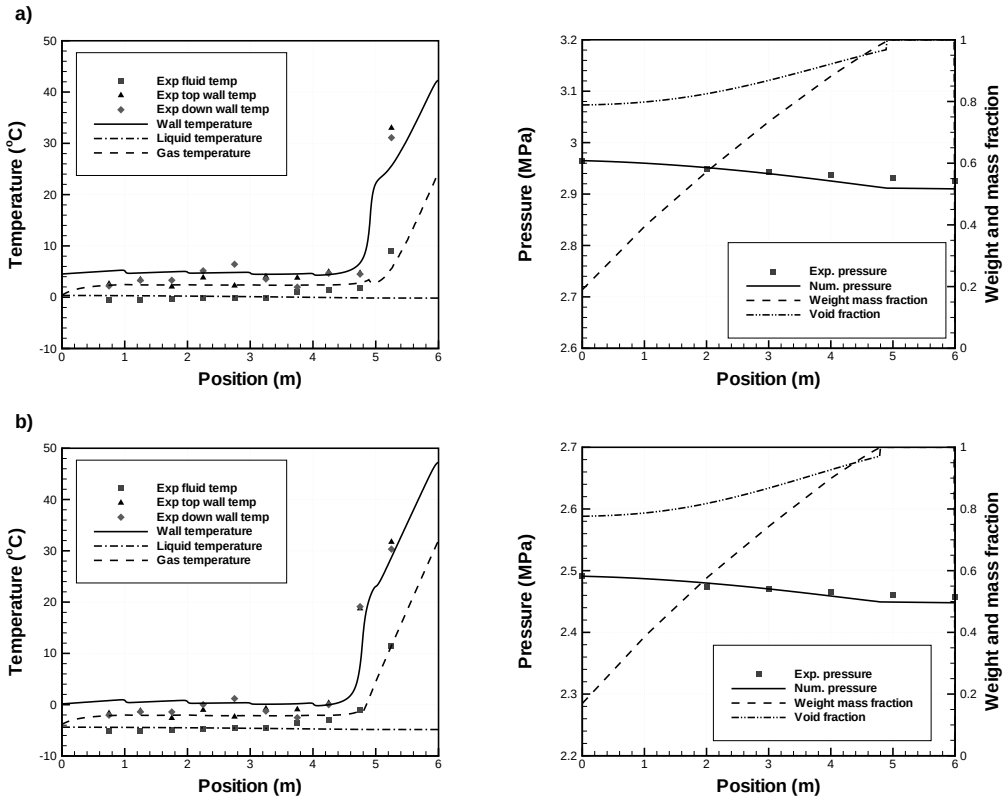


**Figure 5.8:** Numerical and experimental comparison of the temperatures and pressure: a) case D1; b) case D2.

chosen in function of this flow. The wall and fluid temperatures, the pressure drop, the void fraction and the weight mass fraction profiles of each one of the cases are depicted in Figures 5.8 and 5.9.

The numerical wall temperature present an over-prediction in cases D1, D2 and D3, however in case D4 is quite near to the experimental data. The numerical gas temperature predicted by the method is always near to the experimental wall temperature while the fluid is in two-phase zone, when the fluid pass to single-phase gas the gas temperature present the same behaviour of the experimental fluid temperature.

The numerical pressure drop present an under-prediction in cases D1 and D2 at the outlet of the tube, while in cases D3 and D4 the prediction is quite good. The

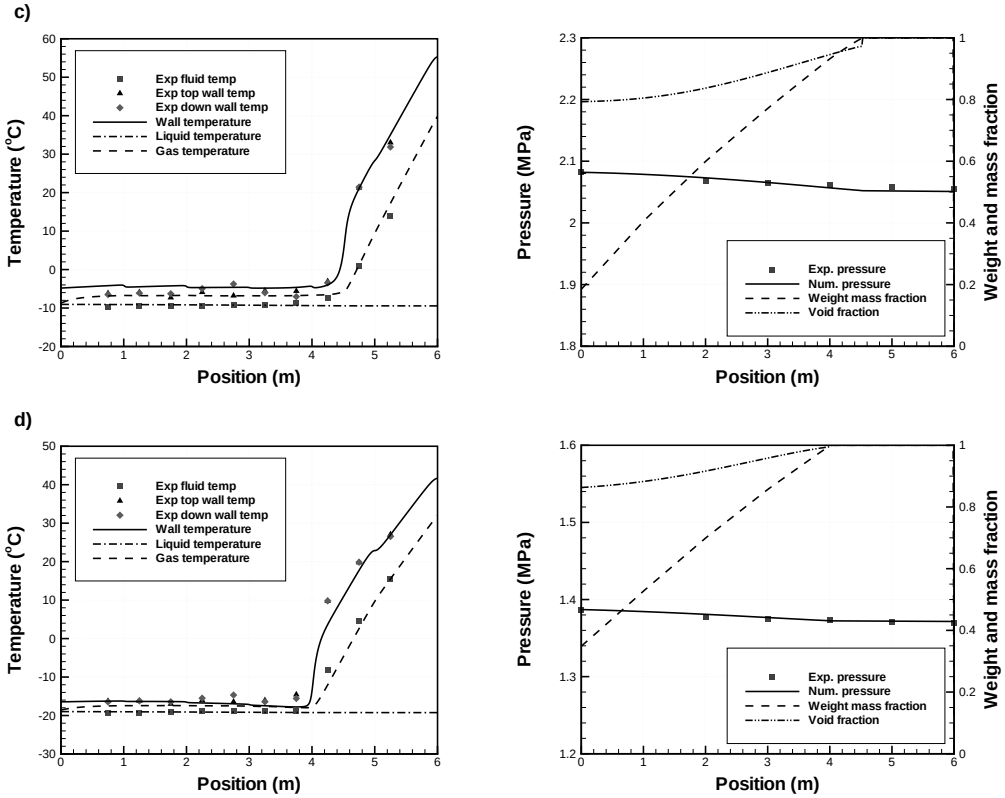


**Figure 5.9:** Numerical and experimental comparison of the temperature and pressure: c) case D3; d) case D4.

quantity of mass flow affect directly the empirical correlation of the frictional forces and as result the pressure drop prediction is not enough good. However, the difference of the pressure drop does not produce a strong effect on the fluid temperature.

Although the agreement between numerical results and experimental data of the temperature and pressure are good in all cases, is important to clarify that the fluid temperature measured is at the middle of the diameter and is not possible predict which phase (liquid or gas) is being measured, only in the point when the fluid is completely gas and an abrupt change of the wall and fluid temperature is detected.

### 5.7.2 Comparative analysis - TFM vs. QHM

The second case is the evaporator explained above with next boundary conditions at the inlet: gas velocity 1.0686 $m/s$, liquid velocity 0.2586 $m/s$, pressure 3.8918e5 $Pa$, fluid temperature 8.12 $^oC$ and a void fraction of 0.769. An external distribution of heat flux is applied along of the tube, following next powers values for meter: 6333.1, 5475.5, 4881.7, 4683.9, 4024.1 and 3364.4 $W/m^2$.

A comparison between numerical results obtained with the quasi-homogeneous model QHM presented in Chapter 2 and the two-fluid model TFM presented in this chapter are shown in Figure 5.10. This case presents stratified flow along of the test tube. This fact have been evaluated by means of the different criteria to define which regimen flow is present in function of velocities and void fraction. Shorts differences have been obtained between both models in temperatures, pressure, void fraction and weight mass fraction values. However, there are a difference in the liquid velocity value between both models. While QHM predict that liquid velocity is always going down until arrive to zero, the TFM predicts that value is increased trying to follow the gas velocity behaviour. Finally, the liquid velocity begins to go down when is near to the point where two-phase flow pass to single-phase gas flow and the value goes to zero. The behaviour of the liquid velocity predicted by the TFM can be understand how the influence of the drag force applied on the liquid phase by the gas phase at the interface, while the QHM only can describe that the value of the liquid velocity always decrease because the mass of liquid is reducing along of the pipe.

After the numerical results comparison between the models proposed in this thesis, the same case is analysed using the TFM model with two different form to evaluate the interfacial drag force term. Then, the influence of the empirical correlation on the numerical results can be seen in the comparison of TFM-A and TFM-B, together with a experimental data. The experimental data has been obtained by means of an experimental unit [30]. Figure 5.11 depicts the behaviour of the pressure, void fraction, temperature and velocity distributions of gas and liquid.

Important differences are noted in the liquid velocity and temperatures between TFM-A and TFM-B results. Firstly, the prediction of the point where the fluid flow pass from two-phase to single-phase gas flow by the TFM-A is better than the TFM-B in comparison with experimental data. This point affects the wall and fluid temperature distribution. Secondly, the liquid velocity value presents an increase in both results. Although a continuous increase of the liquid velocity value until the liquid vanish into the tube is predicted by the TFM-B, the TFM-A predicts smaller increase in the liquid velocity than TFM-B and a decreasing when the liquid phase begin to vanishing into the tube. Finally, both pressure distribution along the pipe present a similar behaviour of the experimental data. However, an over-prediction is reported in TFM-A, while an under-prediction is reported by the results of TFM-B.

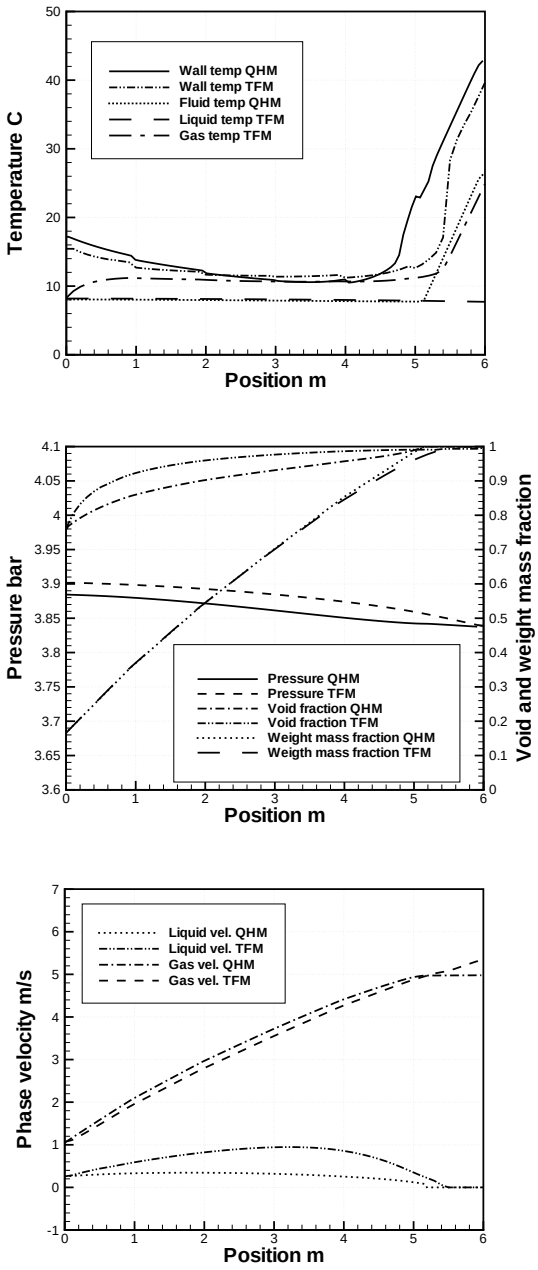


**Figure 5.10:** Numerical models comparison (Quasi-Homogeneous Model QHM and Two-Fluid Model TFM)

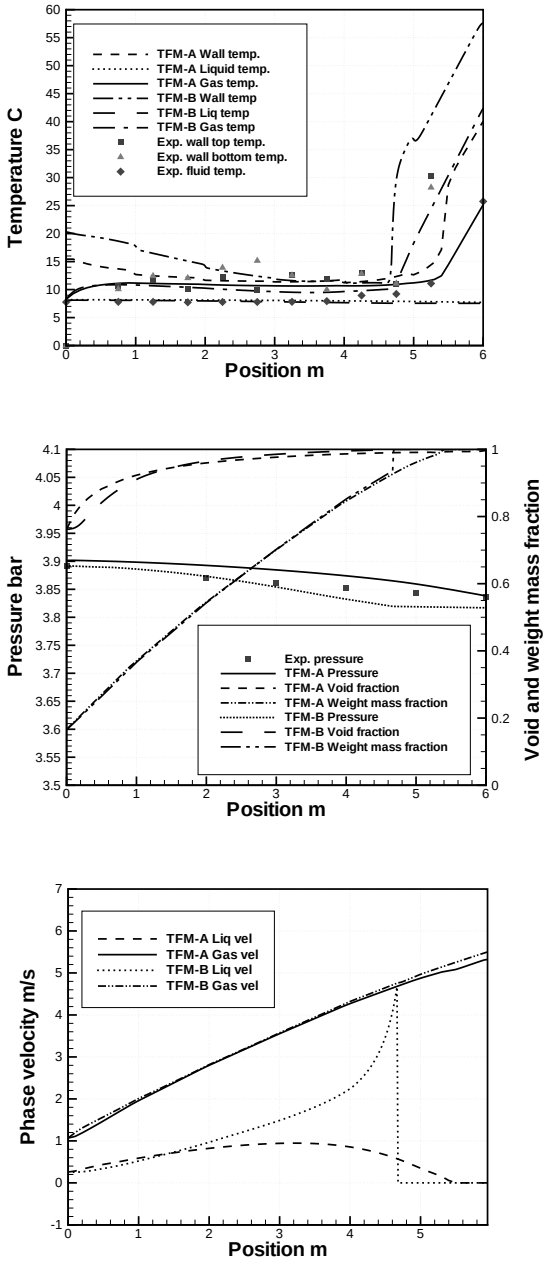


**Figure 5.11:** A numerical and experimental comparison using the two-fluid model

## 5.8 Conclusions

This chapter has presented the mathematical formulation and discretization of the one-dimensional two-fluid model. The solution methodology of the discretized equations is based on a semi-implicit pressure method, quite often used in the solution of the single-phase flow. Some important aspects has been taken into account to solve the two-phase flow into the pipes. A set of empirical correlations have been assumed into the numerical model to evaluate the stratified and the annular regimen flow presented in the steady-state cases shown. The validation and verification of the code have been presented with a benchmark case and a comparison between the numerical results and experimental data. Finally, a comparison between quasi-homogeneous and two-fluid model has been considered and differences between their numerical results have been presented. An important aspect to emphasize is how the two-fluid model gives more detailed information about the fluid flow, i.e. gas and liquid velocities and temperatures, than the quasi-homogeneous model. An important role of the empirical correlations on the good agreement of the numerical results with the experimental data has been shown in this comparison. The application of the two-fluid model to refrigerant systems allows a clearer understanding of the two-phase flow phenomena into evaporators and condensers.

## 5.9 Nomenclature

A cross section area ($m^2$)
C virtual mass coefficient
D diameter ($m$)
$cp$ heat capacity ($J\ kg^{-1}K^{-1}$)
$d_{PE}$ distance between nodes P and E
$d_{PW}$ distance between nodes P and W
$e$ specific total energy ($J\ kg^{-1}$)
$e_c$ specific kinetic energy ($J\ kg^{-1}$)
$e_p$ specific potential energy ($J\ kg^{-1}$)
f friction factor
g acceleration of gravity ($m\ s^{-2}$)
G mass flow rate per area ($kg\ s^{-1}\ m^{-2}$)
H specific enthalpy ($J\ kg^{-1}$)
HT heat transfer coefficient ($W\ m^{-2}K^{-1}$)
$\dot{m}$ mass flow rate ($kg\ s^{-1}$)
M molecular weight ($kg$)
P perimeter ($m$)
p pressure ($Pa$)

$\dot{Q}$ heat flux ($W$)
$\dot{q}$ heat flux per unit area ($W\ m^{-2}$)
S surface area ($m^2$)
T temperature ($^oC$)
V volume ($m^3$)
v velocity ($m\ s^{-1}$)

**Greek symbols**
$\alpha$ void fraction
$\Delta t$ time step ($s$)
$\Delta z$ length of control volume (m)
$\lambda$ thermal conductivity ($W\ m^{-1}\ K^{-1}$)
$\Gamma$ mass transfer rate per unit volume ($kg\ s^{-1}m^{-3}$)
$\rho$ density ($kg\ m^{-3}$)
$\mu$ viscosity ($Nsm^{-2}$)
$\tau$ shear stress ($N\ m^{-2}$)
$\theta$ angle of inclination

**Super- and Subscripts**
i interface
g gas or vapour
l liquid
w wall
e,w,n,s east, west, north and south CV-faces
P main grid node associated to main CVs
E,W,N,S nearest east, west, north and south nodes associated to main grid node P
sat saturation condition

# References

[1] Kleinstreuer C. *Two-Phase Flow: Theory and applications.* Taylor and Francis, 2003.

[2] S. Levy. *Two-phase flow in complex system.* Willey, 1999.

[3] G. B. Wallis. *One-dimensional two-phase flow.* McGraw-Hill, 1969.

[4] T. Hibiki and M. Ishii. One-dimensional drift-flux model and constitutive equations for relative motion between phase in various two-phase flow regimes. *International Journal of Heat and Mass Transfer*, 46:4935–4948, 2003.

[5] Jean-Marc Delhaye. Some issues related to the modeling of interfacial areas in gas-liquid flows I. The conceptual issues. *Comptes Rendus de l'Académie des Sciences*, 329(5):397–410, 2001.

[6] M. Ishii and T. Hibiki. *Thermo-fluid dynamics of two-phase flows.* Springer, 2006.

[7] Idaho National Engineering Laboratory. *RELAP5/MOD3 Code Manual. Volumen IV: Models and correlations*, 2001.

[8] D. Bestion. The physical closure laws in the CATHARE code. *Nuclear Engineering and Design*, 124(3):229–245, 1990.

[9] I. Tiselj, A. Hovard, G. Cerne, J. Gale, I. Parzer, B. Mavko, M. Giot, J. M. Seynhaeve, B. Kucienska, and H. Lemonnier. WAHA3 Code manual. Technical report, Jozef Stefan Institute, 2004.

[10] L. Wojtan, T. Ursenbacher, and J.R. Thome. Investigation of flow boiling in horizontal tubes: part I - a new diabatic two-phase flow pattern map. *International Journal of Heat and Mass Transfer*, 48(14):2955–2969, 2005.

[11] M. Ishii. Two-fluid model and hydrodynamic constitutive relations. *Nuclear Engineering and Design*, 82(2-3):107–126, 1984.

[12] A. Ullmann and N. Brauner. Closure relations for two-fluid models for two-phase stratified smooth and stratified wavy flows. *International Journal of Multiphase Flow*, 32:82–105, 2006.

[13] R. Issa, S. Bonizzi, and S. Barbeau. Improved closed models for gas entrainment and interfacial shear for slug flow modelling in horizontal pipes. *International Journal of Multiphase Flow*, 32:1287–1293, 2006.

[14] J. M. Delhaye, M. Giot, and M. L. Riethmuller. *Thermohydraulics of two-phase systems for industrial design and nuclear engineering.* Hemisphere Publishing Corporation, 1981.

[15] G. Yadigaroglu and R. Lahey. On the various forms of the conservation equations in two-phase flow. *International Journal of Multiphase Flow*, 2(5-6):477–494, 1976.

[16] I. Tiselj and S. Petelin. Modelling of two-phase flow with second-order accurate scheme. *Journal of Computational Physics*, 136:503–521, 1997.

[17] J. Song and M. Ishii. The one-dimensional two-fluid model with momentum flux parameters. *Nuclear Engineering and Design*, 205(1-2):101–115, 2001.

[18] I. Toumi and A. Kumbaro. An approximate linealized Riemmann solver for two-fluid model. *Journal of Computational Physics*, 124:286–300, 1996.

[19] J. Song and M. Ishii. On the stability of a one-dimensional two-fluid model. *Nuclear Engineering and Design*, 204(1-3):101–115, 2001.

[20] J. Zhou and M. Z. Podowski. Modeling and analysis of hydrodynamic instabilities in two-phase flow using two-fluid model. *Nuclear Engineering and Design*, 204(1-3):129–142, 2001.

[21] Yang Liang and Zhang Chun-Lu. Two-fluid model of refrigeration two-phase flow through short tube orifice. *International Journal of Refrigeration*, 28(3):419–427, 2005.

[22] W. Sripattranpan, T. Wongchang, and S. Wongwises. Heat transfer and two-phase flow characteristics of refrigerants flowing under varied heat flux in a double-pipe evaporator. *Heat and Mass Transfer*, 40:653–664, 2004.

[23] C. C. Wang. A numerical method for thermally non-equilibrium condensing flow in a double-pipe condenser. *Applied Thermal Engineering*, 17(7):647–660, 1997.

[24] M. Darwish and F. Moukalled. A unified formulation of the segregated class of algorithms for multiphase flow at all speeds. *Numerical Heat Transfer, Part B*, 40:99–137, 2001.

[25] M. R. Ansari and V. Shokri. New algorithm for the numerical simulation of two-phase stratified gas-liquid flow and its application for analyzing the Kelvin-Helmholtz instability criterion with respect to wavelength effect. *Nuclear Engineering and Design*, 237:2302–2310, 2007.

[26] W. H. Lee and R. W. Lyczkowski. The basic character of five two-phase flow model equation sets. *International Journal for Numerical Methods in Fluids*, 33:1075–1098, 2000.

[27] T. F. Miller and D. J. Miller. A fourier analysis of the IPSA/PEA algorithms applied to multiphase flows with mass transfer. *Computers and Fluids*, 32:197–221, 2003.

[28] C. Moon-Sun, P. Seung-Kyung, and C. Keun-Skin. A numerical study of two-phase flow using a two-dimensional two-fluid model. *Numerical Heat Transfer, Part A*, 45:1049–1066, 2004.

[29] S. V. Patankar. *Numerical Heat Transfer and Fluid Flow*. Hemisphere Publishing Corporation, 1980.

[30] J. Rigola, S. Morales, G. Raush, and C. D. Pérez-Segarra. Analysis of two-phase flow in double-pipe condensers and evaporators with special emphasis on transition zones: Numerical model and experimental comparison. In *Proceedings of the 2004 International Refrigeration and Air Conditioning Conference at Purdue*, pages 1–10, 2004.

[31] S. Morales, J. Rigola, C. D. Pérez-Segarra, and A. Oliva. Analysis of two-phase flow in Condensers and Evaporators based on Two-Fluid models: Numerical Model and Experimental Comparison. In *Proceedings of the 11th International Refrigeration and Air Conditioning Conference at Purdue*, pages 1–8, 2006.

[32] S. Kakac and F. Mayinger. *Two-phase flows and heat transfer*. Hemisphere Publishing Corporation, 1976.

[33] N. Kattan, J.R. Thome, and D. Favrat. Flow boiling in horizontal tubes: part 1 - development of a diabatic two-phase flow pattern map. *Journal of Heat Transfer - Transactions of Asme*, 120(1):140–146, 1998.

[34] N. Kattan, J.R. Thome, and D. Favrat. Flow boiling in horizontal tubes: part 3 - development of a new heat transfer model based on flow pattern. *Journal of Heat Transfer - Transactions of Asme*, 120(1):156–165, 1998.

[35] NIST. Thermodynamic properties of refrigerants and refrigerant mixtures database (REFPROP). Version 6.0, 1998.

[36] A. H. Harvey, A. P. Peskin, and S. A. Klein. NIST/ASME Steam Properties (NIST Standard Database 10), Version 2.2, 2000.

[37] E. R. G. Eckert and R. M. Drake Jr. *Analysis of Heat and Mass Transfer*. McGraw-Hill, 1972.

[38] S. Morales, J. Rigola, C. D. Pérez-Segarra, and A. Oliva. Numerical Resolution of Two-fluid Models Equation for Condensation and Evaporation Flow in Ducts Using a Pressure Based Method. In *Proceedings of the 11th International Refrigeration and Air Conditioning Conference at Purdue*, pages 1–8, 2008.

[39] G.F. Hewitt. *Multiphase Fluid Flow and Pressure Drop,Heat Exchanger Design Handbook*. Hemisphere Publishing Corporation, 1983.

[40] J Cortes. On the construction of upwind schemes for non-equilibrium transient two-phase flows. *Computers and Fluids*, 31:159–182, 2002.

# Chapter 6

# Analysis of two-phase flow using two-fluid models. Two dimensional case

**Abstract.**

A numerical method to simulate the two-fluid model in two spatial dimension is described. The discretization of the governing equations has been developed by means of the finite volume technique, based on a bi-dimensional and transient integration of the conservative equations using a staggered mesh. A semi-implicit pressure based method is used to solve the pressure distribution, the velocity field, and the volume fraction distribution of the each phase.

## 6.1 Introduction

The industrial applications and importance of study the two-phase flow phenomena has been mentioned in last chapters. A technique to solve the two-phase flow phenomena in two spatial dimension using the two-fluid model so-called interpenetrating model will be developed.

Different numerical techniques for the simulation of the multifluid flows have been proposed in the literature. Methods as the direct simulations of multiphase flows involving solid particles, immersed body methods (e.g. Volume-of-fluid VOF, Level set method, the phase-field method), the Lattice Boltzmann model for multiphase flow, the point-particle methods for disperse flows and methods based on the averaging of the conservative equations have been developed by different researchers. A complete description of each one the methods is presented by Prosperetti et al.[1].

The two-fluid models are methods based on the averaging of the conservative equations, which are the most suitable for resolve the complex flows present in real applications such as fluidised beds, pipelines, energy generation, sediment transport, etc.

The two-fluid model is characterised for the continuum formulation proposed by Ishii [2], each point of the domine is occupied simultaneously (in variable proportions) by both phases (e.g. liquid and gas). Each phase is thus governed by its own conservation equations and constitutive laws.

The constitutive laws have a high influence on the solution of the two-phase flow, and different models in function of the regimen flow have been developed to define the interelation between phases (gas and liquid) and each one of the phases with the wall. The one-dimensional two-fluid model always requires a group of empirical expressions, above of nine parameters are needed, to find out the solution.

The extension of the one-dimensional two-fluid model to the two-dimensional two-fluid model represent a first step to the numerical simulation of the two-phase flow based on the CFD methodology usually applied in single-phase. This extension to two-phase flow is defined as computational multi-fluid dynamic CMFD [3]. The CMFD methods are still under developmet in comparison with the CFD methods to solve single-phase. The CMFD methodology is looking for obtain numerical results less dependend of the constitutive laws and a better description the two-phase flow phenomena.

The solution of the two-fluid model is based on a segregated method derived from the pressure-based method widely used in the single-phase flow resolution [4]. Two ways to solve the two-phase flow has been developed, the implicit multi-field algorithms (IMF) proposed by the group of the Los Alamos Scientific Laboratory and the inter-phase slip algorithm (IPSA) developed by the Spalding group at Imperial College. However, Darwich et al. [5] has proposed a new classification of the techniques for simulate the multifluid flow, the mass conservation based algorithm (MCBA) and

the geometric conservation based algorithm (GCBA) formulation.

An alternative methodology to resolve the models based on a averaging of the conservative equations are the coupled methods. These methods have been used widely in the nuclear reactor thermo hydraulic safety codes, such as RELAP5 or TRAC, and are preferable than segregated methods if the time scale are very short, in other words these methods are designed to deal principally with a very fast transient problems. Into these methods there are different strategies to solve the numerical equations. First-order methods [6] using a semi-implicit method or fully-implicit method have been applied to find the solution of the two-phase flow, but the numerical diffusion error as consequence of use upwind or donored schemes is an important problem of these methods. Then, a high-resolution schemes [7] have been implemented to improve the numerical result obtained with first-order (see details in [1]).

This chapter is focused on detailed two-dimensional numerical simulation of phase change phenomena gas-liquid flow, using a only one fluid. The basic field equation, following the transient two-fluid model, consists of two continuity equations and four momentum equations. The volume fraction conservation equation is added to complete the mathematical set of equation to be solved. Then, velocities, pressure and volume fraction are obtained. The numerical mass conservation based algorithm MCBA has been used to solve the two-phase flow, following the methodology to solve the multi-phase flow presented by Moukalled et al.[8].

The energy equation is not considering in the develop of this two-dimensional two-fluid model, because a isothermal condition is assumed in the fluid flow. This hypothesis is used in different papers, where only solve the continuity and momentum equation, non assuming the effect of the energy equations on the pressure correction equation [9][10]. This assumption helps to build a first model capable to resolve numerically the coexistence of two phases in a cavity, and its is a firts step to a complete resolution of the two-phase flow in a cavity by means of the two-fluid model.

After solve the numerical model, two transient cases have been used to verified the numerical results obtained with the present model. The sedimentation case [11] and the collapse liquid column case [12] are used as benchmark cases. These cases are reported widely in the scientific literature. The numerical results and a comparison of each case are shown.

## 6.2 Mathematical formulation

The mathematical formulation proposed in this Chapter to solve the two-phase flow is based on the average volume conservative equations presented in Chapter 5. An extension to two spacial dimensions of one-dimensional mathematical model presented above assuming a negligible influence of the energy, is presented. From the general balance equation 5.4, the mass or continuity equation and the momentum equation

can be expresed as:

$$\frac{\partial(\alpha_k \rho_k)}{\partial t} + \bigtriangledown \cdot (\alpha_k \rho_k u_k) = \Gamma_k \tag{6.1}$$

$$\frac{\partial(\alpha_k \rho_k \vec{u_k})}{\partial t} + \bigtriangledown \cdot (\alpha_k \rho_k \vec{u_k}\vec{u_k}) = - \bigtriangledown (\alpha_k p_k) + \bigtriangledown \cdot [\tau_k] + F_{M,k} \tag{6.2}$$

with

$$\tau_k = \bigtriangledown \cdot \left[ \alpha_k \mu_k \left( \bigtriangledown u_k + \bigtriangledown {u_k}^T - \frac{2}{3} (\bigtriangledown \cdot u_k) I \right) \right] \tag{6.3}$$

$$F_{M,g} = K|u_l - u_g|(u_l - u_g) + \alpha_g \rho_g g \tag{6.4}$$

where $F_{M,g}$ is the forces on the gas phase, K is the interface drag parameter and last terme is the mass force. The evaluation of the $F_{M,l}$ is given by a similar expression with the indices g and l interchanged.

Assuming that the fluid flow is laminar, incompressible, isothermal, both phases have the same pressure and there is not transference of mass through the interface, the mathematical formulation can be re-written as:

$$\rho_k \frac{\partial \alpha_k}{\partial t} + \bigtriangledown \cdot (\alpha_k \rho_k u_k) = 0 \tag{6.5}$$

$$\rho_k \frac{\partial \alpha_k \vec{u_k}}{\partial t} + \bigtriangledown \cdot (\alpha_k \rho_k \vec{u_k}\vec{u_k}) = - \bigtriangledown (\alpha_k p) + \bigtriangledown \cdot (\alpha_k \mu_k \bigtriangledown \vec{u_k}) + F_{M,k} \tag{6.6}$$

Six-equations should be solved, two continuity and four momentum equations, to find a solution of a two dimensional two-phase flow without heat and mass exchanged.

## 6.3 Discretization

The differential equations proposed above can be written in the following form:

$$\rho_k \frac{\partial \alpha_k \phi_k}{\partial t} + \bigtriangledown \cdot (\alpha_k \rho_k u_k \phi_k) = \bigtriangledown \cdot (\Upsilon \alpha_k \bigtriangledown \phi_k) + S \tag{6.7}$$

where the first term $\rho_k \alpha_k \frac{\partial \phi_k}{\partial t}$ is the accumulation of the variable $\phi_k$, the second term is the net flux of the convective stream $\bigtriangledown \cdot (\alpha_k \rho_k u_k \phi_k)$, the third term is the net flux of the $\phi_k$ as consequence of the diffusive stream $\bigtriangledown \cdot (\Upsilon \alpha_k \bigtriangledown \phi_k)$ and the last term is the generation of the variable $\phi_k$ per volume unit $S$.

The mass continuity equation and the momentum equation are expressed in function of the convection-diffusion equation following the convention of next table:

| Equation | $\phi$ | $\Upsilon$ | $S$ |
|---|---|---|---|
| Continuity | 1 | 0 | 0 |
| Momentum in X | $u_k$ | $\mu_k$ | $\alpha_k \frac{\partial p}{\partial x} + F_M$ |
| Momentum in Y | $v_k$ | $\mu_k$ | $\alpha_k \frac{\partial p}{\partial y} + F_M$ |

The convection-diffusion equation can be expressed as an algebraic expression applying the control volume technique based on the finite volume grid depicted in Figure 6.1, a specific control volume is shown in Figure 6.2, where the staggered mesh is used in the x-y plane to solve the velocities. Using an implicit method with a first order scheme, the discretization equation can be written as:

$$\begin{aligned} &\frac{(\alpha\rho\phi)^{n+1}{}_{k,P} - (\alpha\rho\phi)^{n}{}_{k,P}}{\Delta t}\Delta x\Delta y + \\ &[(\alpha\rho u\phi)^{n+1}{}_{k,e} - (\alpha\rho u\phi)^{n+1}{}_{k,w}]\Delta y + [(\alpha\rho v\phi)^{n+1}{}_{k,n} - (\alpha\rho v\phi)^{n+1}{}_{k,s}]\Delta x = \\ &[(\alpha\Upsilon\frac{\partial\phi}{\partial x})^{n+1}{}_{k,e} - (\alpha\Upsilon\frac{\partial\phi}{\partial x})^{n+1}{}_{k,w}]\Delta y + [(\alpha\Upsilon\frac{\partial\phi}{\partial y})^{n+1}{}_{k,n} - (\alpha\Upsilon\frac{\partial\phi}{\partial y})^{n+1}{}_{k,s}]\Delta x + \\ &S_p{}^{n+1}\Delta x\Delta y \end{aligned} \tag{6.8}$$

Using the concept of the total flux (convection plus diffusion) defined as:

$$J_x = (\alpha\rho u\phi - \alpha\Upsilon\frac{\partial\phi}{\partial\times})_k \tag{6.9}$$

$$J_y = (\alpha\rho v\phi - \alpha\Upsilon\frac{\partial\phi}{\partial y})_k \tag{6.10}$$

The general equation that represent the momentum, and continuity equation can be written as:

$$\begin{aligned} &\frac{(\alpha\rho\phi)^{n+1}{}_{k,P} - (\alpha\rho\phi)^{n}{}_{k,P}}{\Delta t}\Delta x\Delta y + \\ &[J_{k,e} - J_{k,w}]^{n+1} + [J_{k,n} - J_{k,s}]^{n+1} = S_c + S_p\phi_p{}^{n+1}\Delta x\Delta y \end{aligned} \tag{6.11}$$

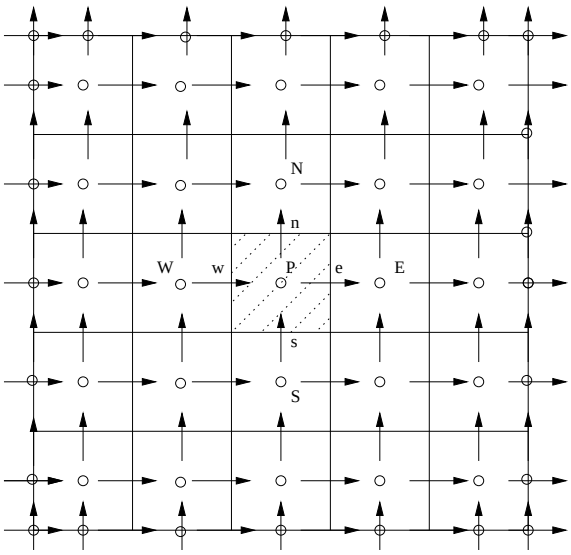


**Figure 6.1:** Partially staggered arrangement on the finite volume grid

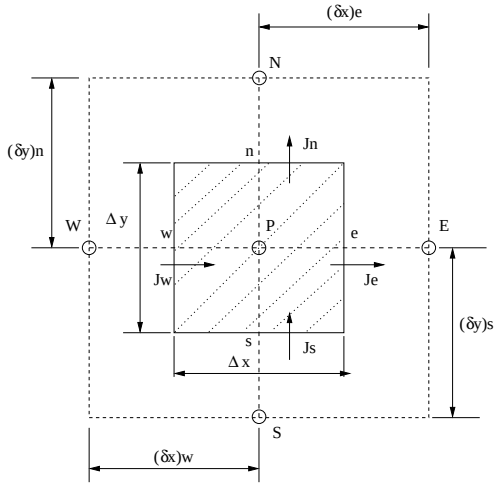


**Figure 6.2:** Control volume for two dimensional situation

The continuity equation formulated from the last equation is expressed as:

$$\frac{(\alpha\rho)^{n+1}{}_{k,P} - (\alpha\rho)^{n}{}_{k,P}}{\Delta t}\Delta x\Delta y + \\ [F_{k,e} - F_{k,w}]^{n+1} + [F_{k,n} - F_{k,s}]^{n+1} = 0 \tag{6.12}$$

Multiplying the equation 6.12 by the variable $\phi_p$ and subtract it from equation 6.11 a new equation to solve the momentum equation is obtained:

$$(\phi^{n+1} - \phi^{n})_{k,P}\frac{(\alpha\rho)^{n}{}_{k,P}}{\Delta t}\Delta x\Delta y + (J_{k,e} - F_{k,e}\phi_{k,P})^{n+1} - (J_{k,w} - F_{k,w}\phi_{k,P})^{n+1} + \\ (J_{k,n} - F_{k,n}\phi_{k,P})^{n+1} - (J_{k,s} - F_{k,s}\phi_{k,P})^{n+1} = S_p{}^{n+1}\Delta x\Delta y \tag{6.13}$$

where

$$\begin{aligned} F_{k,e} &= (\alpha\rho u)_{k,e}\Delta y \quad F_{k,w} = (\alpha\rho u)_{k,w}\Delta y \\ F_{k,n} &= (\alpha\rho v)_{k,n}\Delta x \quad F_{k,s} = (\alpha\rho v)_{k,s}\Delta x \\ D_{k,e} &= (\frac{\alpha\Upsilon}{\delta\times})_{k,e}\Delta y \quad D_{k,w} = (\frac{\alpha\Upsilon}{\delta\times})_{k,w}\Delta y \\ D_{k,n} &= (\frac{\alpha\Upsilon}{\delta y})_{k,n}\Delta x \quad D_{k,s} = (\frac{\alpha\Upsilon}{\delta y})_{k,s}\Delta x \end{aligned} \tag{6.14}$$

Expressing the difference between the total fluxes and the convective flux as:

$$\begin{aligned} J_{k,e} - F_{k,e}\phi_{k,P} &= (D_e + \| - F_e, 0.0\|)(\phi_P - \phi_E) \\ J_{k,w} - F_{k,w}\phi_{k,P} &= (D_w + \|F_w, 0.0\|)(\phi_W - \phi_P) \\ J_{k,n} - F_{k,n}\phi_{k,P} &= (D_n + \| - F_n, 0.0\|)(\phi_P - \phi_N) \\ J_{k,s} - F_{k,s}\phi_{k,P} &= (D_s + \|F_s, 0.0\|)(\phi_S - \phi_P) \end{aligned} \tag{6.15}$$

The general momentum equation can be re-written as:

$$(\phi^{n+1} - \phi^{n})_{k,P}\frac{(\alpha\rho)^{n}{}_{k,P}}{\Delta t}\Delta x\Delta y + \\ (D_e + \| - F_e, 0.0\|)(\phi_P - \phi_E) - (D_w + \|F_w, 0.0\|)(\phi_W - \phi_P) + \\ (D_n + \| - F_n, 0.0\|)(\phi_P - \phi_N) - (D_s + \|F_s, 0.0\|)(\phi_S - \phi_P) = \\ S_p{}^{n+1}\Delta x\Delta y \tag{6.16}$$

The two-dimensional discretization equation for solve the velocity $u_k$ can be written in the general form as:

$$a_P u_P = a_E u_E + a_W u_W + a_N u_N + a_S u_S + b \tag{6.17}$$

where the coefficients are:

$$\begin{aligned}
a_P &= (\alpha\rho)^n{}_{k,P}\frac{\Delta x\Delta y}{\Delta t} + a_E + a_W + a_N + a_S \\
a_E &= (D_e + \| - F_e, 0.0\|) \\
a_W &= (D_w + \|F_w, 0.0\|) \\
a_N &= (D_n + \| - F_n, 0.0\|) \\
a_S &= (D_s + \|F_s, 0.0\|) \\
b &= (\alpha\rho)^n{}_{k,P}\frac{\Delta x\Delta y}{\Delta t} + \alpha_P{}^{n+1}(p_w - p_e)^{n+1}\Delta y + F_M
\end{aligned}$$

Following the same way, the momentum equation to solve the velocity $v_k$ can be expressed as:

$$a_P v_P = a_E v_E + a_W v_W + a_N v_N + a_S v_S + b \tag{6.18}$$

where the coefficients are:

$$\begin{aligned}
a_P &= (\alpha\rho)^n{}_{k,P}\frac{\Delta x\Delta y}{\Delta t} + a_E + a_W + a_N + a_S \\
a_E &= (D_e + \| - F_e, 0.0\|) \\
a_W &= (D_w + \|F_w, 0.0\|) \\
a_N &= (D_n + \| - F_n, 0.0\|) \\
a_S &= (D_s + \|F_s, 0.0\|) \\
b &= (\alpha\rho)^n{}_{k,P}\frac{\Delta x\Delta y}{\Delta t} + \alpha_P{}^{n+1}(p_s - p_n)^{n+1}\Delta y + F_M
\end{aligned}$$

The pressure correction equation can be obtained from the continuity equation of the liquid and gas phases. Summing both equations, a new expression can be obtained:

$$\frac{\partial(\alpha\rho)_g}{\partial t} + \frac{\partial(\alpha\rho)_l}{\partial t} + \bigtriangledown\cdot(\alpha\rho u)_g + \bigtriangledown\cdot(\alpha\rho u)_l = 0 \tag{6.19}$$

The discretization of the equation 6.19 on the main control volume give as result:

$$\begin{aligned}&\frac{(\alpha\rho)_{g,P}{}^{n+1} - (\alpha\rho)_{g,P}{}^{n}}{\Delta t}\Delta x\Delta y + \frac{(\alpha\rho)_{l,P}{}^{n+1} - (\alpha\rho)_{l,P}{}^{n}}{\Delta t}\Delta x\Delta y + \\ &[(\alpha\rho u)_{g,e} - (\alpha\rho u)_{g,w}]^{n+1}\Delta y + [(\alpha\rho u)_{l,e} - (\alpha\rho u)_{l,w}]^{n+1}\Delta y + \\ &[(\alpha\rho v)_{g,n} - (\alpha\rho v)_{g,s}]^{n+1}\Delta x + [(\alpha\rho v)_{l,n} - (\alpha\rho v)_{l,s}]^{n+1}\Delta x = 0 \end{aligned} \tag{6.20}$$

Considering the relations between the assuming values of $u_k{}^*$ and their respective correction value $u_k{}'$ as a function of the pressure correction value $p'$, the convective term can be evaluated as:

$$\begin{aligned}&(\alpha\rho u)_{k,e} = (\alpha\rho)_e u_e{}^* + (\alpha\rho)_e u_e{}' \\ &u_e{}' = d_e{}^u(p_P{}' - p_E{}') \\ &(\alpha\rho u)_{k,e} = (\alpha\rho)_e u_e{}^* + (\alpha\rho)_e d_e{}^u(p_P{}' - p_E{}')\end{aligned}$$

Using last expressions the pressure correction equation can be expressed in the general discretization form for two spatial dimension as:

$$a_P p'_P = a_E p'_E + a_W p'_W + a_N p'_N + a_S p'_S + b \tag{6.21}$$

where the coefficients are:

$$\begin{aligned}
a_E = &\quad \left[(\alpha\rho)_{g,e} d_e{}^{u_g} + (\alpha\rho)_{l,e} d_e{}^{u_l}\right]\Delta y \\
a_W = &\quad \left[(\alpha\rho)_{g,w} d_w{}^{u_g} + (\alpha\rho)_{l,w} d_w{}^{u_l}\right]\Delta y \\
a_N = &\quad \left[(\alpha\rho)_{g,n} d_n{}^{v_g} + (\alpha\rho)_{l,n} d_n{}^{v_l}\right]\Delta x \\
a_S = &\quad \left[(\alpha\rho)_{g,s} d_s{}^{v_g} + (\alpha\rho)_{l,s} d_s{}^{v_l}\right]\Delta x \\
a_P = &\quad a_E + a_W + a_N + a_S \\
b = &\quad [(\alpha\rho)_{g,P}{}^{n} + (\alpha\rho)_{l,P}{}^{n} - (\alpha\rho)_{g,P}{}^{n+1} - (\alpha\rho)_{l,P}{}^{n+1}]\frac{\Delta x\Delta y}{\Delta t} - \\
&(\alpha\rho)_{g,e} u_{g,e}{}^* - (\alpha\rho)_{l,e} u_{l,e}{}^* + (\alpha\rho)_{g,w} u_{g,w}{}^* + (\alpha\rho)_{l,w} u_{l,w}{}^* - \\
&(\alpha\rho)_{g,n} v_{g,n}{}^* - (\alpha\rho)_{l,n} v_{l,n}{}^* + (\alpha\rho)_{g,s} v_{g,s}{}^* + (\alpha\rho)_{l,s} v_{l,s}{}^*
\end{aligned}$$

The volume fraction equation for each phase can be obtained from the continuity equation of the gas and liquid phases equation, respectively.

$$\frac{\partial(\alpha\rho)_k}{\partial t} + \bigtriangledown \cdot (\alpha\rho u)_k = 0 \tag{6.22}$$

The discretization of the equation 6.22 on the main control volume give as result:

$$\frac{(\alpha\rho)_{k,P}{}^{n+1} - (\alpha\rho)_{k,P}{}^{n}}{\Delta t}\Delta x\Delta y + [(\alpha\rho u)_{k,e} - (\alpha\rho u)_{k,w}]^{n+1}\Delta y + [(\alpha\rho v)_{k,n} - (\alpha\rho v)_{k,s}]^{n+1}\Delta x = 0 \tag{6.23}$$

The volume fraction equation expressed in the general discretization form is:

$$a_P\alpha_P = a_E\alpha_E + a_W\alpha_W + a_N\alpha_N + a_S\alpha_S + b \tag{6.24}$$

with

$$\begin{aligned}
a_P = \quad & [\rho_{k,P}]^{n+1}\frac{\Delta x\Delta y}{\Delta t} + \|(\rho_P u_e)_k, 0.0\|\Delta y - \| - (\rho_P u_w)_k, 0.0\|\Delta y + \\
& \|(\rho_P v_n)_k, 0.0\|\Delta x - \| - (\rho_P v_s)_k, 0.0\|\Delta x \\
a_E = \quad & -\| - (\rho_E u_e)_k, 0.0\|\Delta y \\
a_W = \quad & \|(\rho_W u_w)_g, 0.0\|\Delta y \\
a_N = \quad & -\| - (\rho_N v_n)_g, 0.0\|\Delta x \\
a_S = \quad & \|(\rho_S v_s)_g, 0.0\|\Delta x \\
b = \quad & [\alpha_{k,P}\rho_{k,P}]^n\frac{\Delta x\Delta y}{\Delta t}
\end{aligned}$$

The volume fraction of liquid and gas phase can be obtained from the solution of the last equation. However, the values obtained may not satisfy the constraint $\alpha_l + \alpha_g = 1.0$, due to numerical errors. Then, a way to solve this problem is re-evaluate the volume fraction values using the following expression:

$$\alpha_k = \frac{\alpha_k{}^*}{\alpha_l{}^* + \alpha_g{}^*} \tag{6.25}$$

where the $\alpha_k{}^*$ values are obtained from solution of equation 6.24 for each phase.

This is one kind of solution to avoid the accumulation of numerical error and the negative effect on the volume fraction value. Different strategies can be applied on the volume fraction equation to avoid numerical error in the evaluation of the value. One

of these is solve the volume fraction of gas phase implicitly accounting the influence of the liquid phase on the gas. Bounding the volume fractions value (i.e. between 0 and 1) is other mechanism to avoid errors during the iterative process (for details on these improvements see [1] [5] ).

## 6.4 Numerical solution

The numerical solution of the velocities, pressure correction and volume fraction equations described above has been carried out. The set of algebraic equations are solved using a successive over-relaxation method known as SOR. By means of this method, the value of the variable ${\phi^{n+1}}_P$ is obtained as function of the discretized coefficient above detailed, the neigbouring values of the variable $\phi$ and the relation factor $w$, (for details see [13]):

$$ {\phi^{n+1}}_P = \omega \frac{Q_P - a_S {\phi_S}^{n+1} - a_N {\phi_N}^{n+1} - a_E {\phi_S}^{n} - a_W {\phi_S}^{n}}{a_P} + (1-\omega){\phi^{n}}_P \qquad (6.26) $$

The coupling between momentum and continuity is solved by means of the semi-implicit pressure based method similar to SIMPLE method use in single phase flow [4]. Although this method has been commonly used in single-phase flow due to it is quite robust, if two-phase flow is present in the flux, some improvements will be taken into account to avoid problems in the convergence [5]. One of these is the evaluation of the interfacial force terms, which should be evaluated explicitly.

The global algorithm consists of solving implicitly velocities $u_K$ and $v_k$ from equation 6.17 and 6.18, using guess pressure $p^*$ field. After that, solve the pressure correction equation 6.21. The pressure correction value $p'$ helps to correct the velocities $u_k = {u_k}^* + {u_k}'$ and $v_k = {v_k}^* + {v_k}'$ values, and the pressure $p = p* + p'$. Next, the volume fraction $\alpha_k$ is solved from equation 6.24 using the updated values of pressure and velocities. The volume fraction values should be re-evaluated in function of the equation 6.25 to satisfy the constraint $\alpha_l + \alpha_g = 1.0$. Finally, the errors of each one of the variables calculated, velocities, pressure correction and volume fractions, together with the mass residue are compared with the value of the convergence criteria selected. If not convergence is reached return to the first step and an iterative process should be make until the errors will be less than convergence criteria value. When, errors and mass residue satisfy the convergence criteria a new time step should be resolve until steady-state conditions or a specif time in a transient case will be reach. The global algorithm is shown in Figure 6.3.

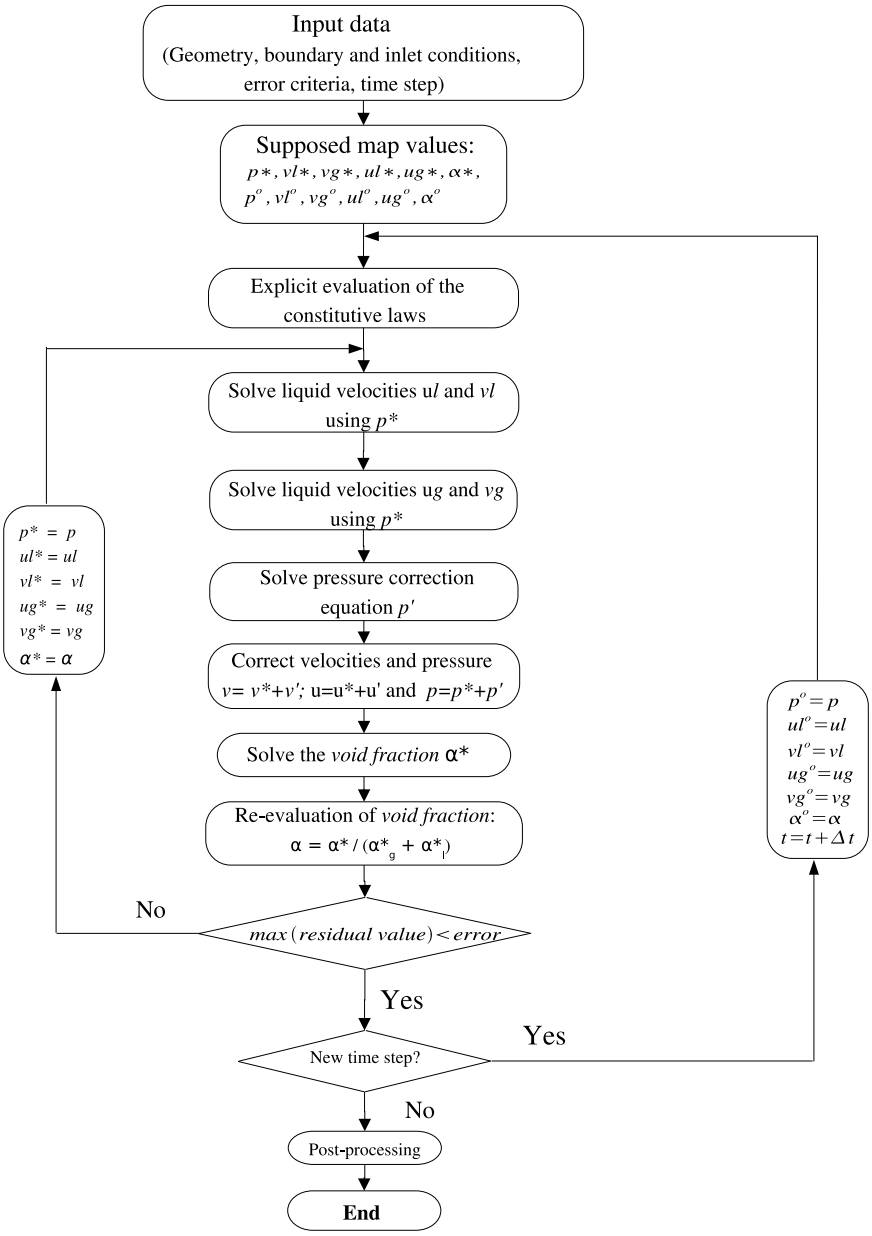


**Figure 6.3:** Algorithm to solve two-phase flow in two dimensional cases

## 6.5 Validation and verification

The validation and verification of the numerical method developed to solve the two-phase flow explained above have been carried out using two cases. The first case is a separation problem or sedimentation problem proposed by Coquel et al. [11], and the second case is a collapse of a liquid column proposed by Moe and Bendiksen [12].

### 6.5.1 Sedimentation case

The sedimentation case consist of a a vertical tube of 7.5 m length. In the initial state, the tube is filled with stagnant liquid and gas with a uniform pressure of 0.1 $MPa$ and a uniform volume fraction of 0.5. The tube is closed at both ends. The velocities are considered as zero at the end points. The phase separation is due to gravity force only, any other forces are considered in this case. The liquid phase falls down to the bottom of the tube, while the gas come up to the top of the tube. An schematic representation of the case is depicted in Figure 6.4.

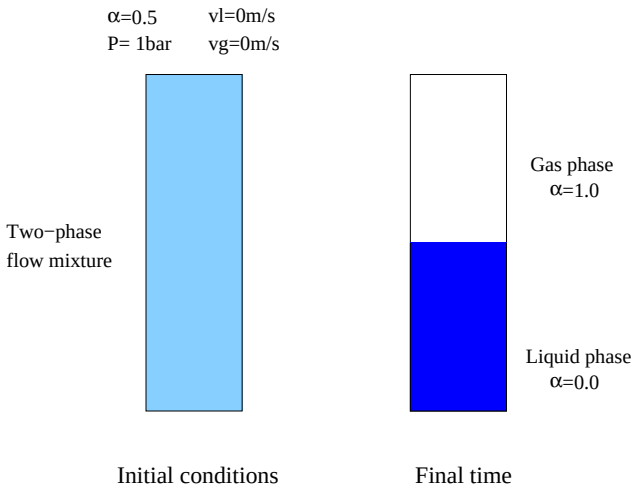


**Figure 6.4:** Sedimentation case.

The results have been obtained using a mesh of 40x40 CVs, a time step of $\Delta t = 1e^{-3}$s and assuming the liquid and gas density as 1000 $kg/m^3$ and 1.0 $kg/m^3$, respectively.

The numerical results have been compared with a analytical solution obtained from scientific literature, where a mathematical expressions assuming that the pressure variation can be negleted and the liquid is accelerated by gravity only until it is

abruptly brought into the stagnant conditions at lower part of the tube are proposed (for details see Evje and Fläten [7][14]).

The numerical results of the volume fraction of gas and the liquid velocity at 0.6s and 1.0s are used to compare with the analytic reference results. The numerical results obtained with the two-fluid model explained in this chapter are represented by the continuous line while the reference is shown with broken line in Figure 6.5.

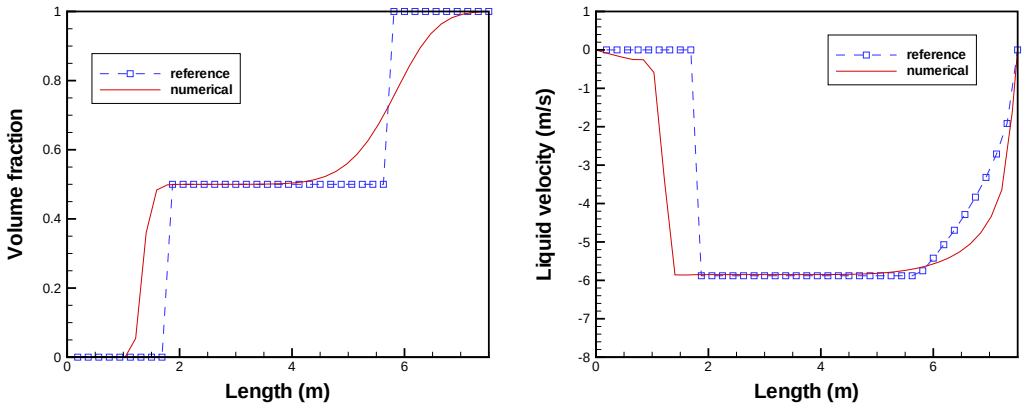


**Figure 6.5:** Comparison between numerical and reference results of volume fraction and liquid velocity at 0.6s.

The volume fraction of gas, the pressure, the liquid velocity and the gas velocity profiles along the vertical length of the tube at 1.0s are depicted in Figure 6.6.

The comparison between numerical results and analytical expression show how the numerical model proposed give a similar result, following the same tendency along the tube of the variables presented, volume fraction of gas, liquid velocity and pressure. Some differences appear between the numerical and reference results, the separation point between gas and liquid phases is predicted to occur before in the numerical model proposed in this work than the analytic results. The pressure and the liquid velocity profile are affected for this under prediction of the separation point.

An illustrative description of the volume fraction variable in the domine is depicted in figures 6.7, where the evolution of the volume fraction in the time along the vertical tube has been registred. This figure shows how the phases begin to separated and both configure two fronts, one upward and another downward.

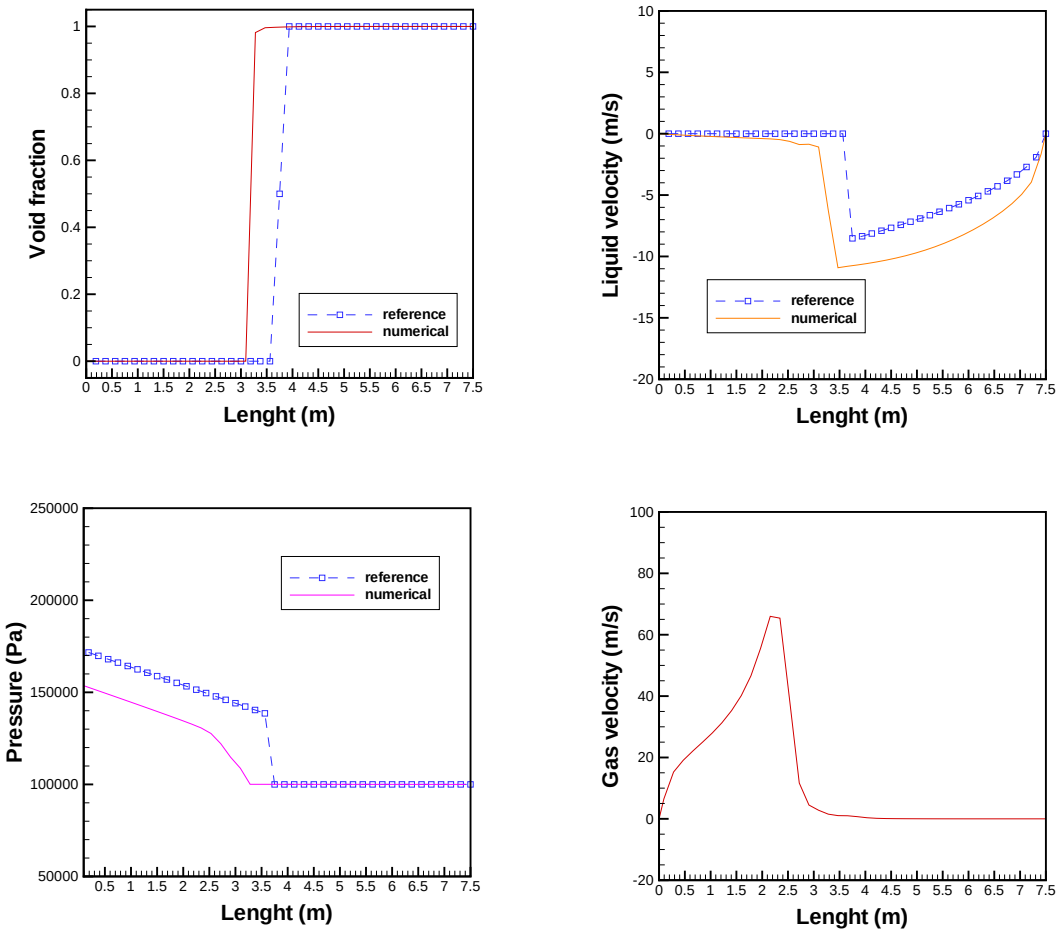


**Figure 6.6:** Profile of the variables calculated, evaluated along the vertical tube at the middle.

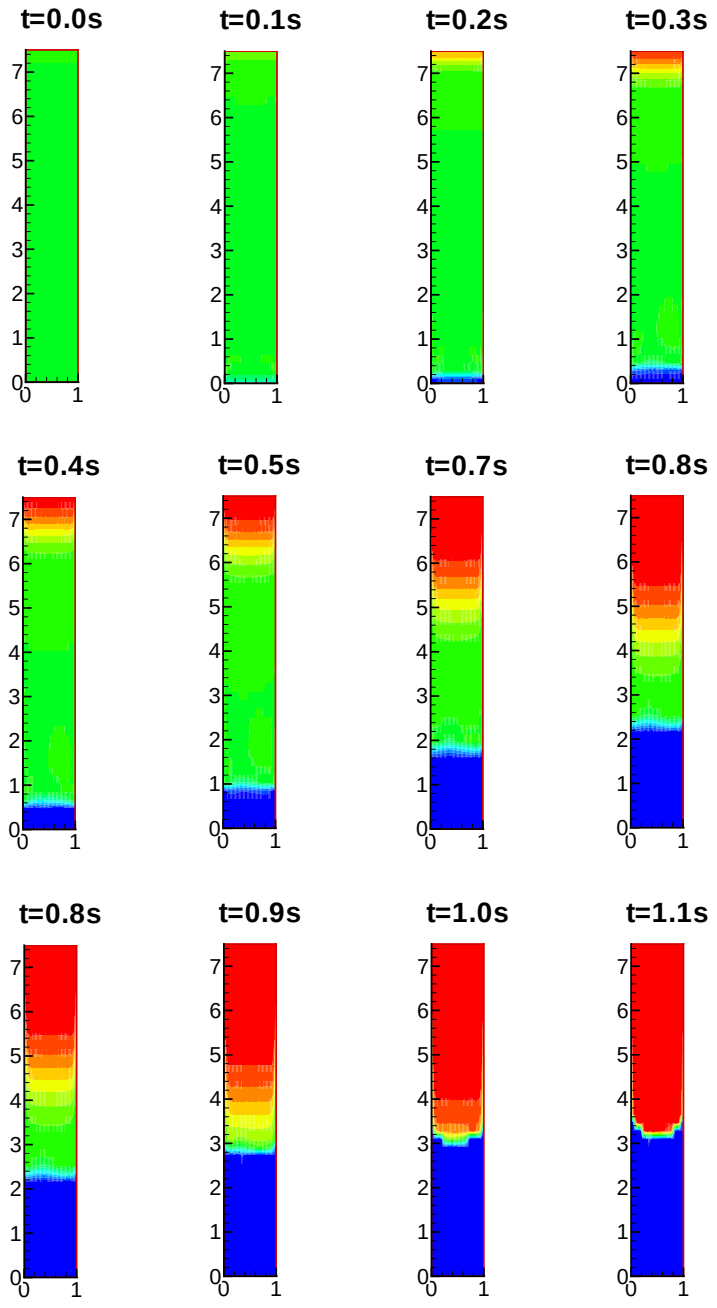


**Figure 6.7:** The volume fraction evolution

### 6.5.2 Collapse of the liquid column case

The second case is a collapse of the liquid column, this cases is a two-dimensional cavity of side 0.2m. This cavity is filled with gas and liquid, half the volume is occupied by the liquid on the left side of the cavity, and the other part is occupied by gas. The interface is aligned with the vertical. The only force that affect is the gravity, which acts in the negative y-direction. The mesh used in this case is 40x40 and the step time used was $1e^{-3}$s. The density of each phase are 1000 $kg/m^3$ for liquid and 1 $kg/m^3$ for gas phase. The liquid will move from one side to other before it come to rest at the bottom of the cavity. An schematic representation of this case is depicted in Figure 6.8.

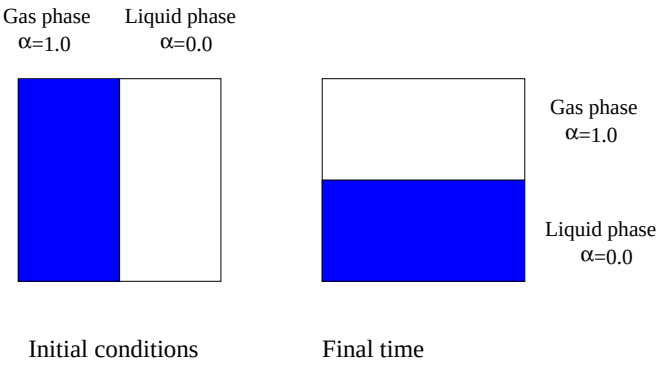


**Figure 6.8:** Collapse of the liquid column case.

A comparison between the numerical results obtained with the model presented in this chapter and the reference results from Moe and Bendiksen [12] are depicted in Figure 6.9.

The comparison between the present model and the model proposed by Moe and Bendiksen, shows a similar behaviour of the volume fraction at three different time step. The line represent the interface when the value of the volume fraction is 0.5, and this line can be compared with the band generated between gas and liquid phases at 0.5. Although there are some differences at the first time step, in the final time step the results are quite similar in both models.

Illustrative results of this case at different time steps are depicted in Figures 6.10 and 6.11. The evolution of the volume fraction into the cavity is presented, from a initial vertical column to a final deposition of the liquid phase on the bottom of cavity. The results at 0.1s show how the liquid column fall down and the liquid begins to take up the gas volume, and the gas phase is moved to the up cavity. The liquid phase movement from the left to the right part of the cavity is shown along the time

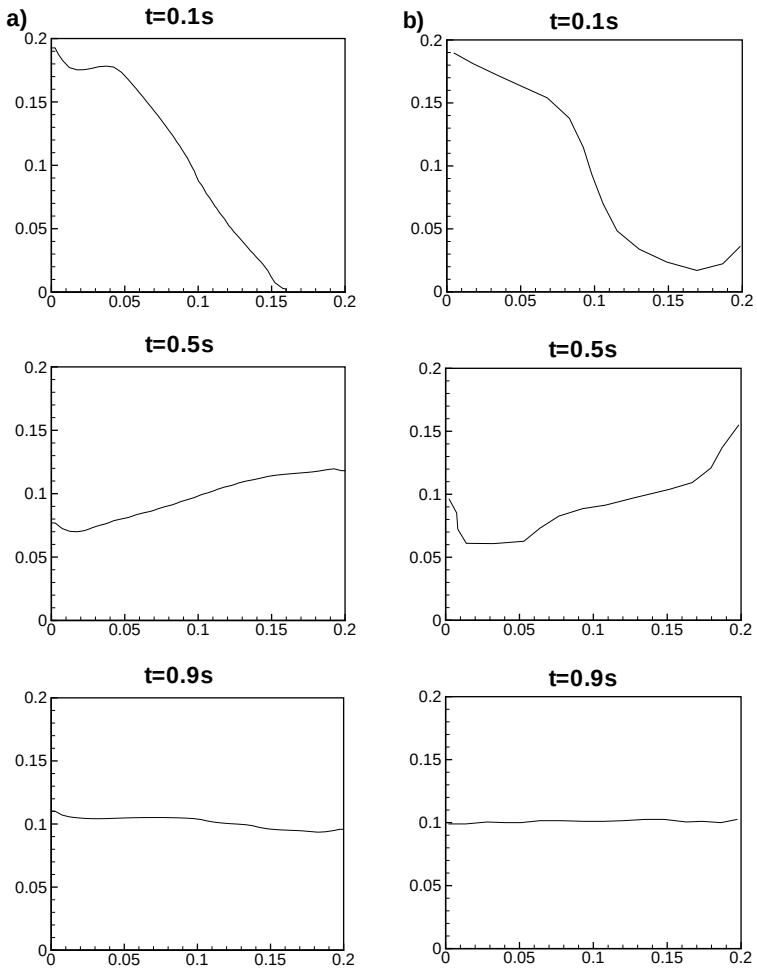


**Figure 6.9:** Collapse of a liquid column. Prediction: a) present model; b)Moe and Bendiksen

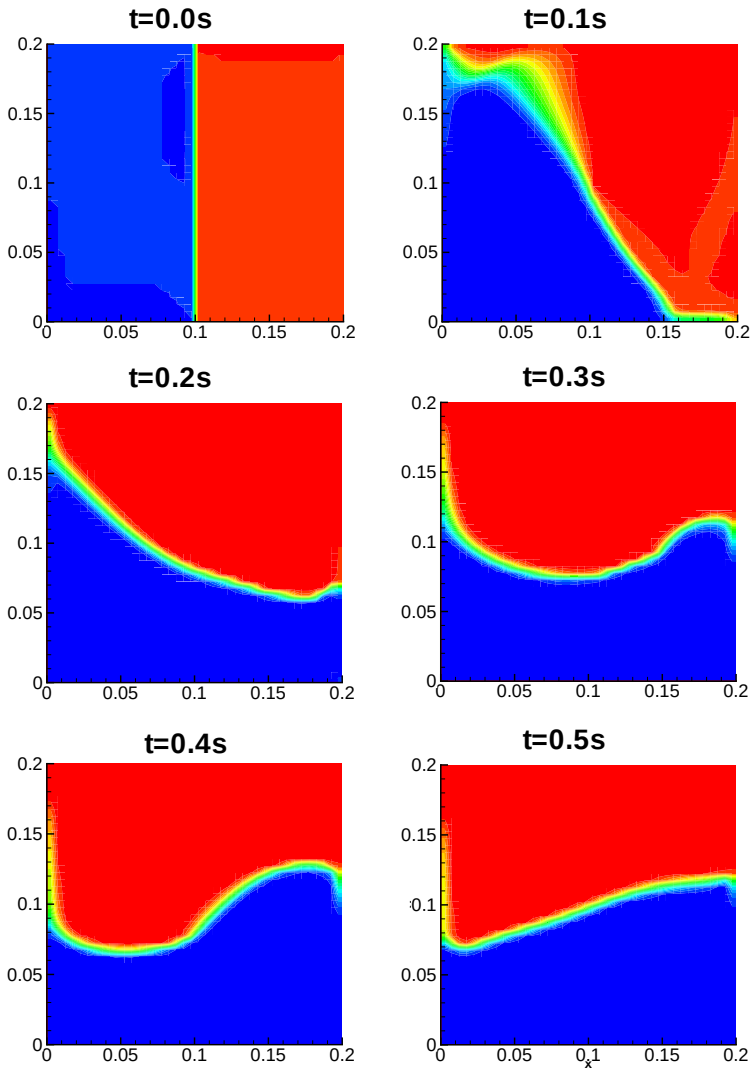


**Figure 6.10:** Collapse of liquid column. The volume fraction evolution (part a)

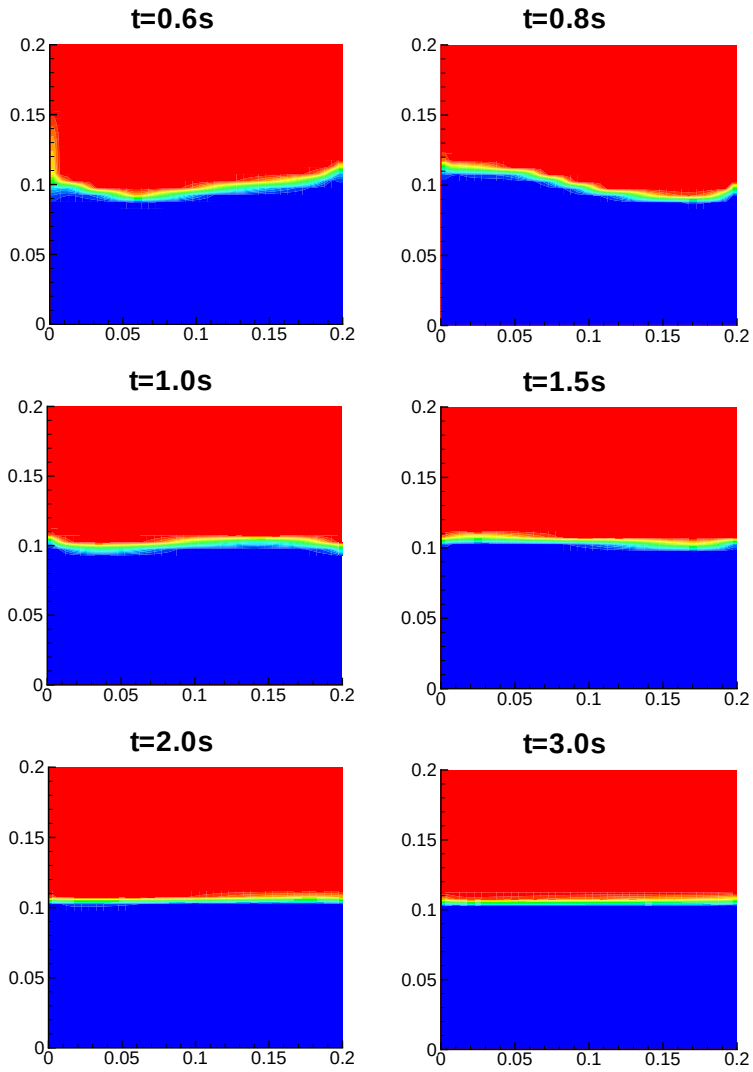


**Figure 6.11:** Collapse of liquid column. The volume fraction evolution (part b)

from 0.1s to 0.5s. After that, the stabilisation of the liquid phase at the bottom of the cavity can be seen.

## 6.6 Conclusions

This chapter has presented the mathematical formulation and discretization of the two-fluid model on two spatial dimension using a staggered mesh. The solution methodology of the discretized equations is based on a semi-implicit pressure method using a first order scheme. The method solve at each time step the velocities and the pressure first, next the volume fraction is obtained and re-evaluated to assure the volume conservation. Two transient cases have been solved by means of the numerical model proposed, the numerical results and a comparative analysis have been depicted.

## 6.7 Nomenclature

$F_M$ forces on the phase
H interfacial drag parameter
$J_x$ $J_y$ total flux
S generation of the variable $\phi$ per volume unit
CV control volume
g acceleration of gravity ($m\ s^{-2}$)
p pressure ($Pa$)
u velocity in x-direction ($m\ s^{-1}$)
v velocity in y-direction ($m\ s^{-1}$)

**Greek symbols**
$\alpha$ void fraction
$\Delta t$ time step ($s$)
$\Delta x$ length of control volume in x direction (m)
$\Delta y$ length of control volume in y direction (m)
$\Gamma$ mass transfer rate per unit volume ($kg\ s^{-1}m^{-3}$)
$\rho$ density ($kg\ m^{-3}$)
$\tau$ stress tensor
$\mu$ viscosity ($Nsm^{-2}$)

**Super- and Subscripts**
k phase g gas or vapour
l liquid
e,w,n,s east, west, north and south CV-faces

P main grid node associated to main CVs
E,W,N,S nearest east, west, north and south nodes associated to main grid node P
* assume value
' correction value

# References

[1] A. Prospereti and G. Tryggvason. *Computational Methods for Multiphase Flow*. Cambridge University Press, 2007.

[2] M. Ishii. *Thermo-fluid dynamic theory of Two-phase flow*. Eyrolles, 1975.

[3] G. Yadigaroglu. Computacional fluid dynamics for nuclear applications: from CFD to multi-scale. *Nuclear Engineering and Design*, 235:153–164, 2005.

[4] S. V. Patankar. *Numerical Heat Transfer and Fluid Flow*. Hemisphere Publishing Corporation, 1980.

[5] M. Darwish and F. Moukalled. A unified formulation of the segregated class of algorithms for multiphase flow at all speeds. *Numerical Heat Transfer, Part B*, 40:99–137, 2001.

[6] J Cortes. On the construction of upwind schemes for non-equilibrium transient two-phase flows. *Computers and Fluids*, 31:159–182, 2002.

[7] S. Evje and K. Fjelde. On a rough AUSM scheme for a one-dimensional two-phase model. *Computers and Fluids*, 32(10):1497–1530, 2003.

[8] F. Moukalled, M. Darwish, and B. Sekar. A pressure-based algorithm for multi-phase flow at all speeds. *Journal of Computational Physics*, 190:550–571, 2000.

[9] M. R. Ansari and V. Shokri. New algorithm for the numerical simulation of two-phase stratified gas-liquid flow and its application for analyzing the Kelvin-Helmholtz instability criterion with respect to wavelength effect. *Nuclear Engineering and Design*, 237:2302–2310, 2007.

[10] T. F. Miller and D. J. Miller. A fourier analysis of the IPSA/PEA algorithms applied to multiphase flows with mass transfer. *Computers and Fluids*, 32:197–221, 2003.

[11] F. Coquel, K. El Amine, E. Godlewski, B. Perthame, and P. Rascle. A numerical method using upwind schemes for the resolution of two-phase flows. *Journal of Computational Physics*, 136:272–288, 1997.

[12] R. Moe and K. H. Bendiksen. Transiente simulation of 2D and 3D stratified and intermittent two-phase flows. Part I: Theory. *International Journal for Numerical Methods in Fluids*, 16:461–487, 1993.

[13] J.H. Ferziger and M. Peric. *Computational methods for fluid dynamics*. Springer-Berlag, 1996.

[14] S. Evje and T. Flatten. CFL-Violating numerical schemes for a two-fluid model. *Journal of Scientific Computing*, 29(1):83–114, 2006.

# Chapter 7

# Conclusions and future actions

## 7.1 Concluding remarks

This Thesis resume the work developed in the simulation of the two-phase flow (gas-liquid) into the pipes. Different strategies to simulate the thermal and fluid-dynamic behaviour of the two-phase flow have been used. Two different numerical models have been studied and explained in this work, together with the advantages and disadvantages of each one, the quasi-homogeneous model (QHM) and the two-fluid models (TFM). Validation with experimental data and analytic results obtained from CTTC's experimental set-up and scientific literature, respectively, have been used to compare the numerical results given for the models proposed in this work. Applications of the methods in different thermal devices have been taken into account and the numerical results have been presented along the development of this work.

The quasi-homogeneous model has been analysed in the first part of the Thesis. The numerical model formulation of the one-dimensional two-phase flow and the discretization using the volume control technique has been presented. A pressure based method SIMPLE liked algorithm has been applied to solve the coupling between mass flow and pressure. The verification of the numerical code has been carried out to show the influence of the convergence criteria and mesh size, which has taken into account the evaporation and condensation process. Different empirical correlations have been implemented with this model to evaluate the heat transfer coefficient, void fraction and friction factor, and their influence on the numerical results has been explained. The validation has been carried out with experimental data from scientific literature and with CTTC's experimental set-up results.

The first numerical method proposed has been applied in the simulation of different cases where the two-phase flow occur. All of them show, how this model integrated

together with a general numerical simulation models for thermal systems and equipments (fin-and-tubes heat exchangers, double-pipe heat exchanger and solar receivers) became an important and useful tool into the design and the performance evaluation of different thermal devices, where two-phase flow occur.

A parametric study of a double-pipe heat exchanger working as an evaporator and a condenser have been carried out using the QHM and different parameters have been analysed. The influence of the flow configuration, the mass flow value through the tube, the insulator thickness, and the inlet conditions as a function of time have been studied. The parametric study shows how the numerical simulation based on a QHM is a robust tool, which can help to analyse the performance of a double-pipe heat exchanger in different working conditions.

The QHM has been implemented into a CTTC code (CHESS) to simulate the two-phase flow into the fin-and-tube heat exchangers. The influence of the two-phase flow behaviour along of the different heat exchanger channels on the wall tubes and fins have been evaluated, using an evaporator and a condenser. The use of the QHM in a the simulation of a real industrial application has been shown a good agreement with experimental data.

The numerical analysis of the critical heat flux into the tube has been implemented based on a Look-up table method proposed by Groeneveld. An application where this phenomena can be present has been analysed. The numerical results of this case give a high jump of the wall temperature along the tube as a consequence of a high heat flux applied. The average and the local behaviour of the wall temperature has been depicted, together with the temperature and the heat transfer coefficient of the fluid flow. This kind of conditions should be avoid in a real application to prevent the possible damages of the solid parts that make up the structure.

After simulate a hypothetic case where the critical heat flux is present, a solar receiver with steam generation has been studied, where the influence of the incident heat flux applied has been taken into account to avoid the critical heat flux condition. The simulation of the complete thermal device has been carried out by means of a CFD&HT code (TermoFluids). This code is capable to link the solution of the two-phase flow, the heat conduction through the solid parts and the heat radiation on the complete solar panel. The numerical results obtained have been shown in a group of figures, where the behaviour of different variables are presented. This code helps to evaluate the performance of the solar receiver in function of different parameters, one of this is the incident heat flux. However, others parameters can be analysed, such as the quantity of mass flux, the geometry of the tubes or the inlet conditions of the fluid flow.

The QHM is a robust numerical method to solve the two-phase flow phenomena. However, this method assume the two-phase flow as a homogeneous mixture with one mixture temperature, one mixture mass flux and one pressure. This assumption can

generate mistakes in the performance prediction in some applications where each one of the phases have different thermal and fluid-dynamic behaviour.

The TFM appear as an alternative to resolve the two-phase flow phenomena and supply a solution of each one of the phases separately. Then, using the TFM a numerical results of the volume fraction, liquid and gas velocities, liquid and gas temperature and a pressure can be obtained.

The mathematical formulation and discretization of the one-dimensional two-fluid model has been presented. The numerical solution is obtained following a similar strategy of the QHM, by means of a pressure based method. However, the number of variables to be found is bigger than QHM. The volume distribution or void fraction value is a new variable to be solved with the TFM, in comparison with the QHM where this value has been evaluated from a empirical correlation. An special attention should be put in the volume fraction solution, where the volume fraction value has to satisfy the conservation condition to avoid error during the iterative solution method.

The validation of the TFM has been evaluated by means of the comparison between the numerical results predicted for the present model and an analytic expression from literature of a transient case. A good agreement between results are shown for the velocities, the pressure and the void fraction along the different time steps.

Although the two-fluid model has been usually applied in nuclear applications, the numerical model developed in this Thesis has been used to simulate an evaporator of a refrigerant system. The numerical results obtained with TFM have shown a good agreement with the experimental data from CTTC's experimental facility.

A good definition and choose of the regimen flow present in the fluid flow should be done to find the more suitable empirical expression. This task is not easy, because there are several flow regime maps and empirical expressions in function of the fluid and field application. In the present Thesis different variables such as the kind of fluid, the working conditions and the position of the fluid flow have been taken into account to choose the more reliable flow regime map.

A group of constitutive laws proposed to water and steam water flow obtained from the nuclear field, which has a lot of experience with TFM, has been adapted to be used with a refrigerant fluid. These criteria has been followed due to there are not enough information about the applicability of the two-fluid model in refrigerant flows.

A comparison between QHM and TFM has been presented, using an evaporation case, the numerical results of both models have been compared and similar behaviour of the fluid temperatures, pressure, void and weight mass fraction have been obtained. However, the prediction of the liquid velocity is different in both models. The TFM predict a higher value of the liquid velocity than the QHM prediction, this difference occurs as a consequence of the interfacial drag friction force, quantified in the TFM and not take into account in QHM.

The numerical results obtained with the TFM are very susceptible to the evaluation of the heat transfer coefficient and the frictional forces of each one of the phases at the interface and at the wall. So, the empirical correlation and the regimen flow definition influenced the numerical results. A comparison between TFM-A and TFM-B shows an example of this critical dependence, where the liquid velocity profile present a different behaviour in function of the empirical expressions applied to evaluate the drag force.

Not exist a clear criteria to the evaluation of the different empirical parameters needed in the resolution of the one-dimensional TFM. Then, a lot of alternatives or strategies to predict the value of these have been proposed in the literature. In general, a big number of empirical expressions can be found in the nuclear field to define the constitutive laws for TFM, but not occur the same in other fields such as the refrigeration, where more experimental studies are necessary.

The extension of the one-dimensional two-fluid model to the two-dimensional two-fluid model represents a first step to the numerical simulation of the two-phase flow based on the CFD methodology usually applied in single-phase. This extension to two-phase flow is defined as computational multi-fluid dynamic CMFD. These kind of methods will be capable to offer more details about the thermal and fluid-dynamic behaviour of the fluid flow than other classical methods. However, the development of the CMFD is coupled to the classical methods to analyse the two-phase flow. The CMFD methods are still under developmet in comparison with the CFD methods to solve single-phase.

The two-dimensional two-fluid model proposed in this Thesis has solved the coupling between velocity and pressure. The momentum and mass conservation equations by each one of the phases have been proposed and suitably formulated to find the volume fraction, the pressure and the gas and liquid velocities. The mathematical formulation on a two spatial dimension and the discretization on a two-dimensional grid using a staggered mesh has been explained. The numerical resolution is based on a pressure based method classified as a mass conservation based algorithm MCBA.

The numerical results obtained with the two-dimensional TFM have been presented, together with a comparative analysis of the numerical results. A good agreement between the numerical results and the references have been obtained for two cases. These cases have shown the influence of the gravity on the dynamical behaviour of the two-phase flow into the cavities.

## 7.2 Future actions

The future actions on the development of numerical methods to predict the thermal and fluid-dynamic behaviour of the two-phase flow and their applications are going to be focused within the general research strategy of the Research Group. In that

sense, a group of subjects to improve the use and the application of this methodology to simulate and analyse the two-phase flow is proposed here.

- Improve the applications and the criteria to select the suitable set of empirical correlations into the one-dimensional two-fluid models increasing the possibility of simulate a lot of conditions in the two-phase flow. This model is very dependent on the empirical correlations and a hard work to verify and validate the evaluation of the different parameters should be carried out. This kind of methods has been used extensively in the simulation of nuclear system and the empirical information used in this field should be extrapolated to other applications.

- Extent the numerical analysis of the two-phase flow into the tubes using the one-dimensional two-fluid model to different operation conditions and evaluate the thermal and fluid dynamic behaviour of the fluid flow at different regimen flows.

- Implement mathematical strategies into the code in order to improve and reduce the high empirical information influence on the convergence process when a change of regimen flows occurs.

- Implement the application of the one-dimensional two-fluid model in the numerical analysis of a critical conditions in different thermal devices. The critical heat flux is a conditions where the physical conditions of each one of the phases are quite different. Then, the TFM can gives more details information than QHM for this condition.

- Following the development of the quasi-homogeneous model, the two-fluid model should be linked inside general numerical simulation models to be capable of solve thermal devices where a detailed description of the two-phase flow is required.

- Build a complete two-dimensional two-fluid model to study the thermal and fluid dynamic behaviour of each one of the phases. In this Thesis a simplified model without energy equation has been proposed. This new task might require a modification of the model proposed, and use other strategies or methodologies to find a more suitable result.

- The two-fluid model presented in this work does not assume the influence of the turbulence phenomena into the two-phase flow. This effect should be considered and some turbulence models can be implemented into the formulation to can simulate cases where the turbulence has an important effects.

- The connection of the two-fluid models and the level-set methods is a new strategy to find good result in some cases. Researchers in the two-phase field have explained the need to link this two kind of models to build a strong resolution method.
- The computational methods for multiphase flow have had an important development in last years and today there are a lot of things about two-phase flow phenomena that are not clear. The numerical simulation of the thermal and fluid dynamic of two-phase flow phenomena using a CMFD methodology in 2D and 3D in Cartesian coordinate is a suitable tool to understand the phenomena and find good results.